Experimental and Numerical Spray Characterization of Biofuels and Pure Components

Ph.D. Thesis

By

Lanjekar Rajan Deorao

DISCIPLINE OF MECHANICAL ENGINEERING
INDIAN INSTITUTE OF TECHNOLOGY INDORE
March 2018

Experimental and Numerical Spray Characterization of Biofuels and Pure Components

A THESIS

Submitted in partial fulfillment of the

requirements for the award of the degree

of

DOCTOR OF PHILOSOPHY

by

LANJEKAR RAJAN DEORAO

DISCIPLINE OF MECHANICAL ENGINEERING

INDIAN INSTITUTE OF TECHNOLOGY INDORE

March 2018

INDIAN INSTITUTE OF TECHNOLOGY INDORE

CANDIDATE'S DECLARATION

I hereby certify that the work which is being presented in the thesis entitled "**Experimental and Numerical Spray Characterization of Biofuels and Pure Components**" in the partial fulfillment of the requirements for the award of the degree of DOCTOR OF PHILOSOPHY and submitted in the DISCIPLINE OF MECHANICAL ENGINEERING, Indian Institute of Technology Indore, is an authentic record of my own work carried out during the time period from January 2013 to March 2018 under the supervision of Dr. Devendra Deshmukh, Associate Professor, Discipline of Mechanical Engineering, Indian Institute of Technology Indore, India.

The matter presented in this thesis has not been submitted by me for the award of any other degree of this or any other institute.

Signature of the student with date
(Lanjekar Rajan Deorao)

This is to certify that the above statement made by the candidate is correct to the best of my knowledge.

Signature of Thesis Supervisor with date
(Dr. Devendra Deshmukh)

Lanjekar Rajan Deorao has successfully given his Ph.D. Oral Examination held on

Signature of Chairperson (OEB)	Signature of External Examiner	Signature of Thesis Supervisor
Date: 5/9/18	Date: 5/9/18	Date: 5/9/18
Signature of PSPC Member:1	Signature of PSPC Member:2	Signature of Convener, DPGC
Date: 05/09/18	Date: 5/9/18	Date: 5-9-18

Signature of Head of Discipline
Date: 5/9/18

Dedicated to
God: Shri Krishna
and
Father: Mr. Deorao Krishnaji Lanjekar

ACKNOWLEDGEMENTS

I am immensely grateful to my supervisor Dr. Devendra Deshmukh for giving me an opportunity to do the Ph.D. under his guidance. His untiring patience towards correcting my mistakes and his faith in me for given tasks makes me complete the present work. I thank him for his invaluable guidance, suggestions, and encouragement throughout the work.

I would like to thank Prof. Pramod Mehta, for providing valuable suggestions during the experiments which were performed at NCCRD facility of IIT Madras, Chennai, India. I thank Mr. Ashwin Patil, proprietor of Avishkar Enterprise Pvt. Ltd. for manufacturing the optical chamber window which is used for spray experiments at IIT Madras, India. I would also appreciate Mr. Sibin Roberts of Arabin Technologists, Chennai, India for performing microwelding of the fuel injector used in the present work. I would like to give special thanks to Mr. Manas Pal and Mr. Anurag from Mechanical Engineering Department, IIT Madras, Mr. Aniket Kulkarni and Mr. Vasudev Choudhari from the discipline of Mechanical Engineering, Spray and Combustion Laboratory, IIT Indore, without their kind support and help the experiments may not be possible. I would like to express my heartfelt gratitude towards my PSPC committee members Dr. Ritunesh Kumar and Dr. Amod Umrikar, including DPGC Convenor Dr. Shailesh Kundalwal for their valuable suggestions towards the research work.

I thank my grandmother Smt. Anusaya Bhuyarkar, my mother Smt. Ameeta Deorao Lanjekar and my in-laws for their blessings. I thank my wife Mrs. Shweta, my children Ved and Vansh and my younger brother Mr. Rohit for their love, care and constant moral support which enables me to carry out the present work. I would also like to thank God for showering me his blessings and have given me a chance to carry out the present work in an association of the wonderful personalities. Last but not the least, I thank my Father, whose teachings and principles always guide me and empower me to go through the difficult times. Finally, I want to thank everyone who has, in one way or another, helped me to conduct the present research work.

RAJAN DEORAO LANJEKAR

ABSTRACT

The biodiesel fuelled CI engines are observed to produce higher NO_x emission. The emissions depend on spray characteristic along with the composition and physiochemical properties of the biodiesel. The non-evaporating and evaporating spray characteristics are analyzed using numerical models for biodiesel and their pure components. The CFD code is modified to incorporate the physiochemical properties of pure components of biodiesel and model multi-component evaporation. The spray models are validated with experimental data available in the literature for various fuels.

The spray characteristics of evaporating spray, liquid length, and vapor length are predicted and compared for pure components of biodiesel and SVO at engine-relevant conditions. The spray tip penetration of karanja biodiesel is found to be similar to that of the methyl oleate. The spray tip penetration of coconut biodiesel is found to be similar to that of methyl laurate. The liquid and vapor length are found to be the function of the fuel properties and ambient gas conditions. The liquid length of methyl oleate is higher than methyl laurate under late-cycle post-injection conditions studied. It may lead to impingement of liquid fuel on the combustion chamber walls. The FAME components studied under near top-dead-center injection conditions are found to have a shorter liquid length, which can avoid wall impingement. A single component representative of biodiesel is found to be sufficient to predict the spray tip penetration of biodiesel and its blend in their respective category.

The vapor length for all the biodiesel pure components is similar at near top-dead-center conditions. However, at lower ambient gas density and ambient gas temperature conditions methyl oleate is found to produce higher vapor length, which decreases with increase in an ambient gas temperature. The SVO pure components have longer liquid length than that of their corresponding FAME. A linear correlation is observed between the liquid length and the boiling temperature of the biofuels. The vapor distribution for a multi-component surrogate is considerably different than that of single component fuel. The spatial mass fraction distribution of biodiesel is found to be the function of the volatility differential of the pure components and their proportion in the composition. The vapor mass fraction distribution for biodiesel of palm and soybean are found to be similar to that of their single component surrogate due to a similar volatility of components of these biodiesels. The change in the percentage of methyl laurate in coconut composition is found to have a strong impact on vapor distribution. The accurate determination of the biodiesel composition is essential to get correct prediction of combustion characteristics and emission profile for the given engine conditions.

Contents

List of Figures

List of Tables

NOMENCLATURE

C	Coconut
$C_{10}H_{22}$	Decane
$C_{12}H_{26}$	Dodecane
$C_{14}H_{30}$	Tetradecane
$C_{16}H_{34}$	Hexadecane
$C_{18}H_{38}$	Octadecane
C_7H_8	Toluene
C_a	Inter-Diffusion Coefficient of Fuel and Air
CA	Cranck Angle
CFD	Computational Fluid Dynamics
CI	Compression Ignition
CME	Coconut Methyl Ester
CN	Cetane Number
CO	Carbon Monoxide
CP	Cloud Point
C_p	Mean Specific Heat of Gas Mixture and Fuel Vapor
$C_{p_{gas}}$	Specific Heat of an Ambient Gas at Constant Pressure
$C_{p_{liq}}$	Specific Heat of Liquid Fuel at Constant Pressure
CRDI	Common Rail Direct Injection
CVC	Constant Volume Chamber
d	Average Diameter
DIPPR	Design Institute for Physical Properties
d_p	Diameter of Droplet
ECN	Engine Combustion Network
EGR	Exhaust Gas Recirculation
EO	Ethyl Oleate
Expt.	Experiment
FAEEs	Fatty Acid Ethyl Esters
FAMEs	Fatty Acid Methyl Esters
h_i	Heat Transfer Coefficient between Droplet Interior and Droplet Surface
HO	High Oleic Sunflower Oil
h_o	Heat Transfer Coefficient between Ambient Gas and the Droplet Surface
HTC	Heat Transfer Coefficient
h_{vap}	Latent Heat of Vaporization
ID	Ignition Delay
IV	Iodine Value
K	Karanja
k	Turbulence Kinetic Energy
kappa	Vapor or Gas Thermal Conductivity
KH	Kelvin-Helmholtz
KH-RT	Kelvin-Helmholtz Rayleigh-Taylor

$\ddot{m}$	Evaporated Mass Flux
ML	Methyl Laurate
MLLn	Methyl Linolenate
MLn	Methyl Linoleate
MM	Methyl Myristate
MO	Methyl Oleate
MP	Methyl Palmitate
MS	Methyl Stearate
MUFA	Mono-Unsaturated Fatty Acid
n	Number of Pure Components in Biodiesel
n-decane	Normal Decane
n-dodecane	Normal Dodecane
n-heptane	Normal Heptane
n-hexadecane	Normal Hexadecane
n-octadecane	Normal Octadecane
NO	Nitric Oxide
NO_2	Nitroge Di-Oxide
n-tetradecane	Normal Tetradecane
N_2	Nitrogen Gas
NBP	Normal Boiling Point
NO_x	Oxides of Nitrogen
NSRDS	National Standard Reference Data
Nu	Nusselt Number
OpenFOAM	Open Field OperationAir Fuel Ratio
P	Palm
P_{amb}	Ambient Gas Pressure
Pe_l	Droplet Peclet Number
P_{inj}	Fuel Injection Pressure
PK	Palm Kernel
PLN	Pump-Line-Nozzle
PM	Particulate Matter
PME	Palm Methyl Ester
P_n	Property of the n^{th} Component of Biodiesel
PP	Pour Point
Pr	Prandtl Number
PUFA	Polyunsaturated Fatty Acid
R	Rapeseed
R_d	Droplet Radius
Re	Reynolds Number
RME	Rapeseed Methyl Ester
RO	Rapeseed Oil
RT	Rayleigh-Taylor
S	Soybean
SFA	Saturated Fatty Acid
Sh	Sherwood Number
Sim.	Simulation
SMD	Sauter Mean Diameter
SME	Soybean Methyl Ester

SOC	Start of Combustion
SVOs	Straight Vegetable Oils
t	Characteristic Turbulence Scale Time
T90	Temperature at which 90% of Fuel Vaporized
T_{boil}	Normal Boiling Point Temperature of Liquid
T_d	Droplet Temperature
T_{fuel}	Fuel Temperature
T_{gas}	Temperature of an Ambient Gas
TO	Triolein
T_{ref}	Reference Temperature
T_s	Surface Temperature
UHC	Unburnt Hydrocarbon
Y_{fs}	Mass Fraction of Fuel at the Droplet Surface
Y_{fsur}	Mass Fraction of Fuel at the Droplet Surrounding
Y_n	Liquid Mass Fraction of the Biodiesel n^{th} Pure Compenent
α_{eff}	Effective Thermal Diffusivity
α_{liq}	Liquid Fuel Thermal Diffusivity
ϵ	Rate of Dissipation
η	Correlation Factor
ρ_{gas}	Ambient Gas Density

1 Introduction

1.1 Background

Compression Ignition (CI) engine exhibits higher thermal efficiency than that of spark ignition engines. This makes CI engine a popular choice for industrial, transport, and domestic power generation applications. The hazardous emissions, such as Particulate Matter (PM), Unburnt Hydrocarbon (UHC), Carbon Monoxide (CO) and Oxides of Nitrogen (NO_x) which are the threat to human health and environment are the problems of CI engine. The CI engine fuel, diesel, is a fossil fuel having limited reserves all over the Globe.

The biodiesel is a renewable fuel for CI engine. Biodiesel gives similar engine performance as that of diesel with a lower PM and UHC emissions. However, higher NO_x emission of biodiesel has become a major hurdle for its use in CI engines [1]. Many numerical and experimental investigations are available in the literature analyzing the causes of higher NO_x emission of biodiesel. The higher NO_x emission of biodiesel is correlated to the fuel composition and properties. The dependence of emission on biodiesel composition motivates the researchers to find the optimal composition of biodiesel, which will have minimum engine emissions.

The advanced combustion technologies, to control NO_x emission, such as Exhaust Gas Recirculation, multiple injection and Low Temperature Combustion strongly depend on air-fuel mixture formation. The air-fuel mixture formation depends on spray atomization and properties of fuel. It is important to understand an effect of the biodiesel composition on mixture formation through spray atomization and evaporation.

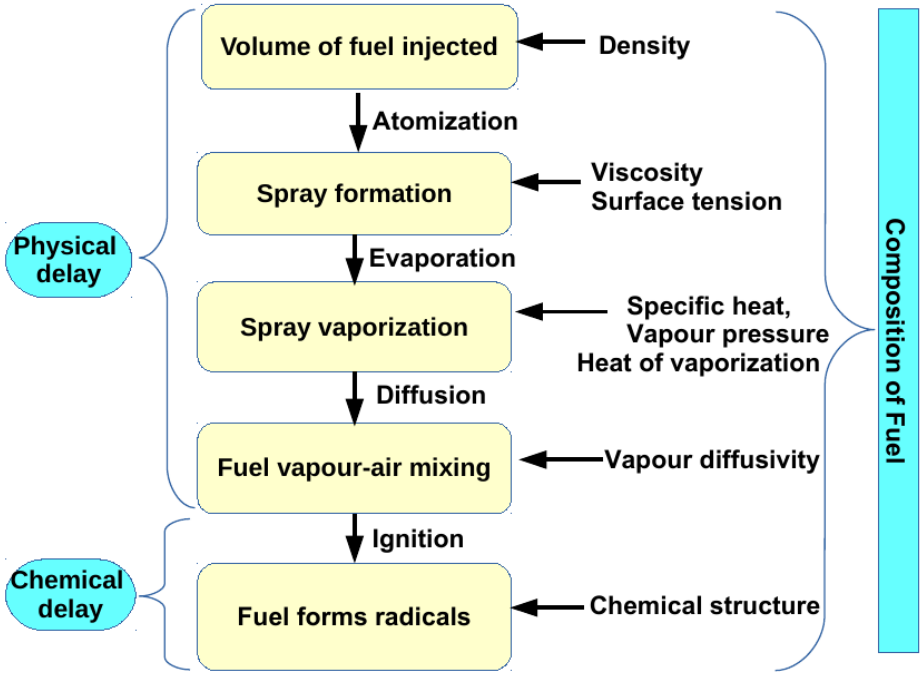

Figure 1.1: Effect of composition and physiochemical properties of biodiesel on air-fuel mixture formation.

1.2 Motivation

The schematic 1.1 shows various processes involved in CI engine combustion. Each of them depends on its preceding process and the composition and physiochemical properties of the fuel. The formation of the fuel spray is the function of fuel properties such as viscosity, and surface tension. The spray characteristics govern the evaporation and the quality of the air-fuel mixture formed. The spatial air-fuel vapor mixture distribution, local equivalence ratio, temperature, and scalar dissipation determine the ignition delay of the mixture.

The difference in chemical kinetics of the each of the component in the mixture formed determines the ignition delay and combustion phasing. The nature and timing of the combustion phases determine the pollutants formed. It is observed that all the processes are interdependent and also depend on the fuel composition and its physiochemical properties. The accuracy of the prediction of each process

affects the overall prediction accuracy. It can be observed from the Fig. 1.1 that the atomization and mixture formation process is crucial to determine the nature of following processes till the combustion and the formation of pollutants.

1.3 Scope of the Study

The combustion of the fuel is preceded by fuel evaporation and mixing with compressed air in the combustion chamber. The atomization of the injected fuel facilitates the vaporization of the fuel into fine droplets. Thus, the nature of atomized fuel governs the vaporization, mixture formation and hence combustion and nature of pollutants produced. The present study investigates atomization of biofuels and their pure components under non-evaporating and evaporating conditions. The air-fuel mixture formation is analyzed with multi-component evaporation models. The spray characteristics of diesel, biodiesel, straight vegetable oil and their respective pure components and surrogate fuels are studied at engine-relevant conditions. The vapor mass fraction distribution of individual components of biodiesel is analyzed using multi-component evaporation model.

1.4 Thesis Structure

A literature study on the relationship between biodiesel properties and engine performance is presented in Chapter 2. A detailed review of spray characteristics and their importance in combustion is discussed in this chapter. The numerical and experimental methodology used in the research work is presented in Chapter 3. Chapter 4 provides the experimental and numerical results of non-evaporating diesel and biodiesel spray. The evaporating spray characteristics at engine-relevant conditions for diesel, biodiesel, and their pure components are presented in Chapter 5. Chapter 6 presents an analysis of multi-component diesel and biodiesel spray with respect to the mass fraction distribution. Finally, the conclusions and scope for future work is summarized in Chapter 7.

2 Literature Review

2.1 Biodiesel

The biodiesel, which is a renewable fuel, can be produced from oil from various sources, including edible and non-edible vegetable oils, waste oils, and fats. *Transesterification* is a widely used process for converting oils into biodiesels. The biodiesels are also termed as Fatty Acid Methyl Esters (FAMEs) or Fatty Acid Ethyl Esters (FAEEs), based on the alcohol moiety (methanol or ethanol) attached to the fatty acid chain. The *Transesterification* reaction for production of FAMEs from triglycerides is shown in the Eq. 2.1.

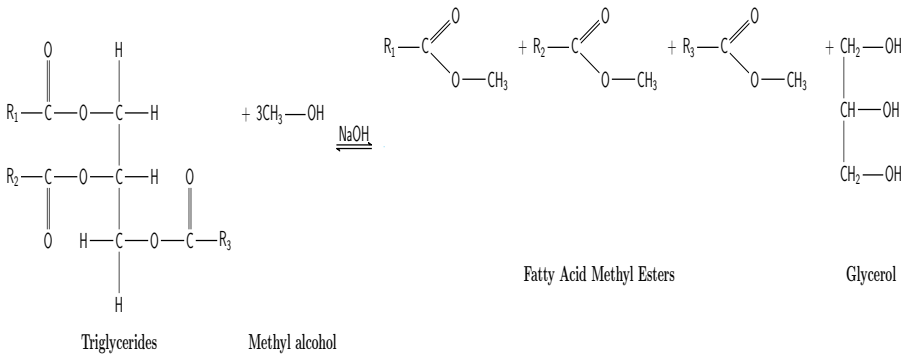

(2.1)

The *Transesterification* reaction (Eq. 2.1) replaces a heavy molecule of glycerol with a comparatively lighter molecular weight alcohol molecule, such as methanol or ethanol and produces mono-alcohol esters such as FAMEs or FAEEs [2–6]. The fatty acid composition of various oils used for producing biodiesel is given in Table. 2.1. The Table. 2.1 shows that most of these oils contain five fatty acids, namely palmitic (hexadecanoic; C16:0), stearic (octadecanoic; C18:0), oleic (9(Z)-octadecanoic; C18:1), linoleic (9(Z), 12(Z)-octadecanoic; C18:2) and linolenic (9(Z), 12(Z), 15(Z)- octadecanoic; C18:3) acids [5–8]. The fatty acids can be classified by the number of double bonds or the degree of unsaturation and chain length. The

Table 2.1: Fatty acid composition of oils used for biodiesel production [5, 6].

Common name	Carbon no. : double bond no.	Composition of oil (%)										
		PN	RS	OL	CO	CR	P	PK	SA	SU	SB	TL
Caproic	6:0	—	—	—	0-0.8	—	—	T-1.5	—	—	—	—
Caprylic	8:0	—	—	—	5-9	—	T	3-5	—	—	—	—
Capric	10:0	—	—	—	6-10	—	T	3-7	—	—	T	—
Lauric	12:0	—	—	—	44-52	—	T	40-52	—	—	T	T-0.2
Myristic	14:0	T-1	—	0.1-1.2	13-19	T-1.7	0.5-6	14-18	T	—	T	2-8
Palmitic	16:0	6-9	1-3	7-16	8-11	8-12	32-45	7-9	3-6	3-6	7-11	24-37
Stearic	18:0	3-6	0.4-3.5	1-3	1-3	2-5	2-7	1-3	1-4	1-3	2-6	14-29
Arachidic	20:0	2-4	0.5-2.4	0.1-0.3	0-0.4	T	T	T-1	T-0.2	0.6-4	0.3-3	T-1.2
Behenic	22:0	1-3	0.6-2.1	—	—	T	—	—	—	T-0.8	T	—
Palmitoleic	16:1	T-1.7	0.2-3	T	0-1	0.2-1.6	0.8-1.8	T-1	—	T	T	1.9-2.7
Oleic	18:1	53-71	12-24	65-85	5-8	19-49	38-52	11-19	13-21	14-43	15-33	40-50
Gadoleic	20:1	—	4-12	—	—	—	—	—	—	—	—	—
Erucic	22:1	—	40-55	—	—	—	—	—	—	—	—	—
Linoleic	18:2	13-27	12-16	4-15	T-2.5	34-62	5-11	0.5-2	73-79	44-75	43-56	1-5
Linolenic	18:3	T	7-10	T-1	—	T	T	—	T	T	5-11	—

PN - peanut ; RS - rapeseed oil; OL - olive; CO - coconut; CR - Corn; P - palm
PK - palm kernel; SA - safflower oil; SU - sunflower; SB - soybean; TL- tallow; T-trace

fatty acids can be classified by the number of double bonds or the degree of unsaturation and chain length. In the CX:Y notation for the fatty acid esters, X and Y denotes the number of carbon atoms in the fatty acid chain and the number of carbon-carbon double-bonds which is unsaturation in the fatty acid chain, respectively. The Saturated Fatty Acid (SFA) has zero double bond (palmitic and stearic fatty acids). The C18:0 is saturated Fatty acid containing 18 carbon atoms and zero (0) number of double bonds. The Mono-Unsaturated Fatty Acid (MUFA) has one double bond (oleic fatty acid). The C18:1 fatty acid has 18 number of carbon atoms with one double bond. The oleic (9(Z)-octadecanoic; C18:1), in which (9(Z) or Δ9) notation indicates that the double bond is present at 9^{th} position in fatty chain, counted from carboxylic (-COOH) end of fatty acid chain. The Polyunsaturated Fatty Acid (PUFA) has more than one double bond in its fatty acid chain such as linoleic C18:2 and linolenic C18:3 fatty acid [5, 6].

The olive and peanut oils are of MUFA type containing 65-85% of oleic (C18:1) fatty acids, whereas safflower, sunflower, corn and soybean are of PUFA type oils having 43-79% of linoleic (C18:2) fatty acids. These oils fall in long chain unsaturated fatty acid category. The palm oil with 32-45% of palmitic acid (C16:0) and tallow oil with 14-29% of stearic acid (C18:0) are in the category of long chain saturated oils. The coconut and palm kernel oils are found to be exception and contain 60-90% of C:12-C:16 medium chain saturated fatty acids [6, 7]. Most of the vegetable oils observed to have long chain fatty acids.

2.2 Effect of Fuel Composition on Properties

The various compositional features of biodiesel include type of fatty acid, an alcohol moiety, chain length and number, position and isomers of double bond [9, 10]. The correlations between these compositional features and the properties of biodiesel are discussed in the literature. The correlation between unsaturation (the average number of double bonds) of biodiesel and their properties such as density, cetane number (CN), iodine value (IV), kinematic viscosity, cloud point (CP), pour point (PP) and heating value has been proposed by Hoekman et al. [11] and Giakoumis [12]. The cetane number of the fuel gives an indication of unsaturation and ignition delay. The

cetane number is highest for long chain saturated fuel, it decreases with introduction of double bonds or branching in fuel molecule. It is observed that fuel with lower cetane number, having higher proportion of unsaturated fatty acid components exhibits higher ignition delay. They found a negative correlation between unsaturation and CN, viscosity, CP, and PP, whereas there is a positive correlation was reported with density, heating value and IV [12]. The density of biodiesel is reported to be directly proportional to the average number of double bonds present [11, 13–15]. For example, high oleic sunflower oil (HO) and rapeseed oil (RO) have lower PUFA content than soybean oil, thus, the density of HO and RO is lower than that of soybean oil [15].

Biodiesel exhibits a narrow range of boiling point (325 to 350°C) compared to No.2 diesel (180 to 320°C) [5].

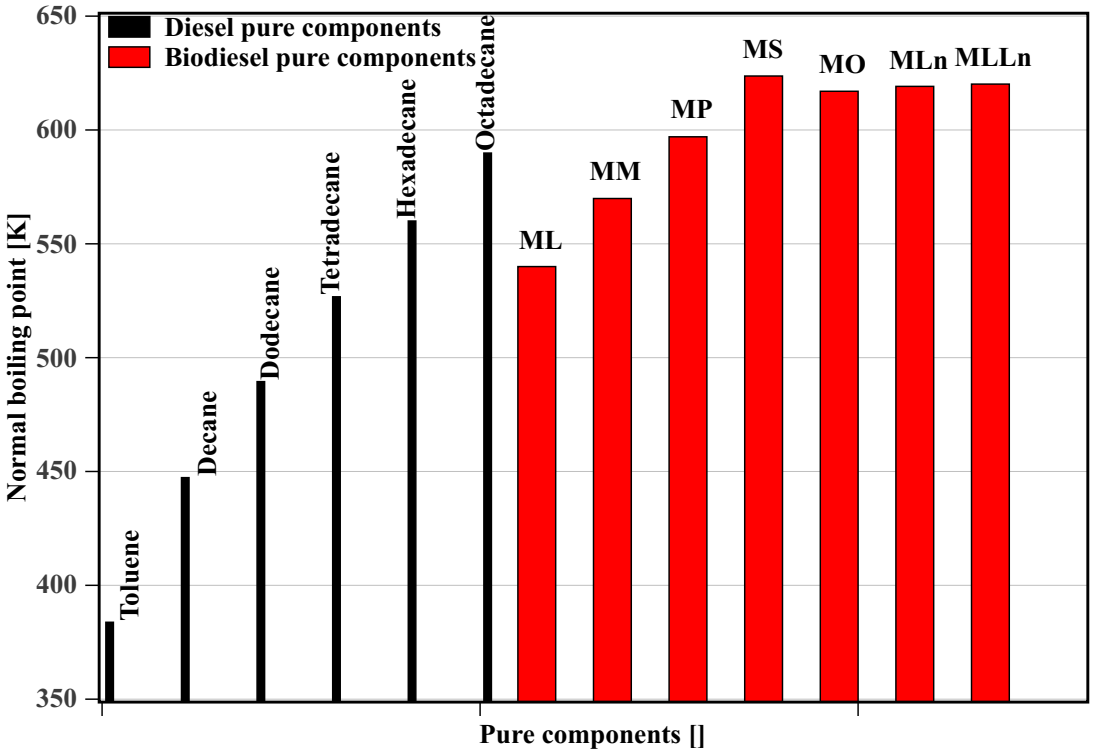

Figure 2.1: Normal boiling point of diesel and biodiesel pure components.

Biodiesel, however, has a higher average boiling point ($\sim$ 331°C) than that of diesel fuel ($\sim$ 263°C) [5]. The energy density and lower heating value of biodiesel are less than that of diesel which is attributed to the presence of oxygen in biodiesel (around 10% by weight) [2]. On comparing normal boiling point of an individual pure component of biodiesel and diesel, methyl laurate in the coconut biodiesel and toluene in the diesel exhibits lowest normal boiling point of 540 K and 380 K respectively among the respective pure components of biodiesel and diesel (Fig. 2.1). This significant difference of normal boiling point among the pure components of biodiesel and diesel in terms of volatility differentials will exhibit different evaporating characteristics, which can be captured with multi-component evaporation model. Thus, there is a need to use multi-component evaporation model to study the vapor mass fraction of each individual species, which helps to improve the prediction of mixture formation, combustion characteristics, and nature of pollutants formed.

Knothe et al. [16] evaluated the influence of the fatty acid chain length, configuration and position of double bonds on the viscosity of biodiesel. The Table. 2.2 compares the kinematic viscosity of MUFA in relation to different chain length, *cis* and *trans* isomers of methyl octadecenoate and position of double bonds in the chain [16]. It is observed that increasing the fatty acid chain length increases the

Table 2.2: Influence of double bond position, configuration and chain length on kinematic viscosity of fatty acids [16]

Chain length and double bond position	Kinematic viscosity (cSt)	
	Double bond configuration	
	cis	*trans*
14:1; Δ9	2.73	–
16:1; Δ9	3.67	–
18:1; Δ6	4.64	5.51
18:1; Δ9	4.51	5.86
18:1; Δ11	4.29	5.41
18:2; Δ9,12	3.65	5.33
20:1; Δ11	5.77	–
22:1; Δ13	7.33	–

viscosity of pure fatty acids. The configuration of double bond such as *cis* and *trans* also influences the viscosity of biodiesel. The *trans* and *cis* are geometric isomers of fatty acids, which differ by the orientation of the double bond. The presence of a

cis double bond induces a 30° bend in the fatty acid chain that obstructs the proper packing of fatty acid chains. The observed reduction in the intermolecular forces is due to the poor packing in fatty acid with *cis* double bonds, resulting in decreased viscosity. The viscosity of fatty acid chain having *trans* double bond configuration is found to be similar to that of saturated fatty acids [7]. The *trans* configuration of the double bond has a higher kinematic viscosity, irrespective of the fatty acid chain length and position of the double bond [16, 17]. It can be said that moving the position of the double bond towards the center of the chain has no effect on the viscosity of the methyl octadecenoate. Therefore, no added advantage in viscosity will be gained by the double bond isomerization of MUFA [16].

Howard et al. [17] studied the influence of polar groups (carboxyl and hydroxyl) on the viscosity of fatty acid derivatives and hydrocarbons. They observed that the polar groups tend to associate more with each other as a result of hydrogen bonding than their non-polar counterparts. Therefore, non-polar hydrocarbons have the lowest viscosities for a given chain length than those of polar hydrocarbons [17]. The high viscosity of fatty acid derivatives can, therefore, be attributed to their polar groups and the highest viscosity of glyceride are due to its molecular weight [17].

Allen et al. [18] tested methyl and ethyl esters at 40°C to observe the influence of the molecular weight and the degree of unsaturation on viscosity. They reported that the kinematic viscosity is proportional to the molecular weight of the saturated ester and has an inverse relation with a number of double bonds [12, 17, 18]. The viscosity is found to decrease by 21% with the addition of one double bond in C18:0. The ethyl esters have 5.4% higher viscosity than that of the methyl esters which is attributed to the difference in their alcohol moiety [18].

It can be inferred from the discussion that the physical properties of biodiesel are influenced by the compositional features of fatty acids. The difference in properties of pure components of biodiesel and diesel affect their combustion and emission characteristics. The lower energy density (calorific value) of biodiesel leads to reduced engine power and increased fuel consumption. The processes such as spray atomization, air-fuel mixing, combustion and formation of pollutants are influenced by density, normal boiling point, viscosity, bulk modulus, the presence of oxygen and surface tension.

2.3 Effect of Fuel Composition on Spray Characteristics

Engine tests with biofuels have shown engine performance comparable to that of diesel fuel [19–22]. However, there is a need to improve the atomization and air-fuel mixture formation processes when using biofuels of various origin [23–25]. The air-fuel mixture formation processes are strongly dependent on spray atomization and evaporation process. These processes are affected by physical properties of fuel depending on their origin. The most commonly studied spray parameters are spray tip penetration, cone angle and mean droplet diameter which are related to the physical properties of biodiesel. Further these properties are found to be a function of fatty acid ester composition [9, 26, 27]. The biodiesel is composed of various fatty acid esters with carbon chain length varying from 12 to 22 [1, 28, 29]. The physical and chemical properties of individual fatty acid esters govern the biodiesel spray characteristics. Allen et al. [18] measured Sauter Mean Diameter (SMD) of five different biodiesels under atmospheric conditions. The viscosity, surface tension and atomization characteristics of 15 commonly used biodiesels were predicted and the atomization characteristics were found to be similar. The similarity in atomization characteristics of commonly used biodiesel was attributed to the long-chain unsaturated fatty acid ester present in these biodiesels. The long-chain fatty acid ester such as methyl oleate may be responsible for the higher viscosity and hence larger SMD for the commonly used biodiesel [18]. The medium-chain length component such as methyl laurate may be responsible for the lower viscosity and hence smaller SMD for the coconut biodiesel which is comparable to that of the diesel. Ejim et al. [30], with statistical analysis, showed that the palm, soybean, cottonseed, peanut and canola biodiesel exhibits similar atomization characteristics with no significant difference in SMD of the spray. The comparison of non-evaporating spray characteristics of biodiesel, diesel, and their blends are carried out by various researchers [31–33]. Gao et al. [34] have observed similar spray tip penetration for the three biodiesel, jatropha, palm and waste cooking oil, which was attributed to their similar viscosity and density. Mancaruso et al. [31] reported similar spray characteristics for the biodiesel such as rapeseed and soybean. From the various studies,

the observed similar atomization characteristics for commonly used biodiesel may be attributed to the similar fatty acid ester composition of biodiesel. Jiaqiang et al. [35] numerically studied biodiesel combustion and emission characteristics in accordance with their fatty acid ester composition. The biodiesels selected for the study, rapeseed, sunflower, soybean and cottonseed biodiesel differ in their degree of saturation. The degree of saturation and kinematic viscosity was observed to have relation with ignition delay (chemical and physical) which consequently determines their combustion and emission characteristics. Balaji et al. [36] investigated spray characteristics of waste cooking oil biodiesel and its 20% blend with diesel fuel. The biodiesel blend spray characteristics were found to be similar to that of diesel fuel. However pure biodiesel showed poor air-fuel mixing which was attributed to the poor atomization. The experimental investigations for establishing the role of pure fatty acid esters on spray characteristics of biodiesel under non-evaporating and evaporating environment is required. The major concern with biodiesel use is the increased NO_x emission, hence it is discussed in more detail in the next section.

2.4 Factors Influencing NO_x Emission

The NO_x emission in a typical diesel engine exhaust is composed of oxides of nitrogen with the major component being NO and lesser amount of NO_2 [10, 37, 38]. The mechanisms of NO formation are: Extended Zeldovich (Thermal NO), Prompt NO (Fenimore) and Fuel NO mechanism [37, 38]. For non-premixed combustion of CI engine, Zeldovich, and Fenimore mechanisms are found to be responsible for NO formation [38]. High temperature (>1800 K) and mixture with equivalence ratio (<1) present at the periphery of diffusion flame are favorable conditions for thermal NO_x formation [39]. Additionally, a residence time of mixture at these conditions determine the amount of NO_x formed. Therefore, any parameter or property which influences combustion temperature, equivalence ratio or residence time of air-fuel mixture can be responsible for NO_x formation. Increase in NO_x emission with biodiesel as fuel is attributed to advance in injection timing, combustion phasing and flame temperature in most of the studies. The detailed analysis of these parameters is discussed below.

2.4.1 Advanced Injection Timing

The timing at which fuel is injected into the cylinder has a significant effect on combustion efficiency and engine NO_x emission [37, 40–43]. Old diesel engines, which used pump-line-nozzle (PLN) injection system, observed an advance in injection timing with biodiesel as compared to diesel fuel due to the higher bulk modulus of biodiesel. The advance in injection timing up to 1° CA has been reported for soyester biodiesel owing to its higher speed of sound and bulk modulus than that of diesel [43, 44]. The bulk modulus of biodiesel is proportional to density, which has a positive correlation with unsaturated fatty acid content in biodiesel [12, 14, 45]. Thus, biodiesel with higher unsaturated fatty acid content will result in an advanced injection. Many researchers have reported an increase in NO_x emission due to advanced fuel injection with biodiesel [13, 43, 45–47]. However, the increase in NO_x emission is observed to be higher than that can be expected from an advance in injection timing [44]. The CRDI system for biodiesel gives a negligible advance in injection timing but produce higher NO_x emission than that of diesel [13].

In summary, high bulk modulus and speed of sound for biodiesel lead to an advance in injection timing in PLN injection system. However, increase in NO_x cannot be completely attributed to advanced injection timing in biodiesel [42].

2.4.2 Flame Temperature

The NO_x formation in diesel is largely attributed to high combustion temperature. Ban-Weiss et al. [48] studied combustion of propane and propene, methyl butanoate and methyl *trans*-2-butenoate numerically. The adiabatic flame temperature of propene and methyl *trans*-2-butenoate is higher than that of their saturated counterparts. Consequently, following the hypothesis of high flame temperature, both propene and methyl *trans*-2-butenoate showed higher NO_x emission.

Graboski et al. [14] conducted the detailed experimental investigation to analyze the influence of fatty acid chain length and unsaturation on NO_x emissions. It is found that emissions of NO_x increased with increase in the proportion of unsaturated fatty acids in biodiesel derived from soybean, canola and soap-stock oils [14, 49, 50]. The unsaturation of fatty acids is also indicated by Iodine Value (IV). The NO_x

emissions are linearly related to IV of the biodiesel [11, 12]. Regression analysis study predicted that a biodiesel with an IV of 38 (corresponding to 1.5 double bonds/molecule) would be a NO_x neutral fuel relative to diesel [14]. Knothe et al. [51] reported that fuel having IV of 40 would be NO_x equivalent to diesel. Wyatt et al. [52] investigated NO_x emission of soymethyl ester and methyl esters of animal fat origin in 20% blend with petroleum diesel. They observed that methyl esters animal fats with lower unsaturation produced lower NO_x emissions. In summary, studies indicate that higher unsaturation of biodiesel results in higher NO_x emissions [11, 12, 14, 48–50, 52, 53].

Long chain saturated esters (C16:0 and C18:0) produce lower NO_x emissions compared to short chain saturated esters. However, saturated methyl laurate (C12:0) is an exception, which produces NO_x equal or less than that of diesel fuel [14]. Methyl esters of coconut oil and palm kernel oils, which has methyl laurate more than 50% by weight, may act as NO_x neutral fuel. The experimental investigation on pure coconut oil produced 12% lower NO_x than that of diesel fuel [54]. Kalam et al. [55] also observed the reduction in NO_x emissions for 50% blend of coconut oil with diesel. They attributed the observed decrease in NO_x emissions to lower combustion temperature based on temperature of exhaust gas. However, separately it is reported that the exhaust gas temperature for biodiesel may be low due to its lower heating value [56]. Experimental investigation with pure and 50% CME blend with diesel resulted in a consistent reduction of NO_x emission [57]. It was attributed to lower peak pressure value of premixed combustion due to their shorter ignition delay periods, which was further related to its saturated nature. Kinoshita et al. [58] compared NO_x emissions from CME, PME and RME biodiesel and found lowest NO_x emission for CME (8% less than that of diesel). This was due to its highest saturated fatty acid contents (90% in CME compared to 50% in PME, and 6% in RME) and lower combustion temperature of CME [58–60]. Similar results and attributions are reported for palm kernel methyl esters and coconut oil biodiesel [59, 61]. It has been suggested that exhaust gas emissions of FAME can be improved by mixing relatively short chain saturated FAME. The ignitability of mixture can be adjusted by varying the composition ratio of saturated and unsaturated FAME [56].

2.4.3 Combustion Phasing

The combustion process in CI engine comprises of an ignition delay, a period of uncontrolled combustion (premixed), and a diffusion controlled combustion. The lower ignition delay results in lesser premixed and higher diffusion controlled combustion period [40, 41, 62]. A significant amount of NO_x is formed during premixed combustion duration, hence in the modern CI engine amount of fuel burned in premixed phase is reduced [48]. The ignition delay is influenced by physical and chemical properties of the fuel such as viscosity, density, surface tension, liquid thermal conductivity, heat capacity, and thermal diffusivity [40, 46, 63]. The lower compressibility, high density, and high CN of the biodiesel are responsible for shorter ignition delay and advanced injection timing [40, 41, 43, 64, 65].

The researchers have investigated different mechanisms of NO_x formation through combustion phasing [10, 40, 43]. Sahoo and Das [65] observed that pure biodiesel and their blends with diesel have shorter ignition delay than that of diesel. Ignition delay is reduced with an increase in engine load for pure biodiesel of jatropha, karanja, and polanga and their blends with diesel. The maximum heat release rate of biodiesel is lower and occur earlier than that of diesel due to shorter ignition delay. Cheng et al. [66] observed 10% increase in NO_x emission of pure biodiesel for same premixed burn period and the start of combustion as that of diesel. These observations show that factors other than the start of combustion and premixed-burn fraction are responsible for the increase in NO_x emission of biodiesel. Mueller et al. [67] reported that combustion process of biodiesel is faster than that of diesel irrespective of ignition delay. It leads to higher in-cylinder temperature and longer residence time at high temperature. This may result in higher NO_x than that of petroleum diesel. The shorter ignition delay (4°) and early start of combustion (5°) could allow the fuel mixture and initial combustion products to have a longer residence time at elevated temperature, thereby increasing formation of thermal NO_x [10, 11, 37, 40, 43, 65]. The NO_x emission of SME remained higher than that of PME, even when the rate of heat release of SME is matched to that of PME by adding the cetane number improver. These studies indicate that cetane number is not the only factor which influences the NO_x emission in biodiesel [68].

Studies in the literature have observed that the lower ignition delay of biodiesel alone has minimal effect on NO_x emission. Biodiesel with the higher percentage of saturated components produces lower NO_x compared to that of high unsaturated components. The unsaturated fatty acids in biodiesel are responsible for higher adiabatic flame temperature and lead to higher NO_x emissions. It is observed that long chain saturated fatty acid produce lower NO_x with methyl laurate (C12:0) being an exception. Biodiesel from coconut oil and palm kernel oil contains a high percentage of lauric fatty acid and are reported to produce lower NO_x than that of diesel fuel. Shorter ignition delay and higher CN of biodiesel cannot be directly correlated to NO_x emission. Various theories of NO_x formation discussed are summarized in Table. 2.3.

2.5 Fuel Spray Characteristics

Several empirical and semi-empirical correlation are present in literature, Dent (1971), Wakuri (1960) and Hiroyasu and Arai (1990), to predict the spray characteristics such as spray tip penetration and cone angle. These correlations predict spray tip penetration as a function of orifice diameter, injection pressure, gas density and time after start of injection with difference in their weighing coefficients [69]. These coorelation are found to predict the spray characteristics with acceptable accuracy within their validation limit. Payri et al. [70] studied diesel spray characteristics with five injectors having orifice diameters (119, 140, 165, 183 and 206) μm. They observed that for given injection pressure and orifice diameter, spray tip penetration increases with decrease in ambient gas density. In the case of higher injection pressure and larger orifice diameter, spray tip penetration is observed to be longer than that of lower injection pressure and smaller orifice diameter. The density ratio of air and fuel injected is observed to be an important parameter for studying the spray characteristics as the interaction of fuel and air affects the spray formation process [71]. The injection parameters such as fuel injection timing (IT), start of injection (SOI), needle opening pressure (NOP) and rate of injection are characteristics of the fuel injection system used in engine. It determines the fuel quantity and velocity of the droplets which consequently affect the rate of spray

Table 2.3: Summary of literature on NO_x emission from biodiesel.

Advance in injection timing	References
Influence of advance in injection timing on NO_x emission	[37, 40–43]
Injection timing advance for soyester correlated to higher bulk modulus and speed of sound	[43, 44]
NO_x emissions attributed to advance in injection	[13, 43–47]
Bulk modulus and density of biodiesel correlated to degree of unsaturation	[12, 14, 45]
High flame temperature	**References**
High flame temperature correlated to degree of unsaturation of biodiesel	[48]
NO_x emission increases with unsaturation or IV of biodiesel	[11, 12, 14, 48–50, 52, 53]
Fuel with IV 38-40 act as a NO_x Neutral fuel (coconut and palm kernel oil)	[13, 14, 54]
Saturated esters (C16:0, C18:0, C12:0) produce NO_x emissions Lower than or equal to diesel	[14, 55, 58–61]
SOC and premixed combustion duration	**References**
Combustion phasing (shorter ID and earlier SOC) of biodiesel resulted in higher NO_x emission	[10, 11, 37, 40, 43, 65]
Difference in ignition delay leads to change in premixed and diffusion combustion period	[40, 41, 62]
Ignition delay correlated to physiochemical properties	[40, 46, 63]
Contradictions to combustion phasing theory	**References**
Higher NO_x emission observed for pure biodiesel for same premixed burned and SOC as that of diesel	[66]
SME found to emit higher NO_x than that of PME even when the rate of heat release of SME is matched with PME	[68]

penetration and affect combustion and emission performance of engine [47]. The reduction of nozzle orifice diameter and higher injection pressure exhibits improvement in the combustion characteristics. The higher injection pressure is desirable for reducing particulate matter emission. Diesel engine emissions are observed to be lower with use of smaller orifice diameter fuel injector. The smaller orifice diameter nozzle exhibits shorter penetration length with a similar air entrainment rate. The combined effect of nozzle orifice diameter and fuel injection pressure strongly affects the spray characteristics of the fuel [69].

The observed increase in the NO_x emission is explained by various researchers using spray and combustion studies [24, 72–74]. The increase in NO_x emission with biodiesel is related to atomization and evaporation characteristics of the spray. It also strongly depends on chemical compositional features and nature of pure constituents of the biodiesel [1, 75, 76]. Myo et al. [77] studied the effect of chemical composition by engine experiments with methyl oleate and its blends with methyl palmitate, methyl laurate, methyl stearate and methyl myristate. The NO_x emission is found to be lowest for the blend of methyl palmitate and methyl oleate respectively in the proportion of 40% and 60%. It is observed that the presence of a higher proportion of monounsaturated pure component, such as methyl oleate, produces lower NO_x emissions of the engine [75]. Wyatt et al. [52] reported lower NO_x emissions with animal-derived biodiesel blends than that of the plant-derived soybean biodiesel blends due to saturated nature of fatty acid esters constituents. The presence of the saturated pure components in biodiesel composition is observed to produce lower NO_x emissions [52, 73]. The composition of biofuels, biodiesel, and SVO, determines physical properties of fuel which governs spray atomization, evaporation and air-fuel mixture formation and also affects the emission formation [78–80]. The NO_x and soot emissions are effectively controlled using EGR and multiple injection technology which controls the air-fuel mixture formation [81]. In view of the utility of biofuels, it is important to understand atomization and air-fuel mixture formation of these fuels with advanced combustion control technologies.

Genzale et al. [82] measured soybean biodiesel evaporating spray characteristics at late-cycle post-injection engine conditions, low-density and high-temperature of ambient gas. The liquid length and rate of spray tip penetration of biodiesel were

high compared to diesel fuel [82]. The study pointed that multiple injection can be an effective way to limit the liquid length and hence avoid impingement on the combustion chamber walls. The SVOs are found to have higher liquid length and poor atomization even at high gas densities under non-evaporating conditions [78]. There is no data available on evaporating sprays of SVO. There are few studies available in the literature which reports biodiesel spray characteristics specifically vapor length and liquid length data at the engine-relevant conditions [82–85]. To utilize the SVO and biodiesel as the alternative fuel for diesel engines, the spray characteristics at engine-relevant conditions, such as high ambient temperature and pressure and late-cycle post-injection are required. Additionally, the physiochemical properties of biofuels would be an aggregate effect of properties of each individual pure components present in its composition. The study of the spray characteristics of pure components of biofuels may help to understand spray characteristics of biofuels from various origins. The advance combustion control strategies require detailed knowledge of evaporative spray characteristics of the fuel. Thus, there is a need to study evaporating spray characteristics of biofuels and their pure components which are used in CI engines. The comparative study for liquid length and the vapor length of the biodiesel pure components (both FAME and FAEE) and the pure components of SVO at the engine-relevant conditions is required.

2.6 Multi-Component Fuel Sprays

The objective of studying the multi-component fuel sprays is to predict the behavior of real multi-component fuel under engine relevant conditions. The fuel spray characteristics control the quality of air-fuel mixture formation and engine-out emissions of CI engine. The experimental and numerical investigations for the spray characteristics of diesel and biodiesel available in the literature discuss tip penetration and cone angle at various operating conditions [70, 86–89]. The constant volume combustion chamber spray experiments are performed with the high-speed imaging technique to study the liquid length and vapor length of both single component and multi-component fuel. However numerical spray study use the single component representative of a real multi-component fuel. Single component evaporation

models are available in most of the commercial CFD codes. The predicted liquid length and vapor length using single component evaporation model is found to be in agreement with measured spray characteristics of diesel and biodiesel fuel [85, 90].

The single component fuel cannot represent the vapor mass fraction distribution of real multicomponent fuel. The ignition delay of the fuel is determined by local equivalence ratio, temperature, and scalar dissipation rate [91]. These parameters are different in case of single component fuel and real multi-component fuel. The difference in ignition delay leads to different combustion phasing mechanisms and emission profile. Aggarawal [92] reported that the ignition behavior of the multi-component diesel sprays are extremely sensitive to the liquid mass fraction of the volatile component present in its composition. The ignitability of the mixture is observed to be improved with an increase in the percentage of a volatile liquid mass fraction. A significant improvement in ignitability of the multi-component fuel is observed when the volatile liquid mass fraction is within 10-20% and their NBP temperature is 50 K to 100 K lower than that of other components. Based on the difference in ignitability of multi-component and single component fuel, it can be inferred that the combustion characteristics of the multi-component fuel can be different than that of the single component surrogate fuel. Gopalakrishnan and Abraham [91] studied the ignition behavior of diesel sprays and reported that the predicted ignition delay of the single component heptane is around 20% less than that of the measured ignition delay of multi-component mixture. The single component surrogate fuel could not match the ignition delay of the real multi-component fuel due to the difference in air-fuel mixture and thus equivalence ratio and the temperature of the mixture. Ignition delay affects diffusion and premixed combustion phases and hence heat release rate in an engine. This consequently changes the type and quantity of pollutants formed. For example, the NO_x formation is found to be related to heat release rate and diffusion combustion burn rate of the biodiesel [93]. Ra and Reitz [94] pointed out the difference in the air-fuel mixture distribution of single component tetradecane and multi-component diesel fuel. The average molecular weight of the species at near nozzle and downstream of the combustion chamber was different when using multi-component evaporation model. The spatial variation of average molecular weight indicates that the ignition char-

acteristics of multi-component diesel fuel will be different and cannot be predicted with the single component surrogate fuel. Thus, there is a need to use the multi-component evaporation model to get more accurate prediction of overall processes such as air-fuel mixture formation, ignition, combustion and formation of pollutants.

2.7 Summary

The renewable alternative biofuels, such as biodiesel and Straight Vegetable Oils (SVOs) have various advantages, e.g., local availability and lower greenhouse gas emissions, over fossil fuels for Compression Ignition (CI) engines. Biodiesels obtained by transesterification of the SVOs have properties similar to that of diesel. The higher NO_x emission of biodiesel is a major hurdle for its use in diesel engines. Higher NO_x emission from biodiesel fuel is explained through various theories, such as higher adiabatic flame temperature due to fuel bound oxygen, advanced injection timing, and combustion phasing. The theories proposed are found to be closely related to physiochemical properties of biodiesel. The properties of biodiesel are further found to be the aggregate behavior of pure components present in their composition.

The fuel spray characteristics study is found to be important, as this characteristics govern the air-fuel mixture formation, ignition, combustion and nature of the pollutants formed. The investigations found that the common spray parameters of diesel and biodiesel such as spray tip penetration, cone angle and mean droplet diameter are further found to be related to the properties of the fuel.

However, the spray studies which relate the spray characteristics of biodiesel or straight vegetable oils to the fuel composition are limited in the available literature. Furthermore, multicomponent evaporation studies of biodiesel are important to understand ignition, combustion characteristics, and nature of pollutants formed. It is necessary to have information on contribution of pure component of fatty acid ester on physical properties of biodiesel and their influence on spray atomization and evaporation. The effect of composition of biodiesel on air-fuel mixture formation is important to understand combustion and emission formation.

2.8 Objectives of the Study

The objectives of the present study are as follows:

- To study the role of pure of components and their physiochemical properties on spray characteristics of biodiesel and SVO
- To investigate the role of fuel composition on spray characteristics such as spray tip penetration, liquid length, and vapor length.
- To study effect of fuel composition on distribution of vapor mass fraction of components of biodiesel

Following methods are employed in the study:

1. The experimental and numerical investigation on non-evaporating spray characteristics of pure components of biodiesel and diesel, including validation of models.
2. The numerical study of evaporating spray of diesel, biodiesel, and SVO with their single component surrogate.
3. Evaporating spray study of biodiesel and diesel spray with the multi-component surrogate

3 Methodology

A methodology to study the spray characteristics of biofuels is discussed in this chapter. It is divided into two sections consisting of experimental measurements and numerical models. The numerical methodology includes an introduction of OpenFOAM CFD code and its models. The modified evaporation and heat transfer models are explained. These models are validated with experimental data and results from literature. These models are used to analyze the spatial mass fraction distribution of evaporating multi-component surrogate fuel spray.

3.1 Experimental Methodology

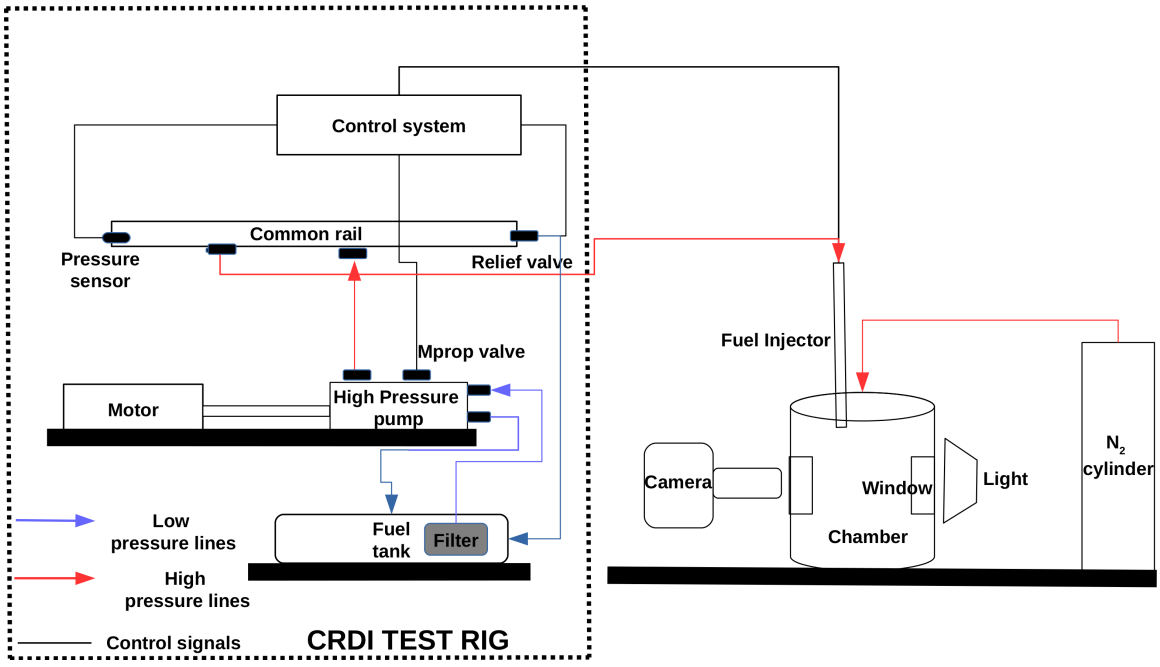

Figure 3.1: Schematic of high-pressure spray visualization facility.

The non-evaporating spray experiments are performed in a constant volume chamber with high-speed shadowgraphy technique. The experimental set-up includes a high-pressure constant volume chamber with an optical access, a high-pressure fuel injection CRDI test rig and a high-speed shadowgraphy arrangement. The schematic of the experimental set-up for high-pressure spray visualization shown in the Fig. 3.1. The technical specifications of the CRDI test rig components are given in the Table. 3.1. The high-pressure constant volume chamber has an internal diameter of 204 mm and height of 260 mm. An optical access is provided on the chamber walls with two quartz window placed diametrically opposite to each other. The quartz windows are rectangular in shape with a size of 70 $mm \times 50\ mm$. To capture the shadow of the spray in the chamber it is illuminated with a LED light. Additionally, a diffuser plate is placed in-front of the LED light to get a uniform back-light illumination. A high-pressure spray injection test rig is developed using a Common Rail Direct Injection (CRDI) system components as shown in Fig. 3.1. A high-pressure fuel is injected at a desired fuel injection pressure and known injection duration. A seven-hole solenoid injector with a nozzle diameter of 130 μm is used for the present study. Six holes of the injector were blocked with micro-welding to study the single spray from one nozzle hole. The fuel injection pressure can be varied in the range from 200 *bar* to 1500 *bar*. A National Instruments fuel injector driver module is utilized to control the start of injection and fuel injection duration of a solenoid fuel injector. The variation of fuel spray characteristics are shown with respect to time after start of injection. A fuel metering of the CRDI fuel pump is governed by an in-house developed Arduino based controller to maintain the desired injection

Table 3.1: Specification of the Experimenta Setup.

Sr.no.	Components	Specifications
1	CRDI fuel injection system	50 to 2200 bar ($\pm$ 15 bar)
2	Pressure transimitter	0 to 3300 bar ($\pm$ 0.25%)
3.	Image acquisition system	ROI 444 $\times$ 182 $pixels$, 30000 $frames/second$, exposure time 1.0 μs
4.	Spray image calibration	6 pixels/mm

pressure. The experiments are carried out at fuel injection pressure of 1000 and 1500 bar against ambient gas pressure of 30 and 40 bar. The maximum velocity of the injected fuel is around 300 to 400 m/s. The minimum possible exposure time is required to get the sharp images, which is just sufficient to freeze the motion of spray. In the present study, exposure time of 1 μs is used to capture the high speed spray. The high-speed camera is used for imaging the fuel spray evolution with a sensor region of interest (ROI) is 1000×1000 pixels which give around 7000 image acquisition rate. The optimum compromise between image acquisition rate and image resolution has been carried out. The image acquisition rate is increased to 30000 frames per second with reduction in ROI to 444 × 182 pixels and a resolution of 0.1 mm per pixel.

The optical spray chamber is filled with N_2 gas at an ambient temperature to ensure an inert environment for the spray. The raw images captured with the high-speed camera are processed with an in-house developed image processing algorithm to get the spray tip penetration. The variation in the spray tip penetration of 6 spray events is observed within 5.0% of mean spray tip penetration.The in-house developed image processing algorithm basic steps are outlined as follows:

1. Acquire the images in series with first image as reference background image.

2. Covert the images to binary images with appropriate threshold. The image matrix pixel value = 0, represent black colour and 1 represent white colour. The image has three parts, white spray, black background and interface which is the periphery of spray.

3. Locate the position of the injector, which act as the starting point for spray tip penetration.

4. Find the width of the spray and central axis of the spray via tracing the image matrix row by row to find the left and right edge of the spray. The edges of the spray can be marked, as it acts as the shift between pixel value from zero to one or one to zero. The axis of the spray will be located at half of the spray width calculated.

5. Find the minimum width of the spray in the matrix generated in above step, it acts as a spray tip. Measure the vertical distance between the user defined

injector tip location and to the spray tip location tracing along the axis of the spray. It gives the value of spray tip penetration.âĂİ

3.2 Numerical Methodology

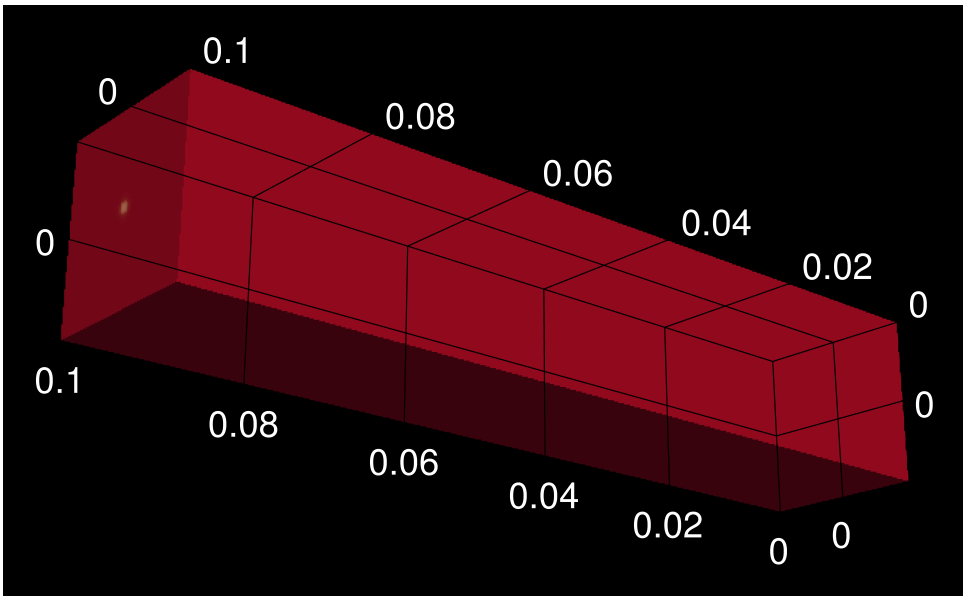

Figure 3.2: Constant volume chamber geometry for numerical study of sprays.

The high-pressure fuel spray is modeled using a "sprayFoam"solver of "OpenFOAM"CFD code. The computational geometry is a constant volume rectangular cuboid with dimensions of 20 mm X 20 mm base and 100 mm height as shown in Fig. 3.2. The mesh size is 1 mm along the height of the vessel, 0.5 mm along the width of the cuboid. The time-step of 2.5 μs is used for the simulations. The fuel injector with an orifice diameter of 130 μm is positioned at a distance of 0.5 mm below the top of the cuboid directed downwards along the central axis. The combustion and chemistry modules of the code are deactivated to study the spray under non-reacting condition.The Eulerian approach requires resolution of nozzle and the flow properties. The nozzle orifice used in the present study is around 130 μm and 90 μm. The cell size should be of equivalent to nozzle orifice diameter, in order to match the boundary conditions. This would result in huge number of cells, which demand huge computational resources. The Lagrangian approach is used to model the spray to avoid resolving the physical length scales of orifice size of injector. It is most popular and suitable approach for practical engineering spray simulations [95].

The pure components of FAMEs, FAEEs, and triglycerides are implemented in the "OpenFOAM"fuel library. The thermodynamic and physiochemical properties required for the implementation of the pure components are obtained from National Standard Reference Data System (NSRDS), Design Institute for Physical Properties (DIPPR) project 801 [96]. The temperature independent properties are normal boiling point, critical temperature, critical pressure and critical volume. Whereas, some of the temperature dependent properties are density, viscosity, surface tension and thermal conductivity.

The evaporating spray study discussed in the Chapter. 5 is conducted under non-reacting ambient conditions. The default liquid evaporation model for droplet evaporation is based on the classical D^2 law [37]. The D^2 law states that the square of evaporating droplet diameter varies linearly with time. It does not consider the effect of natural convection and force convection [97–99]. The equation is as follows:

$$D^2 = {D_0}^2 - K \times t \tag{3.1}$$

Where, D_0 is initial diameter of the droplet at time t=0, K is the evaporation constant includes fluid property such as density of fuel, ambient conditions such as density of ambient gas, Diffuisivity coefficient and Mass fraction of fuel at droplet surface and at infinity from the droplet, t is the time required to decrease the droplet size from D_0 to D and D is Diameter of the droplet after time t.

The parameters such as nozzle diameter and the total mass of fuel injected which are required for validation of the cases are set as given in the experimental sets. The input of transient mass flow rate profile of fuel injected is required in spray simulation. It can be determined experimentally [100] or calculated based on empirical correlations. A standardize rate of injection profile is required for modeling transient spray in CFD. The profile should be free from experimental artifacts present in different experimental data. The transient nature of flow rate profile during opening and closing of the nozzle can be represented with a standardize rate of injection profile. A model for the rate of injection provided by CMT-Motores Térmicos is used to generate the flow rate profile in present study [100]. The parameters required for generating flow rate profile are fuel injection pressure, ambient gas pressure, nozzle diameter, discharge coefficient, fuel injection duration and fuel density. To

maintain the consistency in mass flow rate profile calculation, the flow rate profile is calculated using the CMT-Motores model given by Payri et al. [100]. This model is widely used and well validated method for numerical spray simulation.

The liquid length of the spray is the maximum axial distance from the injector, where 95% of the liquid mass injected is found. The vapor length is defined as the maximum axial distance from the injector where the fuel mass fraction is more than 0.001. The spray vapor area is defined as the surface area bounded by the contour of the fuel mass fraction with a value of 0.001.

3.2.1 Mathematical Model

The numerical study is performed with an open-source CFD code, OpenFOAM. OpenFOAM is a C++ object-oriented library for solving the problems in continuum mechanics [101]. The simulations of spray involved ambient gas phase and the injected liquid fuel phase. The ambient gas phase of the spray simulations is solved using a Eulerian framework with continuous equations in space and time. The liquid phase representing liquid fuel is assumed as non-reacting spherical droplets that exchange mass, momentum, and energy with an ambient gas. The position and velocity of the droplet is calculated by solving a series of discrete differential equations in a Lagrangian framework.

The turbulence is modeled using a k-ϵ model, where k is the turbulence kinetic energy and ϵ is the rate of dissipation. The empirical model constants are tuned to predict the vapor penetration length within an acceptable range of the experimental data. The transport equations for k and ϵ and the model constants are used from research work of Weller et al. [101].

The atomization of the injected fuel is modeled with Kelvin Helmholtz Rayleigh Taylor (KH-RT) break-up model [102]. The WAVE breakup model is also known as the Kelvin-Helmholtz Rayleigh-Taylor (KH-RT) model. The KH-RT model has two modes of breakup. The KH breakup accounts for unstable waves growing on liquid jet due to a relative velocity between the gas and liquid [95]. The liquid jet is approximated by parent droplets of radius equal to nozzle orifice diameter [103]. The KH breakup can also be defined as the phenomenon of aerodynamic stripping of smaller droplets from larger droplets. The RT breakup accounts for waves growing

on the droplet surface due to acceleration normal to the droplet-gas interface. It can be said as the disintegration of larger droplets into smaller droplets due to effect of normal stresses. Analysis of a round liquid jet, yields a fastest growing wave with a wavelength (Λ_{KH}) and a growth rate (Ω_{KH}). The critical droplet radius r_c, which is the radius a parcel stripped off the liquid jet, is assumed to depend linearly on the wavelength Λ_{KH} and the stripping rate, or characteristic breakup time τ_{KH}. The breakup time constant controls the breakup rate and is assumed to be a simple function of the growth rate Ω_{KH} , wave length Λ_{KH}, and droplet radius, r:

$$r_c = B_0 \times \Lambda \tag{3.2}$$

$$\tau_{KH} = \frac{(3.726 \times B_1 \times r)}{(\Omega_{KH} \times \Lambda_{KH})} \tag{3.3}$$

$$\frac{dr}{dt} = -\frac{(r - r_c)}{\tau_{KH}} \tag{3.4}$$

The modeling constant B_1, characteristic breakup time, is found to vary from 1.73 to 60. With increase of value of B_1, the rate of reduction in droplet size lowers and hence spray tip penetration of liquid length may increase due to presence of larger droplets for larger time. It takes into consideration the effect of turbulence on breakup. Rayleigh Taylor breakup, on the other hand, is governed by disturbances growing on the surface of the droplet.The RT breakup equations are as follows:

$$r_c = C_{RT} \times \frac{\Lambda_{RT}}{2} \tag{3.5}$$

$$\tau_{RT} = \frac{C_{tau}}{\Omega_{RT}} \tag{3.6}$$

$$\frac{dr}{dt} = -\frac{(r - r_c)}{\tau_{RT}} \tag{3.7}$$

The C_{RT} controls the size of the new droplets generated after breakup. It takes into consideration the unknown effects of initial conditions such as turbulence and cavitation inside the nozzle on secondary breakup of droplets. The effect of C_{tau} and C_{RT} coefficients on RT breakup are proportional to each other. The C_{tau} is breakup time constant which gives similar effect as of B_1 in the KH mode. The C_{RT} coefficient determines the size of stable droplet after breakup. With increase

in C_{tau} and C_{RT} both leads to increase in spray tip penetration or liquid length due to presence of larger droplet size.

The primary drop size distribution is needed as an input to models that predict the effect of secondary atomization [104]. It is widely used in spray literature, because of its mathematical simplicity. The initial droplet size was set by sampling from a Rosin-Rammler distribution with parameters.The average initial drop size is varied with fuel.It is given as follows:

$$D = D_{inj} \times \Gamma(1 - 1/n) \tag{3.8}$$

Where, n is spread of distribution, D_{inj} is injected droplet diameter and D is average initial diameter.

Table 3.2: Tuned parameters of KH-RT model and Rosin Rammler distribution for n-heptane, methyl laurate and methyl oleate.

Tuned Parameters	Fuels		
	N-Heptane	Methyl Laurate	Methyl Oleate
KH-RT	B_0 = 0.61		
	B_1= 40; C_{tau}=1; C_{RT}=0.1	B_1= 60; C_{tau}=10;C_{RT}=1	
Rosin Rammler D[μm]	D_{min} = 1; n=4		
	D_{max} = 300;D = 160	D_{max} = 400;D = 270	D_{max} =600;D = 400

In the present study, the average initial diameter for heptane is D = 160 μm 270 μm for methyl laurate and 400 μm for methyl oleate with injector orifice diameter of 130 μm. The tuned parameter for nonevaporating spray is shown in the Tabel.3.2. During tuning the parameters, it is observed that predicted results are validated for n-heptane, when injected droplet diameter (D_{inj}) is equal to nozzle orifice diameter, for methyl laurate it is 1.7 times of nozzle diameter and for methyl oleate (D_{inj}) 2.5 times of nozzle diameter.

The "sprayFoam" solver is a transient solver for compressible, turbulent flow with spray parcels is used in the present work. The basic flow chart of the "spray-

Foam" solver with generic file names is shown in the Fig. 3.3. The detailed equation involved here are presented in the paper of OpenFOAM originator [101]. The header file "createTime.H" is used to input the information of all the parameters such as start time, end time and time step required for spray simulation. The mesh information is provided in "createMesh.H" header file. The algorithm and equations required for solving continuity, momentum, and energy equation are taken from "rhoEqn.H", "UEqn.H", and "EEqn.H"code files.

The results presented in chapter 4 and chapter 5 are produced with default codes of "OpenFOAM"with few modifications in the spray breakup constants. The atomization parameters such as Rosin Rammler distribution and turbulence model parameters are tuned for validation with experimental results. The details of the tuned parameters of the respective models are presented in the respective chapters.

3.2.2 Droplet Heating and Evaporation Model

The multi-component evaporating spray study which is presented in chapter 6 is carried out with the modified heat transfer and liquid evaporation model. The equations and algorithm in the code for droplet heating and evaporation are considered valid for the spray study. The droplet evaporation is a surface phenomenon and thus the droplet surface temperature is an essential parameter for determining the evaporation rate.

The droplet surface temperature in the original code is computed as the average of the droplet temperature and surrounding temperature with weighting parameter of (2/3) and (1/3). The equation for the droplet surface temperature is given as:

$$T_s = \frac{2.0 \times T_d + T_{gas}}{3.0} \tag{3.9}$$

Where, T_s is the droplet surface temperature, T_d is the droplet temperature and T_{gas} is an ambient gas temperature.

In the original code, the heat transfer coefficient between droplet surrounding and droplet interior is modeled with the Nusselt number Nu. The Nusselt number is

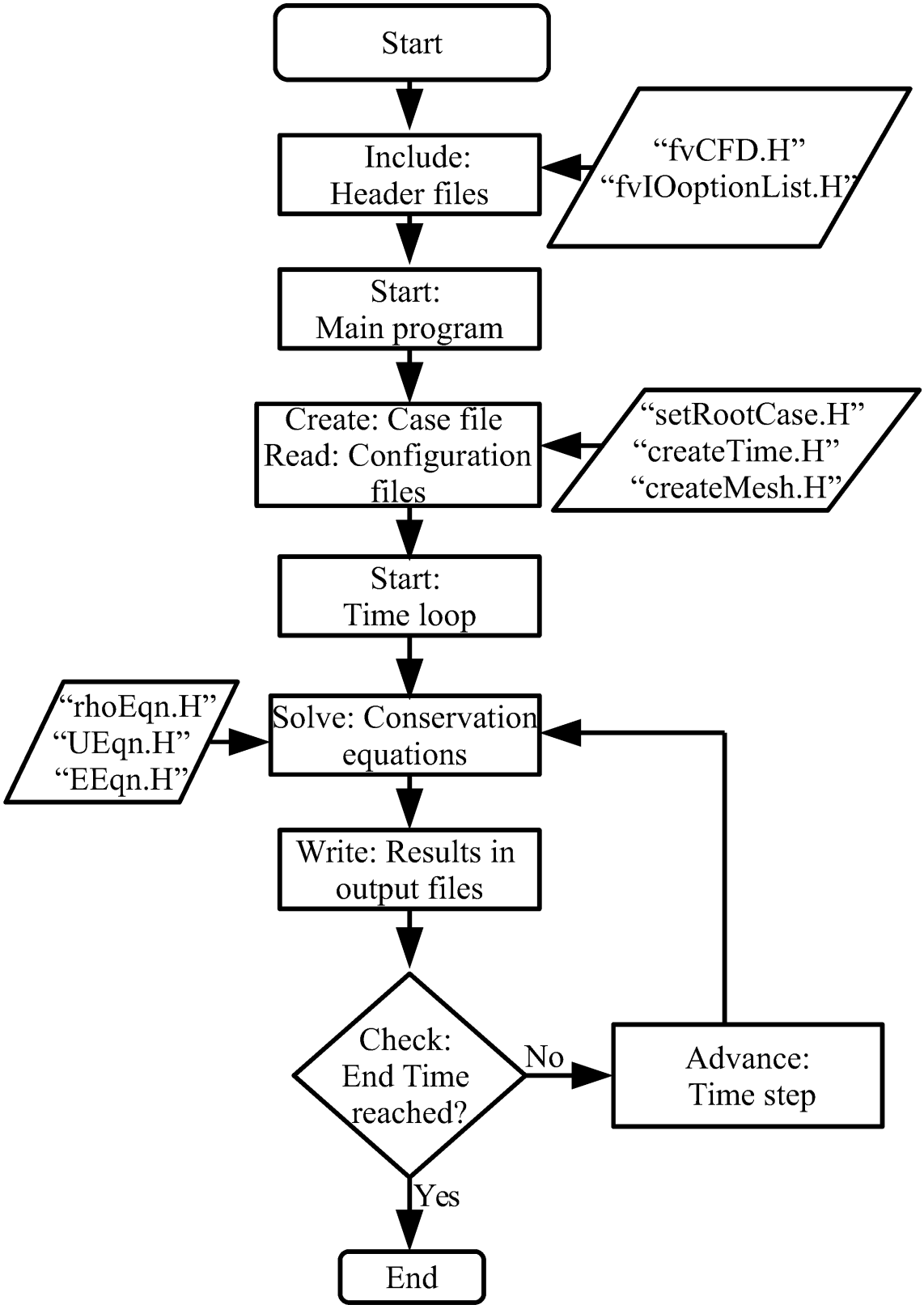

Figure 3.3: Flowchart of a OpenFOAM solver.

determined from Ranz Marshall correlation which is given by:

$$Nu = 2.0 + (0.6 \times Re^{1/2} \times Pr^{1/3}) \tag{3.10}$$

Where, Nu is the Nusselt number, Re is the Reynolds number and Pr is the Prandtl number The equation for calculating heat transfer coefficient between droplet surrounding and the droplet interior using Nu is given by:

$$HTC = \frac{Nu \times kappa}{d_p} \tag{3.11}$$

Where, HTC is heat transfer coefficient, $kappa$ is vapor or gas thermal conductivity and d_p is the diameter of droplet. In the default code, the heat transfer coefficient between droplet surface and droplet interior is neglected. The fuel properties at the droplet surface in original evaporation model are evaluated based on the surface temperature.

3.2.3 Modified Heat Transfer and Evaporation Model

The multi-component droplet heating and evaporation model used in this study is explained in this section. The droplet evaporation process consists of heating of injected droplet, assuming it has the lower temperature than that of compressed gas in the combustion chamber. The injected droplet absorbs heat from the compressed hot air. The droplet heating continues till the droplet attains the saturation temperature. Furthermore, the addition of heat is the latent heat of fuel required for evaporation of the droplet. The droplet vaporization takes place with fuel mass transfer from the surface of the droplet to the surrounding gas with the diffusion of vapor. The vapor diffusion is governed through concentration gradient of vapor. The steady state of vaporization is reached when the rate of mass transfer from droplet surface reaches to equilibrium with the rate of heat transfer from and to the droplet.

The droplet heating model used in the present study includes the effect of droplet internal circulation with the effective thermal diffusivity model [105]. The droplet surface temperature is evaluated with consideration of heat and mass transfer balance taking place at the interface of a droplet and surrounding ambient gas. The

mass transfer rates of the fuel components inside liquid droplet are assumed larger thus, droplet liquid phase is well mixed. However, the heat transfer rates are finite so the droplet temperature is not uniform and thus, a model is required to determine surface temperature.The surface temperature of the droplet is determined from a heat and mass transfer balance at the interface between the droplet and the surrounding gas. The surface temperature evaluation is iterative in nature as both heat transfer and mass transfer flux at the interface of the droplet has to be balanced. The droplet surface temperature based on heat and mass transfer balance is given by Eq. 3.12 [94]:

$$T_s = \frac{((h_i \times T_d) + (h_o \times T_{gas})) - (\ddot{m} \times h_{fg})}{h_i + h_o} \tag{3.12}$$

Where $\ddot{m}$ is evaporated mass flux, h_o is the heat transfer coefficient between ambient gas and the droplet surface, and h_i is the heat transfer coefficient between droplet interior and droplet surface. The equation for h_o is given as [94] :

$$h_o = \frac{\eta \times C_p \times \ddot{m}}{\exp(\frac{2.0 \times R_d \times C_p \times \ddot{m}}{K \times Nu} - \frac{Ca \times (Y_{fsur} - Y_{fs})}{K} \times \frac{Sh}{Nu}) - 1} \tag{3.13}$$

The h_i is evaluated based on the effective thermal diffusivity model given by Sirignano and Williams [106]

$$h_i = \frac{K}{\sqrt{\pi \times \alpha_{eff} \times t}} \tag{3.14}$$

where t is characteristic turbulence scale time. The effective thermal diffusivity α_{eff} is calculated as follows:

$$\alpha_{eff} = \alpha_{liq} \times (1.86 + (0.86 \times tanh(2.225 \times \log_{10}(Pe_l/30.0))) \tag{3.15}$$

Where α_{liq} is the liquid fuel thermal diffusivity, Pe_l is the droplet Peclet number, R_d is the droplet radius, Sh is the Sherwood number, Nu is the Nusselt number, C_p is the mean specific heat of gas mixture and fuel vapor, η is the correlation factor defined by Ra and Reitz [107], C_a is the inter-diffusion coefficient of fuel and air, Y_{fs} and Y_{fsur} are the mass fractions of fuel at the surface and surrounding, respectively.

The surface properties are evaluated as the function of the reference temperature.

The reference temperature given by Eq. 3.16 is chosen for calculating the droplet surface properties in the modified code. The reference temperature evaluated as the average of surface temperature and ambient gas temperature will be more accurate as it includes the effect of surface temperature and ambient gas temperature.

$$T_{ref} = \frac{2.0 \times T_s + T_{gas}}{3.0} \tag{3.16}$$

The properties such as vapor pressure, latent heat of vaporization are evaluated as the function of droplet surface temperature and ambient pressure instead of droplet temperature. The evaluation of the properties at the correct temperature is essential as it affects the overall evaporation characteristics of the fuel spray.

The simulations in the present study are carried out at non-reacting ambient atmosphere maintained with inert N_2 gas. The ambient gas pressure and temperature, chosen for the simulation, is in accordance with the operating conditions of the typical latest generation diesel engines [108]. The injection parameters for validation of cases are set as given in the respective experiments. For comparison of various biodiesel and their representative pure component, the injection parameters are set as follows: nozzle diameter = 90 μm, injection pressure = 150 MPa and the injection duration = 6 ms. The injector is positioned at the distance of 0.5 mm along the axis of the chamber directing downwards below the top surface. The corresponding total injected mass and mass flow rate of injection are used in the simulation. The liquid length of the spray is defined as the maximum axial distance from the injector position where 95% of the total liquid mass injected is found. The vapor length is defined as the maximum axial distance from the tip of the injector where the fuel mass fraction is equal to 0.001.

3.3 Summary

The experimental study on non-evaporating spray characteristics are performed with high-pressure constant volume optical chamber. The high-speed shadowgraphy technique is used to study the spray characteristics of biodiesel, diesel and their pure components. The CRDI set-up and the required control system to perform the experiment is developed. The image-processing code is developed to determine the

spray tip penetration from the raw images obtained from the experiment. The numerical spray study is carried out with "OpenFOAM"CFD code. The thermophysical properties and temperature dependent properties of various fuels are obtained from DIPPR database and implemented in the fuel library. The standardized flow rate profile is generated with respective model constants from the available experimental data used for validation of the numerical models. The droplet heat transfer model is modified to incorporate droplet surface temperature calculation in evaporation.

4 Non-Evaporating Spray Characteristics

The non-evaporating spray characteristics of biodiesel spray characteristics is presented in this chapter. The numerical models used to simulate the spray characteristics of different fuels are calibrated using the experimental results. These calibrated models are then validated under different operating conditions. The models are further used to study spray tip penetration of various biodiesel with the single and multi-component representative.

The present investigation is an attempt to show that the observed spray tip penetration of biodiesel may be due to their pure fatty acid ester composition. Furthermore, the spray tip penetration prediction of single component and multi-component representative is compared with biodiesel, diesel and their blend. The comparative experimental and numerical study is carried out to establish the significance of the single component over the multi-component representative of the biodiesel, diesel and their blends for predicting the spray tip penetration. The single component representatives of biodiesel are methyl oleate, and methyl laurate and for the diesel are *n*-heptane, *n*-dodecane and *n*-tetradecane. Methyl oleate is a commonly used pure component surrogate for biodiesel, with exception of coconut and palm kernel biodiesel where methyl laurate is used.

4.1 Results and Discussion

The spray experiments are performed for pure components, such as n-heptane, methyl oleate and methyl laurate. These fuels are selected such that the n-heptane represents diesel, methyl oleate represents biodiesels such as karanja, rapeseed and

soybean, and methyl laurate represents coconut biodiesel and palm kernel biodiesel. The pure components used in the study are purchased from TCI chemicals with laboratory grade purity. The important physical properties of fuels are compared in the Table 4.1.

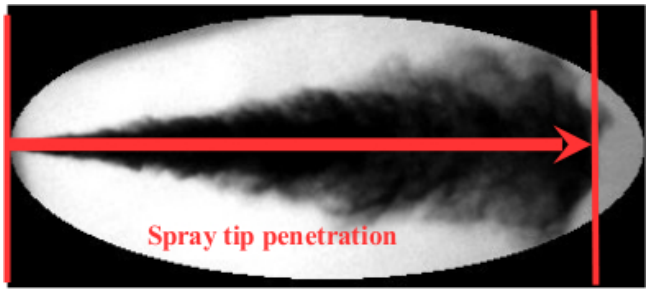

Figure 4.1: Definition of the spray tip penetration.

Table 4.1: Fuel properties of biodiesel, diesel and their pure components [12, 96].

Fuels	Fuel properties		
	Density at $288K$ $[kg/m^3]$	Kinematic viscosity at 313 K $[mm^2/s]$	Surface tension at 313 K $[mN/m]$
Methyl oleate	877	4.57	30
Methyl laurate	872	2.43	28
n-heptane	690	0.5	18
n-dodecane	795	1.9	28
n-tetradecane	771	3.0	27
Diesel	825	2.6	23
Coconut biodiesel	876	3.14	22
Karanja biodiesel	883	5.04	29

The density, viscosity and surface tension of karanja biodiesel is similar to that of methyl oleate while properties of coconut biodiesel are similar to methyl laurate. The n-heptane, n-dodecane, and n-tetradecane are also studied as these are extensively used as representative of diesel in experiments and simulations. The spray tip penetration, the farthest distance of the spray tip from the nozzle, is shown in the Fig. 4.1. The spray tip penetration of pure components is measured at fuel injection pressures of P_{inj} = 1000 and 1500 *bar* and at an ambient gas pressure of P_{amb} = 30 (ρ = 35 kg/m^3)and 40 *bar* (ρ = 46 kg/m^3).

The high-speed shadowgraphy images of pure component fatty acid methyl ester and n-heptane acquired at different injection pressures and ambient gas pressures

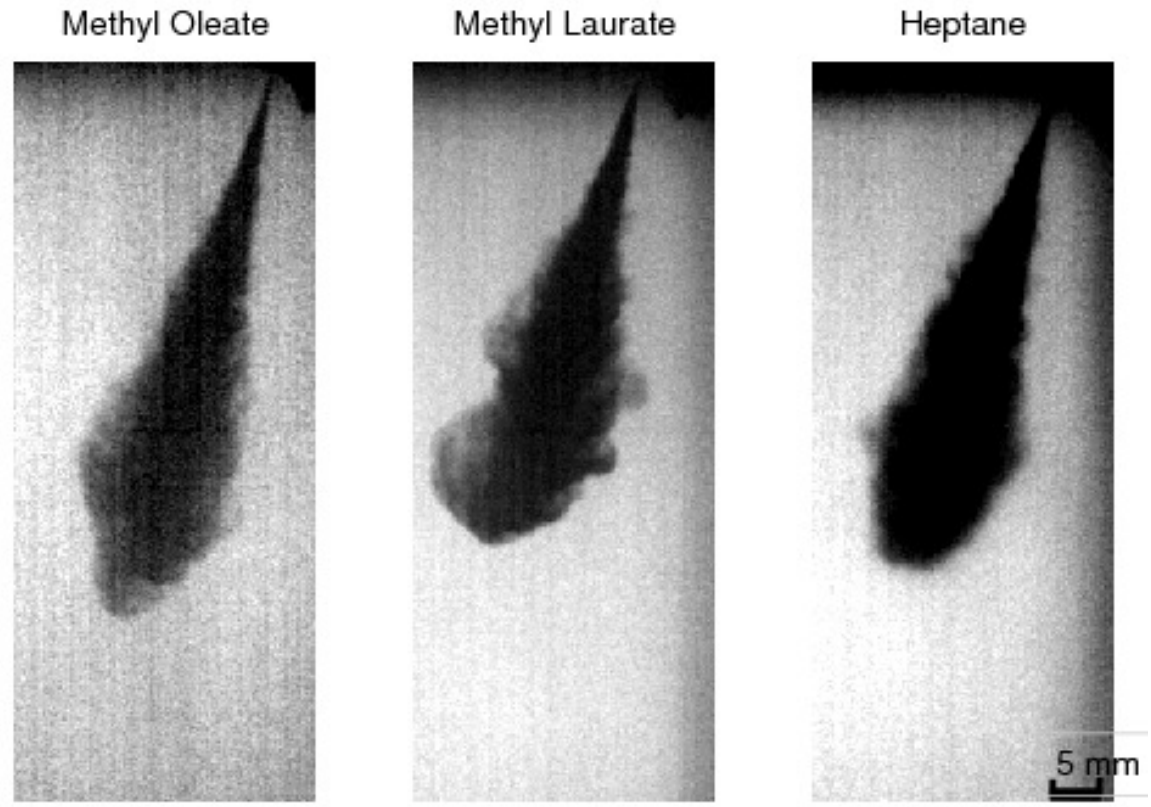

Figure 4.2: Spray structure of different fuels at an injection pressure of 1500 *bar* and a gas pressure of 40 *bar* ($\rho = 46$ kg/m^3) at around 400 μs after the start of injection.

are compared in Fig. 4.2. The instantaneous images of these sprays at around 400 μs after the start of injection are compared. The spray structure of the methyl oleate is observed to be compact and penetrating longer compared to that of the n-heptane and methyl laurate. The spray structure for methyl laurate and n-heptane is similar including cone angle and spray tip penetration. The spray structure indicates more dispersion in sprays of methyl laurate and n-heptane compared to methyl oleate.

4.1.1 Spray Tip Penetration

It is difficult to have one common single component representative for all the biodiesels since the composition of biodiesel differ depending on their origin [109, 110]. Hence, it is important to know whether the selected single component representative has similar spray characteristics as that of the biodiesel. The spray characteristics of individual pure component help to understand their effect in the multi-component fuel such as biodiesel spray behavior and also to identify the dominant component.

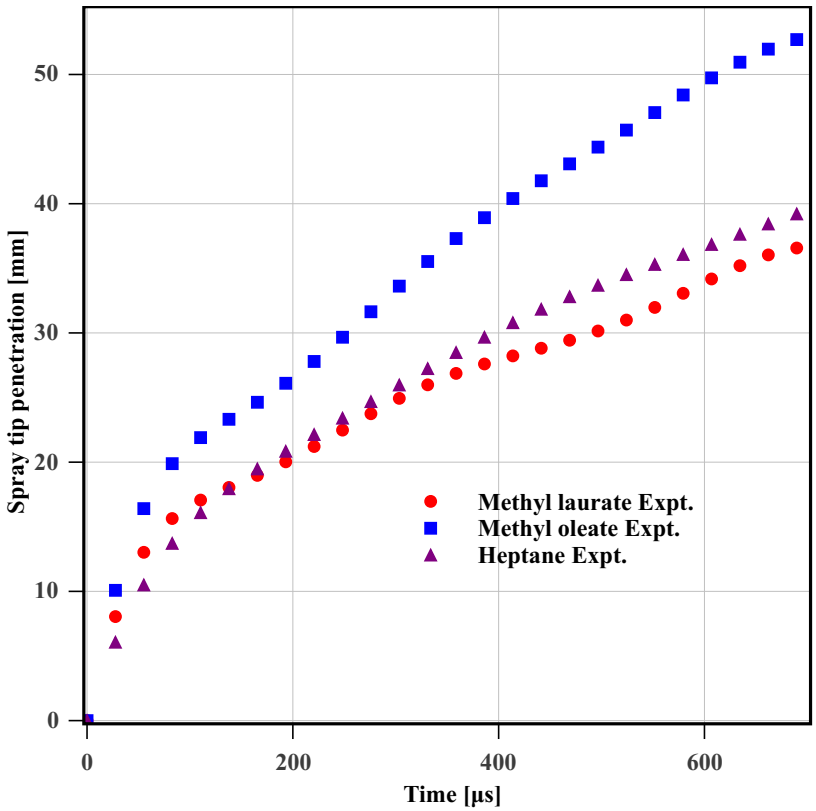

(a) P_{inj}=1500 *bar* and P_{amb}=30 *bar* (ρ = 35 kg/m^3).

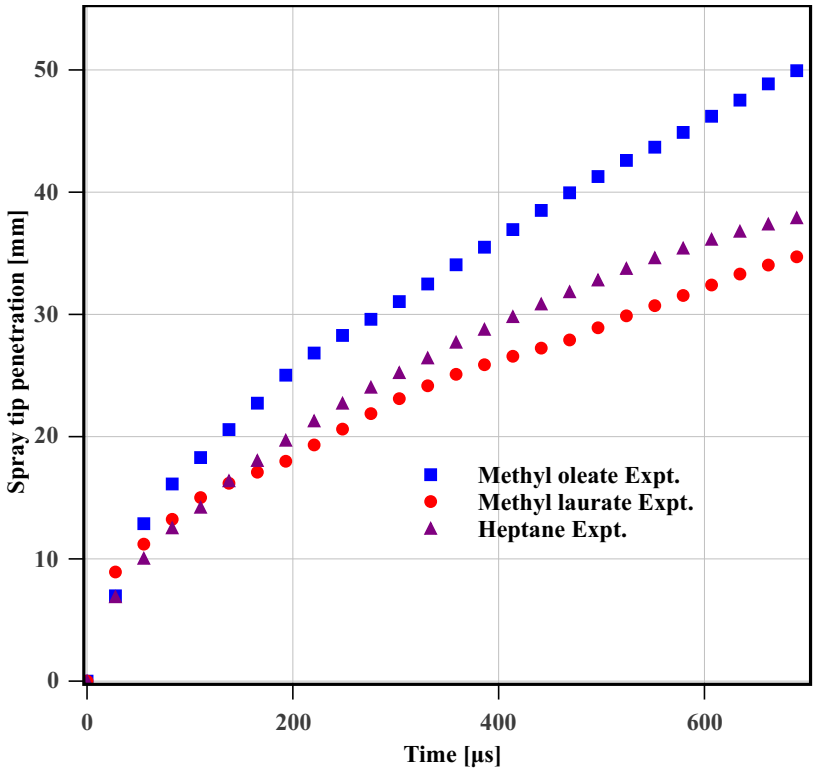

(b) P_{inj}=1500 *bar* and P_{amb}=40 *bar* (ρ = 46 kg/m^3).

Figure 4.3: Measured spray tip penetration of methyl laurate, methyl oleate and *n*-heptane.

In the present study, methyl oleate is selected to represent soybean, karanja and rapeseed biodiesel, and methyl laurate for coconut and palm kernel biodiesel [12, 82]. The biodiesel has a range of the fatty acid esters, from lauric to erucic with a number of carbon atoms ranging from 12 to 22, present in different proportion. The effect of fatty acid chain length of pure components methyl laurate and methyl oleate on their spray tip penetration is compared in the Fig. 4.3. The fuel injection pressure is $P_{inj} = 1500\ bar$ and ambient gas pressures are $P_{amb} = 30$ and $40\ bar$ ($\rho = 35$ and $46\ \mathrm{kg/m^3}$). The spray tip penetration of methyl oleate is longer than that of methyl laurate and *n*-heptane at both the ambient gas pressures. The spray tip penetration of *n*-heptane and methyl laurate is observed to be similar at both the gas pressures studied. This observation gives an indication that the atomization behavior of methyl laurate and *n*-heptane is identical. Moreover, there is a small increase in spray tip penetration of *n*-heptane and methyl laurate with a decrease in ambient gas pressure from 40 *bar* ($\rho = 46\ \mathrm{kg/m^3}$) to 30 *bar* ($\rho = 35\ \mathrm{kg/m^3}$). The spray tip penetration for methyl oleate increases by more than 20% with decrease in ambient gas pressure from 40 *bar* ($\rho = 46\ \mathrm{kg/m^3}$) to 30 *bar* ($\rho = 35\ \mathrm{kg/m^3}$). This may be due to the poor atomization of methyl oleate which may lead to larger droplets at lower gas pressures leading to the longer spray tip penetration.

The spray tip penetration in the Fig. 4.3 also demonstrates the effect of fatty acid chain length. The methyl laurate has 12 carbon atoms and methyl oleate has 18 carbon atoms in their molecule. The long fatty acid chain length, methyl oleate, shows the longer spray tip penetration than that of the methyl laurate irrespective of the operating conditions. The physical properties of methyl oleate such as kinematic viscosity, surface tension, and density exhibit higher value than that of methyl laurate. The kinematic viscosity of methyl oleate is 4.57 mm^2/s, which is around 88% higher than that of methyl laurate. Similarly, the surface tension of methyl oleate is 6% higher than that of methyl laurate. The spray tip penetration of methyl oleate is observed to be 15% to 30% longer than that of the methyl laurate. These physical properties specifically, kinematic viscosity and surface tension govern the mean droplet diameter of the spray through atomization [18]. The higher viscosity and surface tension of methyl oleate tend to produce spray with bigger droplets and hence higher momentum. The spray with higher momentum droplets

is able to penetrate longer, as seen for the case of methyl oleate at the same instant of time after the start of injection. The density of the fuel also affects the mass flow rate profile and the injected mass per unit time. Hence, the fuel with higher density inject more mass per unit time, which is valid for methyl oleate having the higher density than that of methyl laurate.

Furthermore, Allen et al. [18] observed that the physical properties of the pure components such as viscosity and surface tension are higher for long-chain fatty acid ester than that of a medium-chain fatty acid ester. The physical properties compared in Table 4.1 shows higher viscosity and surface tension for methyl oleate than that of methyl laurate. The higher viscosity of fuel shows poor atomization characteristics, larger droplet size and hence, longer spray tip penetration [18]. It can be concluded from the observed results that the measured spray tip penetration of the biodiesel pure component is in accordance with the difference in their molecular characteristics and physical properties.

4.2 Numerical Modeling of Non-Evaporating Spray

The spray models of an "OpenFOAM" CFD code are used to predict the spray characteristics of biodiesel pure components. The model parameters are tuned for the experimental conditions with fuel injection pressure $P_{inj} = 1000\ bar$ and an ambient gas pressure $P_{amb} = 30\ bar$ ($\rho = 35\ kg/m^3$) with fuel injector orifice diameter 130 μm is shown in the Table. 3.2. The KH-RT secondary breakup model and Rosin Rammler distribution parameters are tuned for n-heptane which represent diesel and methyl oleate and methyl laurate which represent biodiesel [95, 102]. One set of KH-RT model parameters is found to be valid for both methyl oleate and methyl laurate. For n-heptane another set of model parameters is used due to the difference in their breakup characteristics. The Rosin Rammler distribution parameters used for the study are different for n-heptane, methyl oleate, and methyl laurate as they represent three different categories of the fuels.

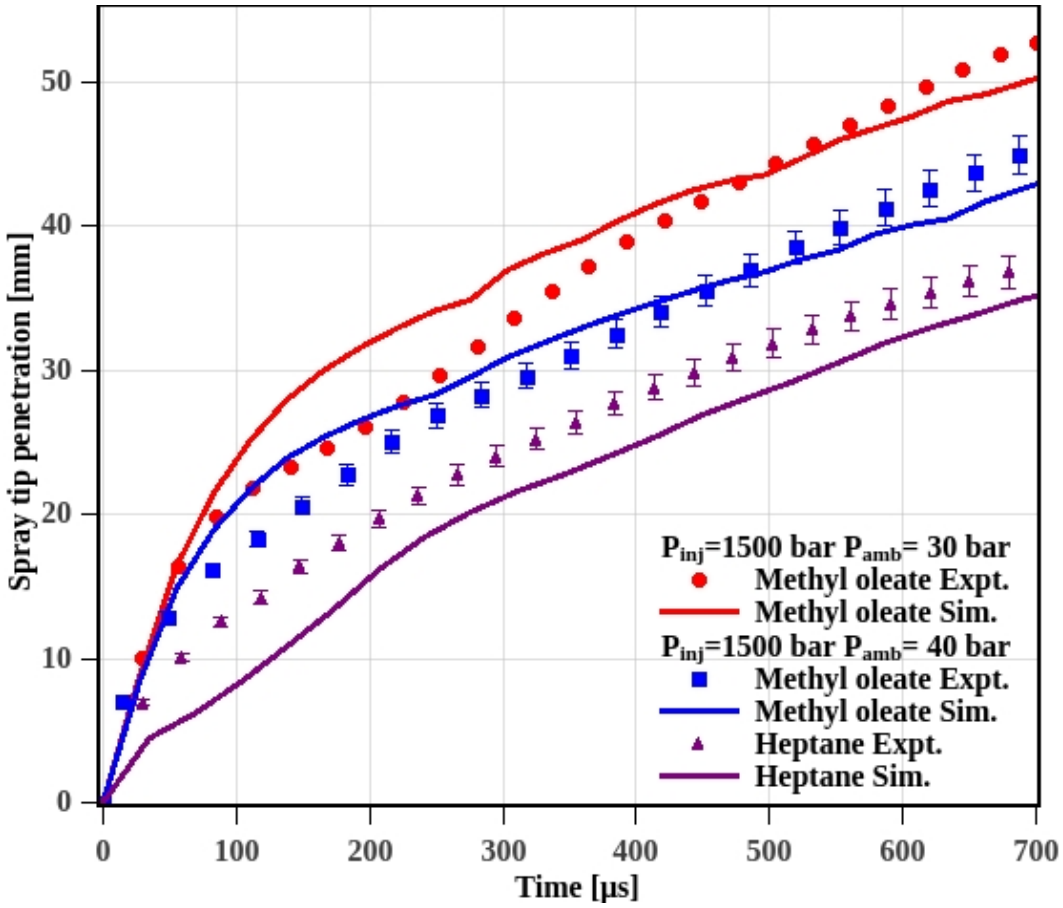

Figure 4.4: Comparison of measured and predicted spray tip penetration of methyl oleate and *n*-heptane at an injection pressure of 1500 *bar*.

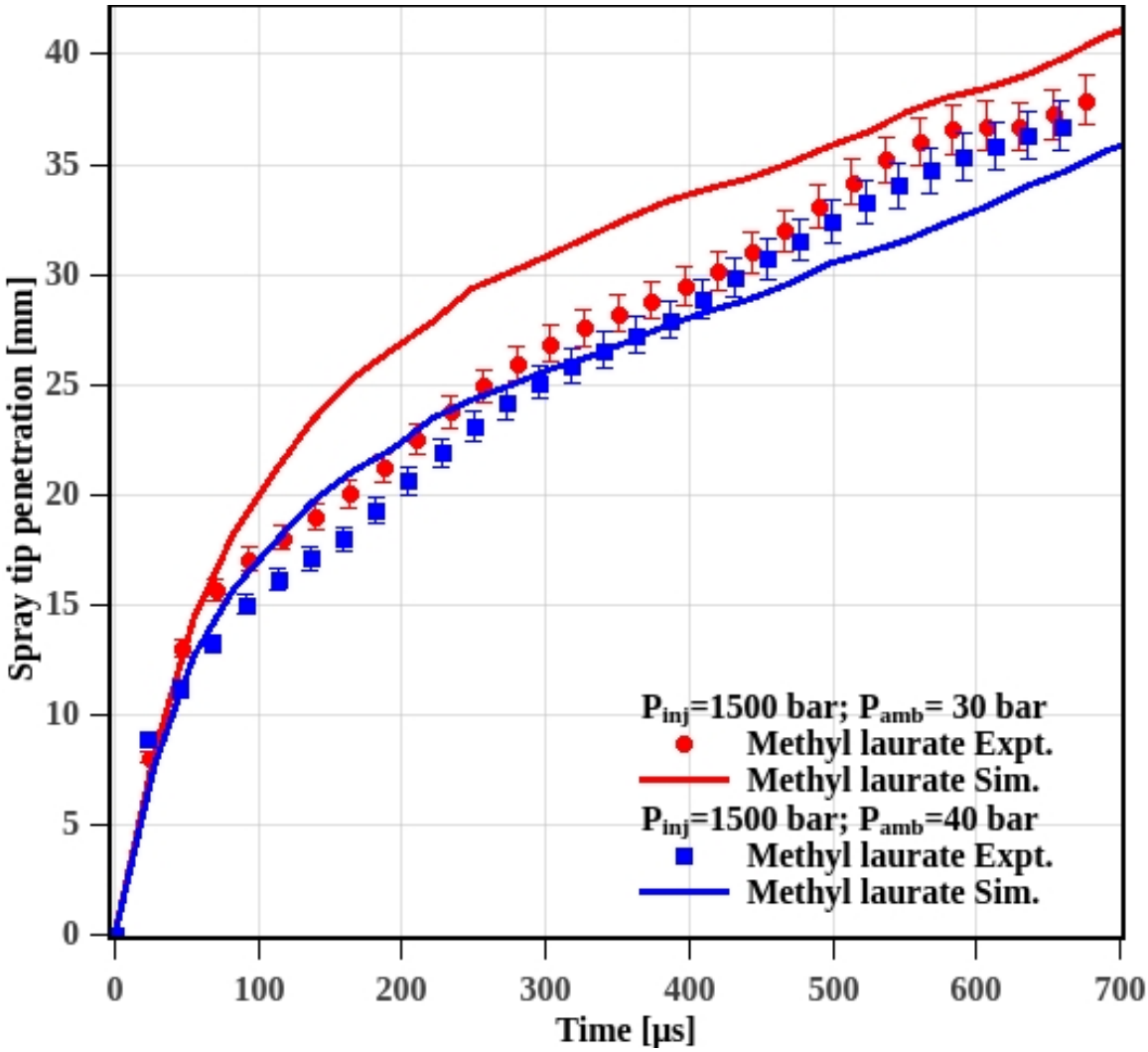

Figure 4.5: Comparison of measured and predicted spray tip penetration of methyl laurate.

The validation of the "OpenFOAM" spray models for biodiesel single component representative of biodiesel and diesel is presented in this section. The validation results for methyl oleate representative of biodiesel and n-heptane representative of diesel are shown in Fig. 4.4 at an injection pressure of 1500 *bar* and gas pressures of 40 *bar* ($\rho = 46$ kg/m^3) and 30 *bar* ($\rho = 35$ kg/m^3). The predicted spray tip penetration of methyl oleate closely follows the measured spray tip penetration at both the gas pressure conditions. The observed difference in the spray tip penetration during an initial part of spray injection is due to the initial transient nature of the spray and assumed fuel mass injection rate for simulation study [111–113]. The predicted spray tip penetration for the n-heptane is also in a close match with the experimental results. Similarly, the predicted spray tip penetration of methyl laurate is found to be in agreement with the measured results at both the ambient gas pressures of 30 *bar* ($\rho = 35$ kg/m^3) and 40 *bar* ($\rho = 46$ kg/m^3) (Fig. 4.5). It is concluded from the observed results that the tuned spray models are able to predict the spray tip penetration of biodiesel and diesel pure components at different operating conditions within measurement error. These tuned spray models are further used to predict the spray characteristics of biodiesel and its blend with diesel.

4.2.1 Spray Tip Penetration of Biodiesel

The biodiesel, depending on their origin has 8 to 10 different fatty acid esters [109]. The CFD simulation is performed with one representative component, whose physiochemical properties are similar to that of the biodiesel. In the literature, methyl oleate has been commonly used as the representative fuel for various biodiesel irrespective of the composition of the biodiesel [82]. From the composition of various biodiesel, it is observed that karanja biodiesel has a high percentage of methyl oleate, and coconut and palm kernel biodiesel have a high proportion of methyl laurate [1]. The spray tip penetration of karanja and coconut is predicted with their single-component and multi-component representative fuel.

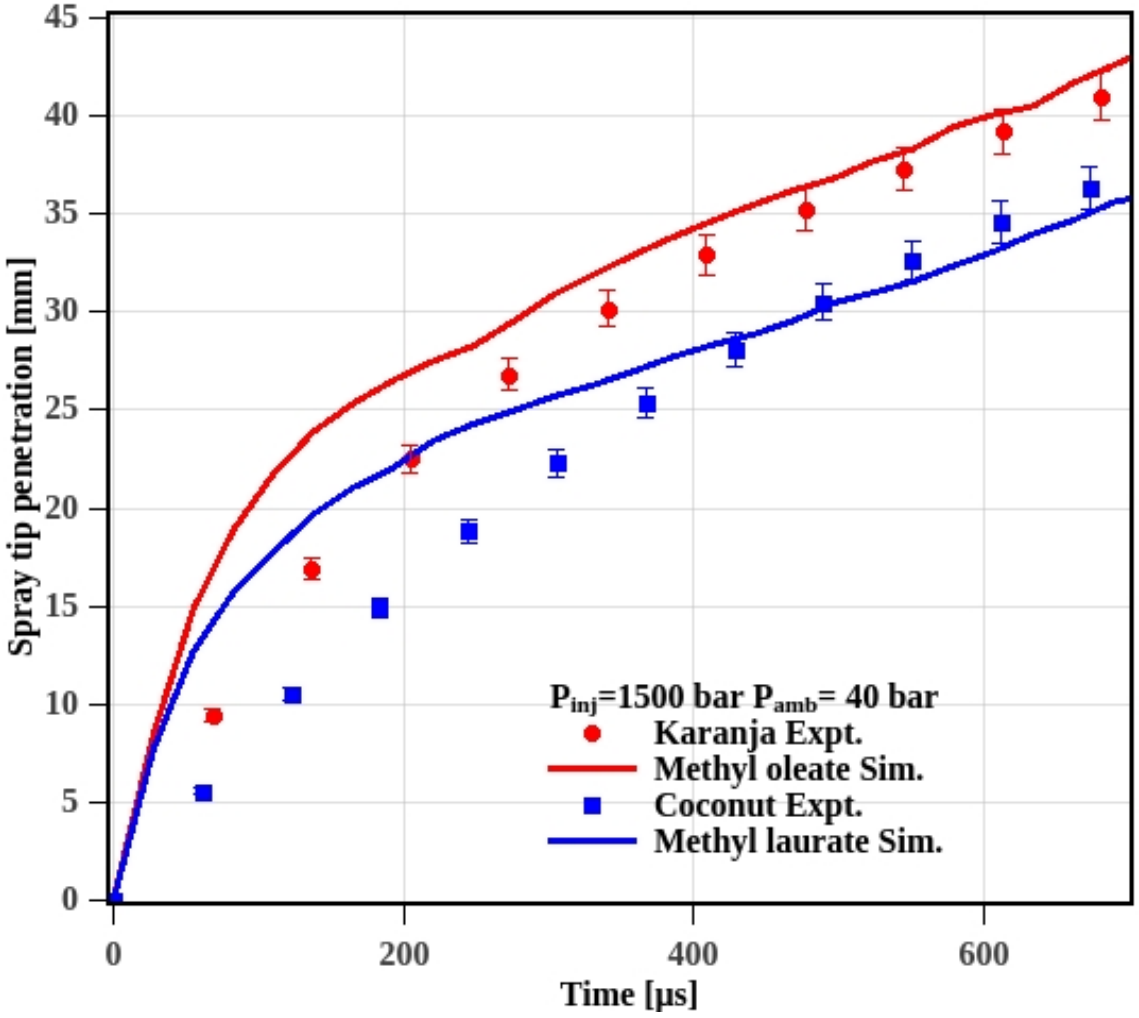

Figure 4.6: Experimental and predicted results for biodiesel at an injection pressure of 1500 *bar* and an ambient gas pressure of 40 *bar* ($\rho = 46$ kg/m^3) .

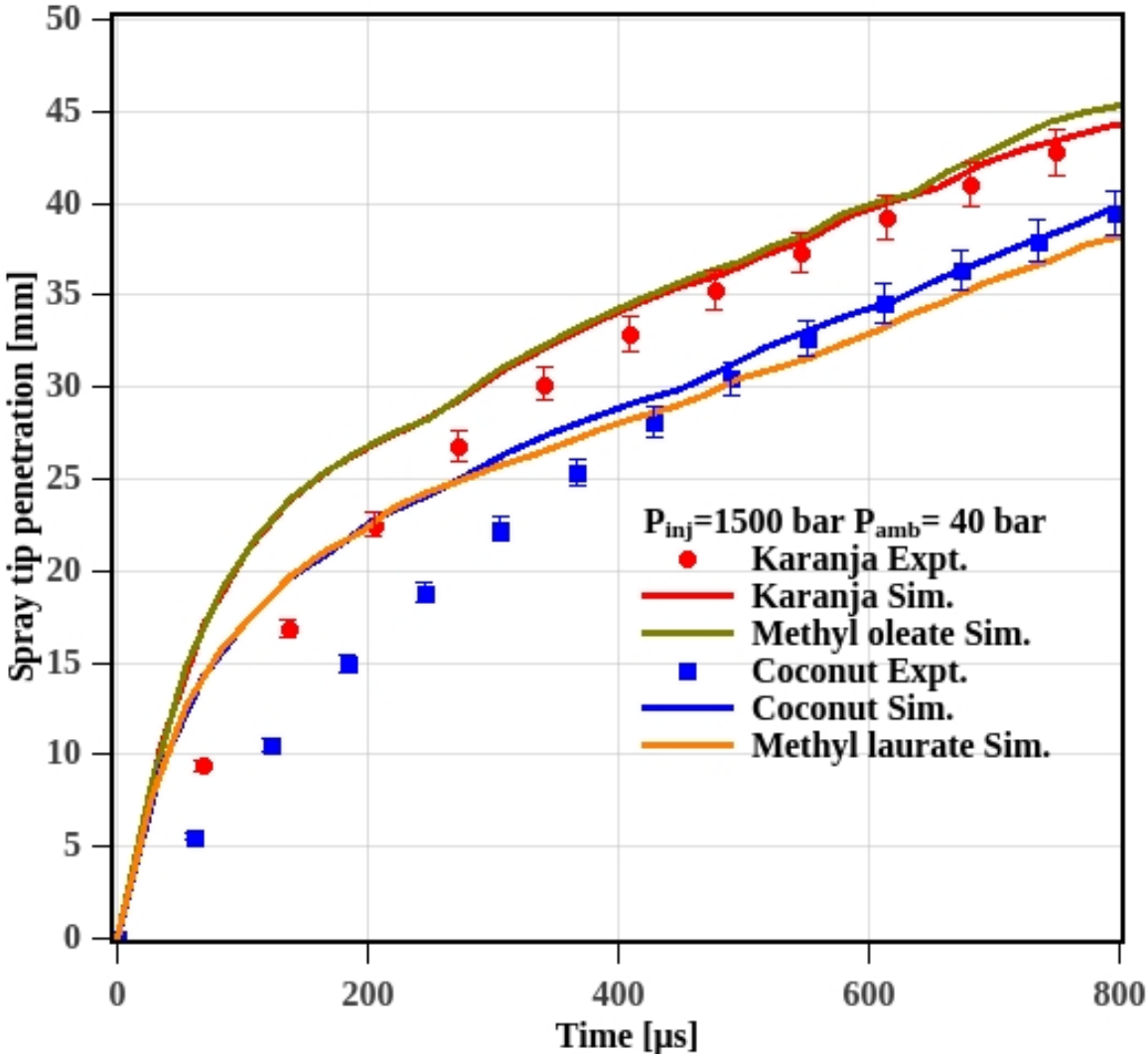

Figure 4.7: Experimental and predicted spray tip penetration of karanja and coconut biodiesel at an injection pressure of 1500 *bar* and an ambient gas pressure of 40 *bar* ($\rho = 46$ kg/m^3).

The predicted results are shown in Fig. 4.6 for, fuel injection condition of P_{inj} = 1500 *bar*, P_{amb} = 40 *bar* (ρ = 46 kg/m^3). It is observed that the predicted spray tip penetration of methyl oleate is similar to the spray tip penetration of karanja biodiesel. Similarly, the predicted spray tip penetration of the methyl laurate has a close match with the measured spray tip penetration of the coconut biodiesel. Thus, it can be said that the spray tip penetration of commonly used biodiesels soybean, rapeseed and karanja which have a high percentage of methyl oleate can be represented by methyl oleate. Similarly, a non-evaporating spray of palm kernel and coconut biodiesel can be represented by methyl laurate.

The Fig. 4.7 shows the comparison of the measured spray tip penetration of biodiesel with predicted spray tip penetration using single component and multi-component surrogate. The karanja biodiesel is modeled with five FAME components in the proportion of methyl palmitate 5.94%, methyl stearate 5.44%, methyl oleate 61.34%, methyl linoleate 23.14%, methyl linolenate 4.14%. The coconut biodiesel is modeled with five FAME components in proportion of methyl laurate 53.82%, methyl myristate 21.22%, methyl palmitate 10.32%, methyl stearate 3.92%, and methyl oleate 10.72%. These compositions are typical to the respective biodiesel found commonly [12]. The spray model parameters are kept same for both the cases of single and multi-component representative simulations. The input to the multi-component model used in the study is the liquid mass fraction of major five components present in the biodiesel. The biodiesel property is evaluated with mixture rule using physical properties of each pure component. The mixture rule for calculating physical properties of the biodiesel is given in the Eq. 4.1.

$$\text{Property of biodiesel} = \sum_{n=1}^{5} (Y_n \times P_n) \tag{4.1}$$

where, Y_n = liquid mass fraction of the nth pure component present in biodiesel, n = number of pure components present in the biodiesel, P_n = property of the nth component of biodiesel. It is observed that (Fig. 4.7) both the single component and the multi-component representative gives similar spray tip penetration which further closely follows the measured spray tip penetration of their respective biodiesel. Since the predicted spray tip penetration of the single component and multi-component

representative is similar to the biodiesel, it can be concluded that the single component modeling for prediction of biodiesel spray tip penetration is sufficient under non-evaporating conditions.

4.2.2 Spray Tip Penetration of Biodiesel Blend with Diesel

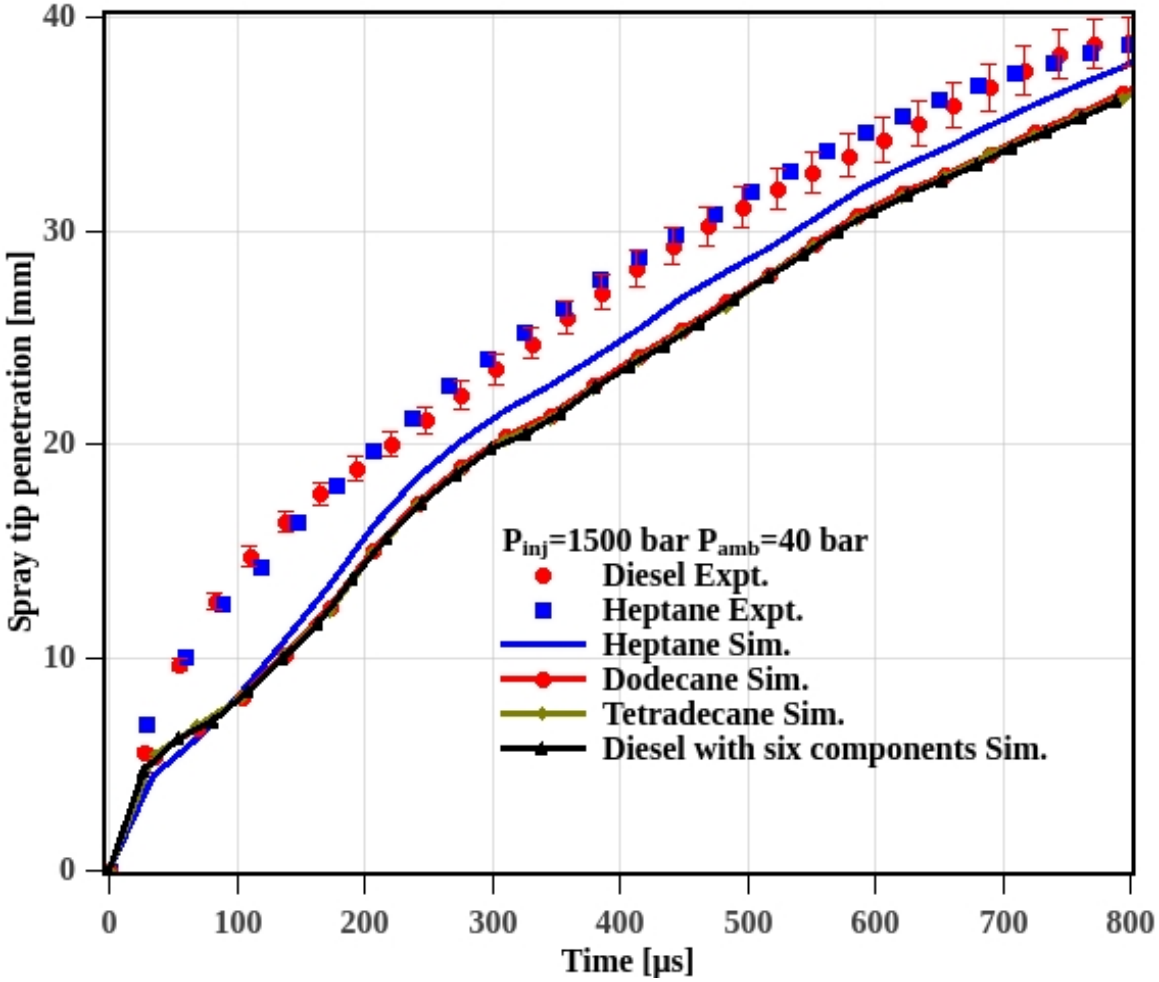

Figure 4.8: Experimental and predicted spray tip penetration of diesel, *n*-heptane, *n*-dodecane, *n*-tetradecane and diesel six components representative at an injection pressure of 1500 *bar* and an ambient gas pressure of 40 *bar* (ρ = 46 kg/m^3).

The biodiesel is extensively used in the blends with diesel in different proportion within the range of 5% to 20%. This avoids extensive engine modifications including injection system and fuel injection mapping. It is important to understand how the blending of biodiesel with diesel affects the spray characteristics. The spray tip penetration of 20% karanja biodiesel blend with diesel fuel is predicted with the single component and multi-component representative of diesel and biodiesel. The spray

model is first validated with different single component and multi-component representative of diesel. The Fig. 4.8 shows the validation of diesel fuel single component and multi-component representatives such as *n*-heptane, *n*-dodecane, *n*-tetradecane and six component diesel representative. The multi-component representative of diesel contains six components: toluene (15%), *n*-decane (14%), *n*-dodecane (22%), *n*-tetradecane (23%), *n*-hexadecane (13%) and *n*-octadecane (11%) [94]. Similar to the biodiesel, the single and multi-component representatives of diesel are found to predict similar spray tip penetration. Thus, the use of single component representative is also found to be sufficient for the prediction of non-evaporating spray tip penetration of diesel fuel. Among, the three single component representatives studied, *n*-heptane, *n*-dodecane and *n*-tetradecane, the *n*-heptane shows the spray tip penetration more close to that of the diesel fuel. Hence, the *n*-heptane is selected as the single component representative for diesel for blending with karanja biodiesel.

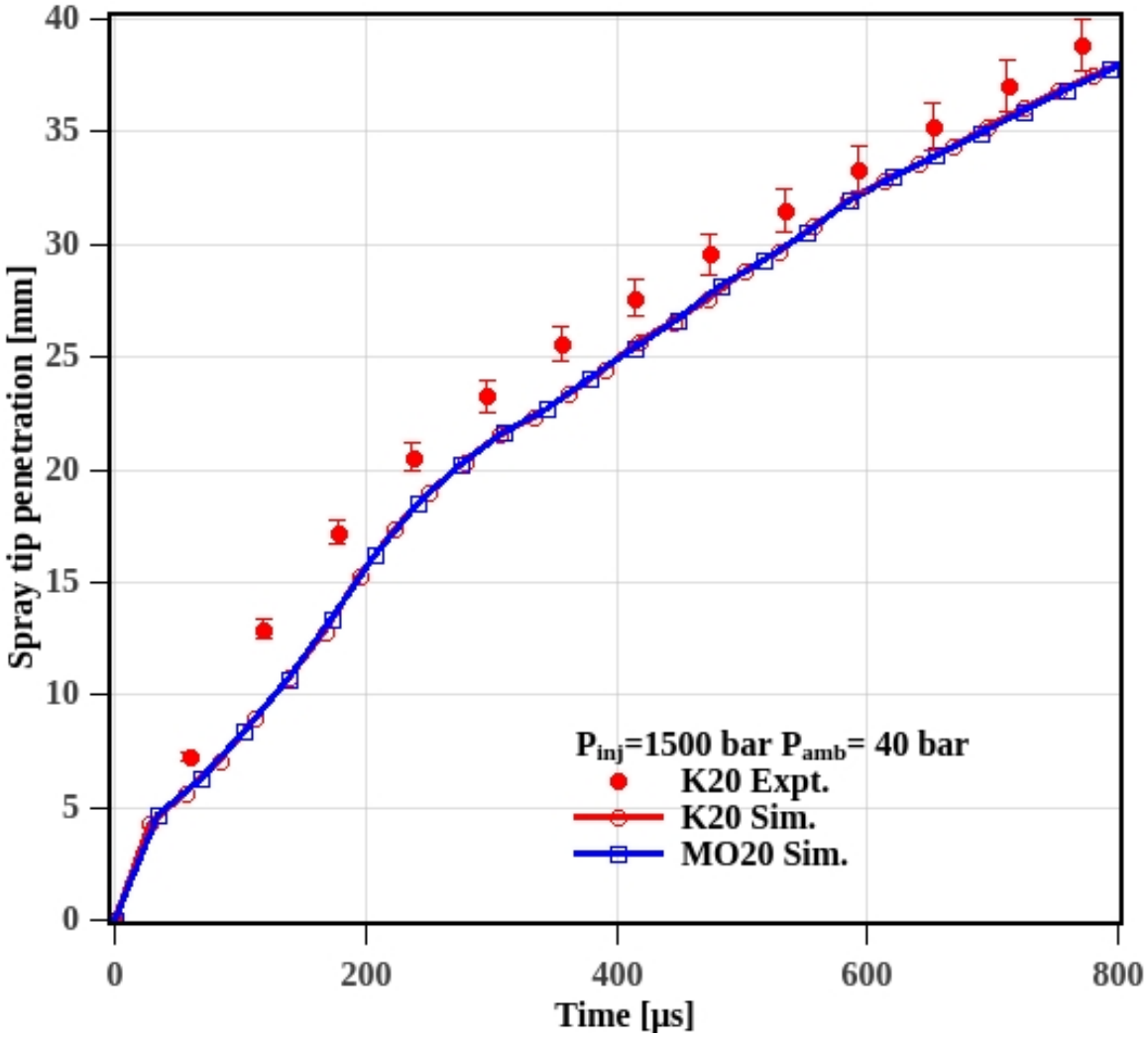

Figure 4.9: Experimental and predicted spray tip penetration of karanja biodiesel blend with diesel at an injection pressure of 1500 *bar* and an ambient gas pressure of 40 *bar* (ρ = 46 kg/m^3). (K20 = karanja biodiesel 20% blend with diesel; K20 Sim = karanja biodiesel five component representative 20% blend with *n*-heptane; MO20 = Methyl oleate 20% blend with *n*-heptane)

The Fig. 4.9 shows the comparison of predicted spray tip penetration of methyl oleate 20% blend with n-heptane and methyl oleate 20% blend with multi-component representative of karanja biodiesel, with the measured results of karanja biodiesel 20% blend with the diesel. It is observed that both the blends of the multi-component and single component representative of karanja biodiesel shows similar spray tip penetration. From the above observations, it is concluded that the blends can be predicted with its corresponding single component representative for biodiesel.

4.3 Summary and Conclusion

The comparative experimental and numerical study is conducted to establish the significance of single component representative of biodiesel, diesel and their blend for predicting their spray tip penetration. The representatives selected in the study categorize the biodiesels in two groups. The methyl oleate represents long-chain fatty acid ester biodiesels such as karanja, soybean, and rapeseed. The methyl laurate represents medium chain fatty acid ester biodiesel such as coconut and palm kernel. The spray tip penetration of karanja biodiesel is predicted with corresponding single and multi-component representatives. The spray tip penetration of karanja biodiesel is found to be similar to that of the methyl oleate. The observed similarity in the spray tip penetration of the biodiesel is due to the presence of methyl oleate in its fatty acid ester composition. The spray tip penetration of coconut biodiesel is found to be similar to that of methyl laurate. Furthermore, the measured spray tip penetration of biodiesel and its 20% blend with diesel is predicted by single component and multi-component representative which is found to be in good agreement. It can be concluded that the single component representative of biodiesel is sufficient to predict the non-evaporating spray characteristics of biodiesel and its blend in their respective category. It is necessary to have knowledge of the composition of the biodiesel and FAME component dominating physical properties of biodiesel to model the biodiesel spray.

5 Evaporating Spray Characteristics

The evaporating spray characteristics of biodiesel and biofuel pure component spray is presented in this chapter. The spray are studied at engine-relevant conditions such as late-cycle post-injection and near top-dead-center injection conditions. The spray characteristics liquid length, vapor length, and spray vapor area are predicted using the validated spray model.

The biodiesel pure components selected for the evaporating spray study are methyl oleate, methyl laurate, and ethyl oleate. The simple triglycerides such as triolein and trilaurin are selected to represent the SVOs for the spray study. The spray study include, the plant-derived SVOs as it forms a closed loop of CO_2 with its use in the agricultural field work [114–116]. It is also widely used as a fuel in stationary engines and agricultural machinery like tractors. The engine tests with the SVOs have concluded that it may give environmental benefits with reduced engine emissions of hydrocarbons and soot [23, 117–119].

The spray models are tuned and validated for diesel surrogate dodecane with experimental data available from the Engine Combustion Network (ECN) experimental spray repository [120]. The spray models are also tuned and validated for biodiesel liquid length and vapor length at different engine-relevant conditions available in the literature. For comparison of various biofuels, the injector hole diameter used here is 108 μm in size, the injection pressure is set to 1500 bar and injection duration is 3 ms. The corresponding mass and mass flow rate of injection is used in the simulation. The CFD study for multicomponent fuel is conducted using one representative pure component. The representative component is selected based on highest contribution of that component in the multi-component biodiesel. Additionally, it should

have properties similar to that of biodiesel [82]. In the present study, the methyl oleate is chosen as the representative pure component for rapeseed, karanja, palm, jatropha and soybean biodiesel. The methyl oleate is chosen as its properties such as liquid density and normal boiling point (816 kg/m^3 at 373 K; 617 K) is found to be comparable to that of the biodiesels it represents [5, 12, 82, 121, 122]. From the Table. 5.1, it is observed that soybean biodiesel contains methyl linoleate at the higher proportion than that of methyl oleate. However, the methyl oleate is chosen as its representative due to its similar physiochemical properties to that of the soybean biodiesel. Similarly, for the jatropha and palm biodiesel, methyl oleate is chosen as their representative due to its similar physiochemical properties although other components have higher contribution in composition. On the similar lines, the methyl laurate is chosen as the representative component for the coconut and the palm kernel biodiesel. The sprays for all these pure component FAME and FAEE is studied to understand their individual contribution in atomization and mixing process.

Table 5.1: Fatty acid composition of various biodiesels [1, 15, 110, 123, 124].

Fatty Acid Methyl Esters	C	PK	P	S	R	J	K
Methyl laurate	**44-52**	**40-52**	–	–	–	–	–
Methyl palmitate	8-11	7-9	32-45	6-10	2-6	13-15	4-8
Methyl stearate	1-3	–	2-7	2-5	1-3	6-7	2-9
Methyl oleate	5-8	11-19	**38-52**	**15-33**	**52-67**	**37-41**	**45-71**
Methyl linoleate	–	–	–	50-60	6-14	35-42	10-18
Methyl linolenate	–	–	–	5-11	6-14	–	–

Note: C-coconut; PK-palm kernel; P-palm; S-soybean; R-rapeseed; J-jatropha K-karanja

5.0.1 Validation

The CFD modeling of evaporating spray requires tuning of various parameters of the spray models [95, 102]. These parameters are tuned so as to match the simulation with the experimental liquid length and vapor length for diesel and biodiesel fuel at one operating condition. The spray simulation for case 2 as shown in Fig. 5.1 with Δt of 0.1 μs and Δx of 125 μm which is of the order of nozzle orifice diameter demands

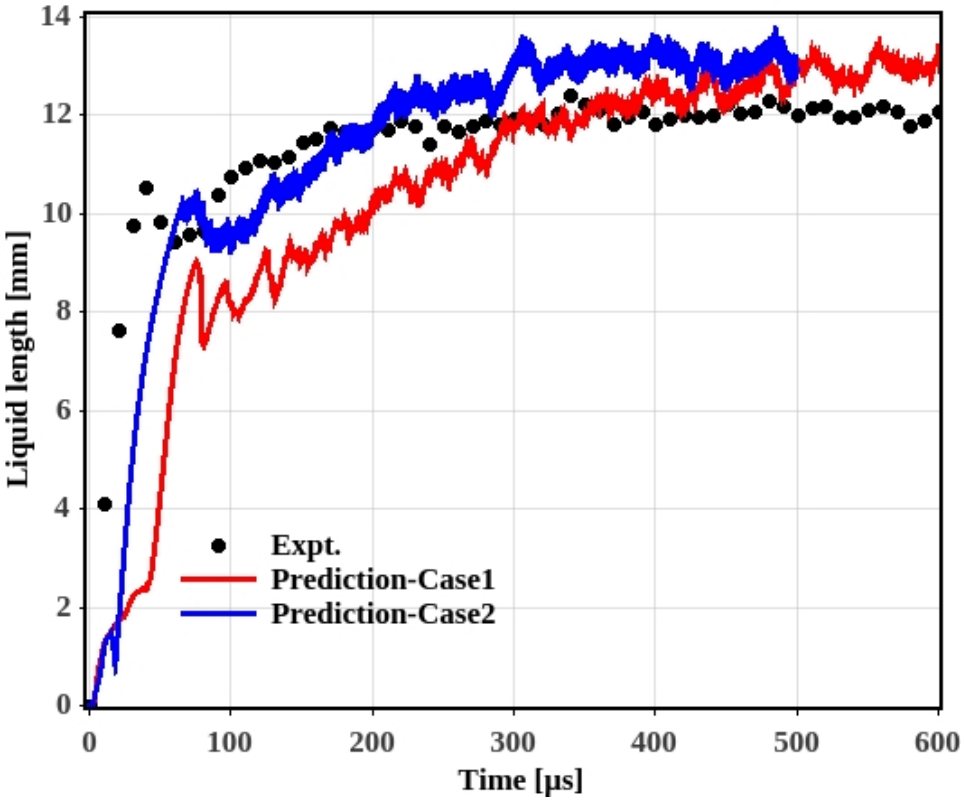

Figure 5.1: Grid independent study of liquid length for dodecane at at T_{gas}=1400 K, ρ_{gas}= 7 kg/m^3 [120]. Note: Case 1: time step size (Δt) =2.5 μs; grid size (Δx) =1 mm and Case 2: Δt =0.1 μs; Δx = 0.125 mm

more computational resources and time. The case 1 spray simulation with Δt =2.5 μs; grid size Δx =1 mm is observed to require less computational time with simiar liquid length prediction as that of case 2. Thus, based on the grid independent study as shown in Fig. 5.1, the spray characteristics are found to be fairly independent for cell size less than 1 mm. Hence, for the study the cell size is 1 mm and the time step of 2.5 μs is used for the present study. The vapor length and liquid length

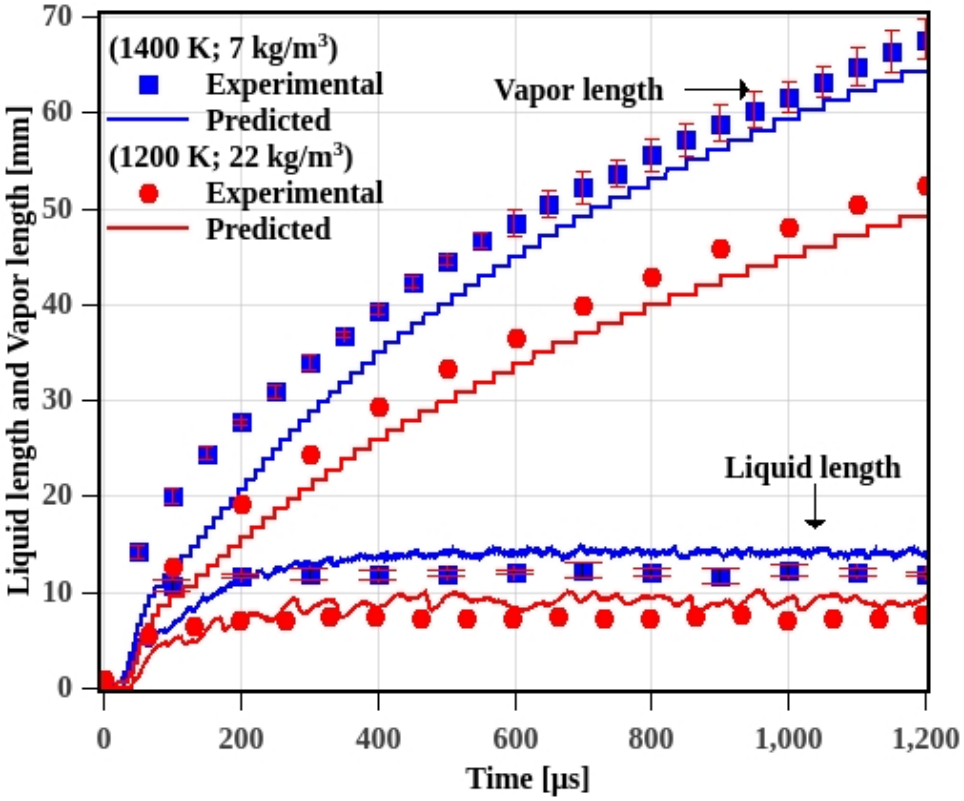

Figure 5.2: Validation of liquid length and vapor length with experimental measurements for dodecane at various ambient temperature and density conditions [120].

for dodecane is compared with experimental measurements in Fig. 5.2. The models are tuned for the condition of T_{gas}=1400 K, ρ_{gas}= 7 kg/m^3 and validated for the condition T_{gas}=1200 K, ρ_{gas}= 22 kg/m^3. While tuning the model parameters, it is observed that the liquid length is sensitive to the KH-RT model parameters and vapor length is sensitive to k-ϵ model parameters specifically value of C_1 used in the present study is 1.52. It can be observed that the liquid length is sensitive to the KH-RT and Rosin Rammler parameters. However, the tuning of the model parameters was not able to give both the liquid length and vapor length prediction close match with the measured data. Hence, it was decided to keep the existing

10% difference in the measured and predicted results. Thus, from the Fig. 5.2 it is observed that the predicted liquid length and vapor length are within 10% of error band with the corresponding measured results for the ambient conditions studied.

The spray model constants are tuned for one operating condition (T_{gas}=1400 K, ρ_{gas}= 1.2 kg/m^3) for biodiesel and kept constant for all other conditions. These constants are not modified for remaining simulations in this chapter. The six cases of tuning for KH-RT and Rosin Rammler Distribution parameters are shown in the Table. 5.2 for soybean biodiesel with methyl oleate as representative fuel. The fifth case, higlighted in bold font is indicating final tuned parameters used for the present study. The predicted liquid length for six cases shown in Table. 5.2 at operating condition (T_{gas}=1400 K, ρ_{gas}= 1.2 kg/m^3) is shown in the Fig. 5.3.

Table 5.2: Tuned parameters of KH-RT model and Rosin Rammler distribution for experimental soybean biodiesel liquid length [82] represented by methyl oleate with fuel injector orifice diameter 108 μm at 1400 K ambient gas temperature and 1.2 kg/m^3 ambient gas density.

Tuned Cases	Tuned Prameters			
	KH model	RT model		Rosin Rammler
	B1	Ctau	Crt	D
1	60	1	0.1	132
2	60	10	1	132
3	60	20	10	132
4	60	40	10	190
5	**60**	**10**	**0.1**	**220**
6	60	10	1	220

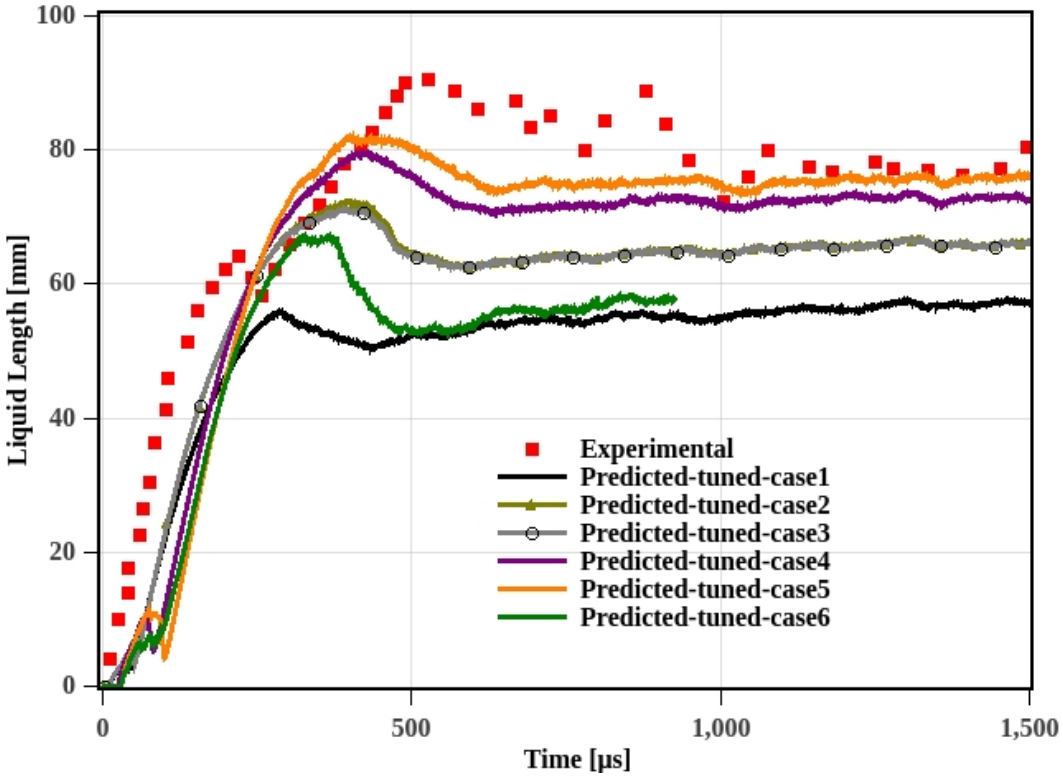

Figure 5.3: Result of tuning exercise of KH-RT model and Rosin Rammler distribution parameters for experimental soybean biodiesel liquid length [82] represented by methyl oleate with fuel injector orifice diameter 108 μm at 1400 K ambient gas temperature, 1.2 kg/m^3 ambient gas density and 1500 bar injection pressure. Note: Cases shown in Table.5.2

The liquid length of biodiesel spray is validated with the available experimental data from the literature. The validation of liquid length for soybean biodiesel is carried out at eight different ambient conditions as shown in Fig. 5.4. The steady-state

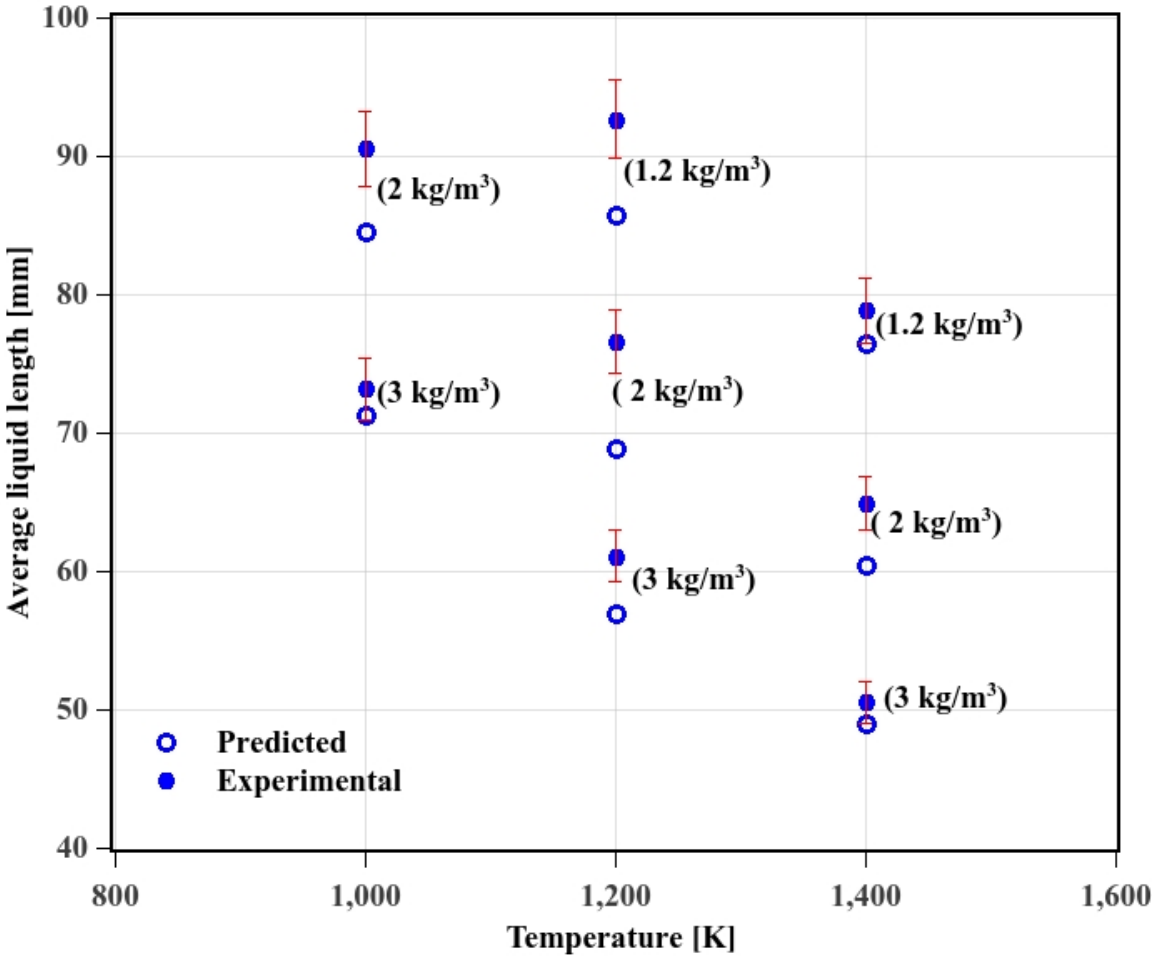

Figure 5.4: Comparison of predicted and measured liquid length of soybean biodiesel at various ambient temperature and gas density. Soybean biodiesel is modeled as methyl oleate [82].

liquid length is used for comparison with experimental measurements. The predicted liquid length is in close agreement with the experimental data. The maximum deviation of 10% is observed at low gas densities and low ambient gas temperatures. The liquid length from simulation closely matches with experimental data at high ambient gas densities. These conditions, give an effect of ambient gas density and temperature on liquid length. It is observed that there is around 5 mm decrease in liquid length for every 100 K increase in ambient temperature.

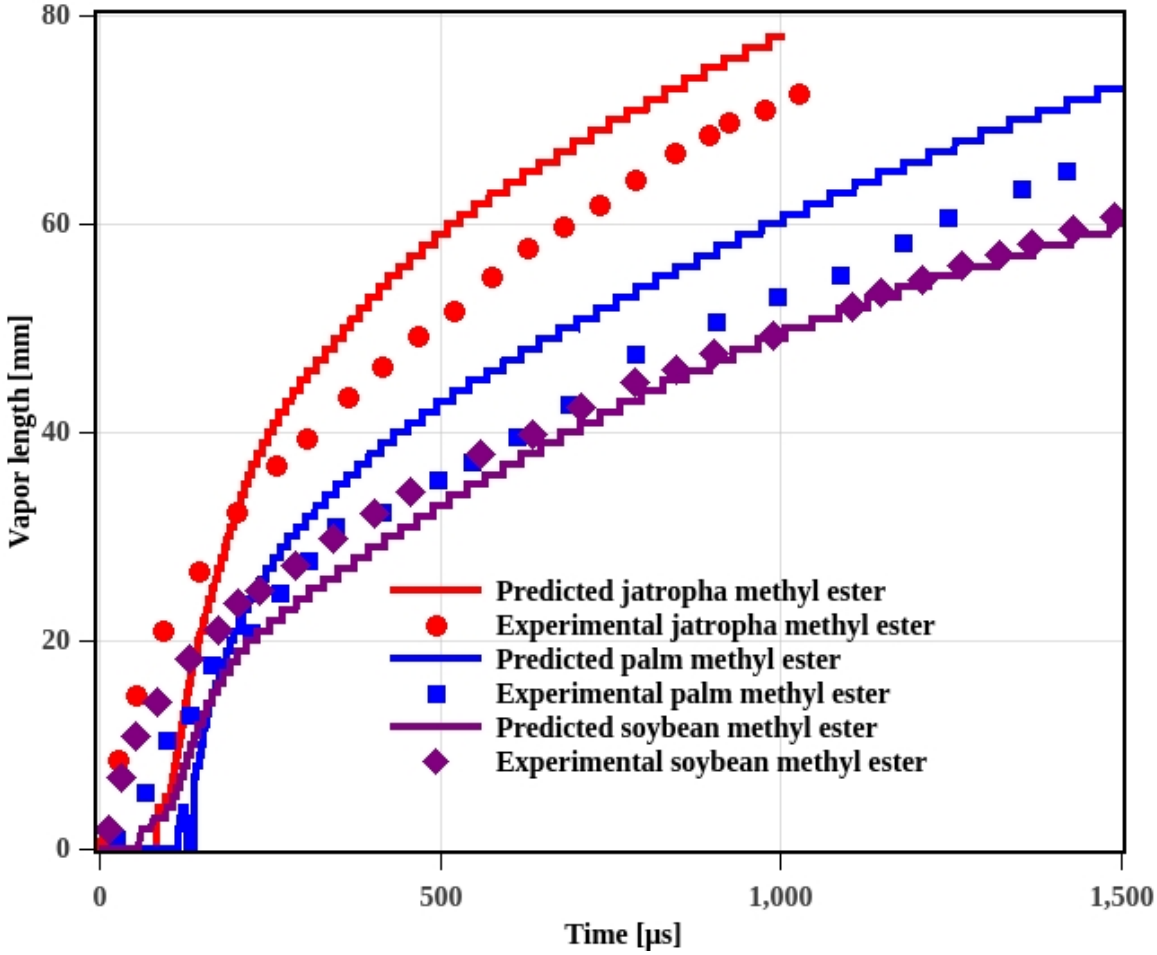

Figure 5.5: Vapor length validation for biodiesel of soybean at 900 K, 22.5 kg/m^3 [90], palm at 830 K, 20.2 kg/m^3 [85] and jatropha at 900 K, 18.7 kg/m^3 [84].

The vapor length of fuel spray plays an important role in ignition and combustion behavior of the fuel which later decides emissions formed in the engine. However, there is very little experimental data available on biodiesel vapor length. Using the available experimental data, predicted vapor length for three biodiesel viz. soybean at T_{gas}= 900 K and ρ_{gas}= 22.5 kg/m^3 [90], palm at T_{gas}= 830 K and ρ_{gas}= 20.2 kg/m^3 [85] and jatropha at T_{gas}= 900 K and ρ_{gas}=18.7 kg/m^3 [84] is compared in Fig.5.5.

The simulations are performed using methyl oleate as the representative component for jatropha and soybean biodiesel whereas methyl palmitate is used as the representative component for palm biodiesel.

The predicted vapor length of soybean, palm and jatropha biodiesel is in agreement with the measured data within 10%. The predicted vapor length of soybean biodiesel shows a close match with the measured vapor length. However, for the palm and jatropha biodiesel over-prediction of around 10% with respect to measured data is observed. It may be due to the use of same spray model parameters which are tuned for the soybean biodiesel. The model parameters for jatropha and palm may slightly differ since the soybean, jatropha, and palm biodiesel experiments are based on different conditions such as different injector dimensions. Another reason for the over-prediction, observed from the measured data might be due to the presence of other components in the biodiesel which are not considered in the simulation study. In summary, the simulation results are in a close agreement with the measured data at higher gas densities and are able to predict trends in all the validation cases. The spray models are successfully validated against experimental data for the spray characteristics such as liquid length and vapor length for biodiesel and diesel. The experimental data of SVO liquid length and vapor length is not available in literature. Hence, the validated spray model for the biodiesel is used to predict the liquid length and vapor length of SVO pure components.

5.1 Liquid Length Prediction

The liquid length of spray determines the impingement of liquid fuel on the combustion chamber wall. The longer liquid length indicates impingement of fuel on

the chamber wall which may lead to higher emissions. The liquid length strongly depends on an ambient gas density and temperature. The advanced fuel injection strategies include multiple-injection in diesel engine to control NO_x and soot emissions. This includes late-cycle post-injections when ambient densities are lower at high gas temperature. The objective of this section is to predict the liquid length, vapor length and spray area of biofuel pure components at operating conditions relevant for diesel engines. The important injection conditions investigated in this chapter are late-cycle post-injection and near top-dead-center conditions in the engine.

5.1.1 Liquid Length under Late-Cycle Post-Injection Condition

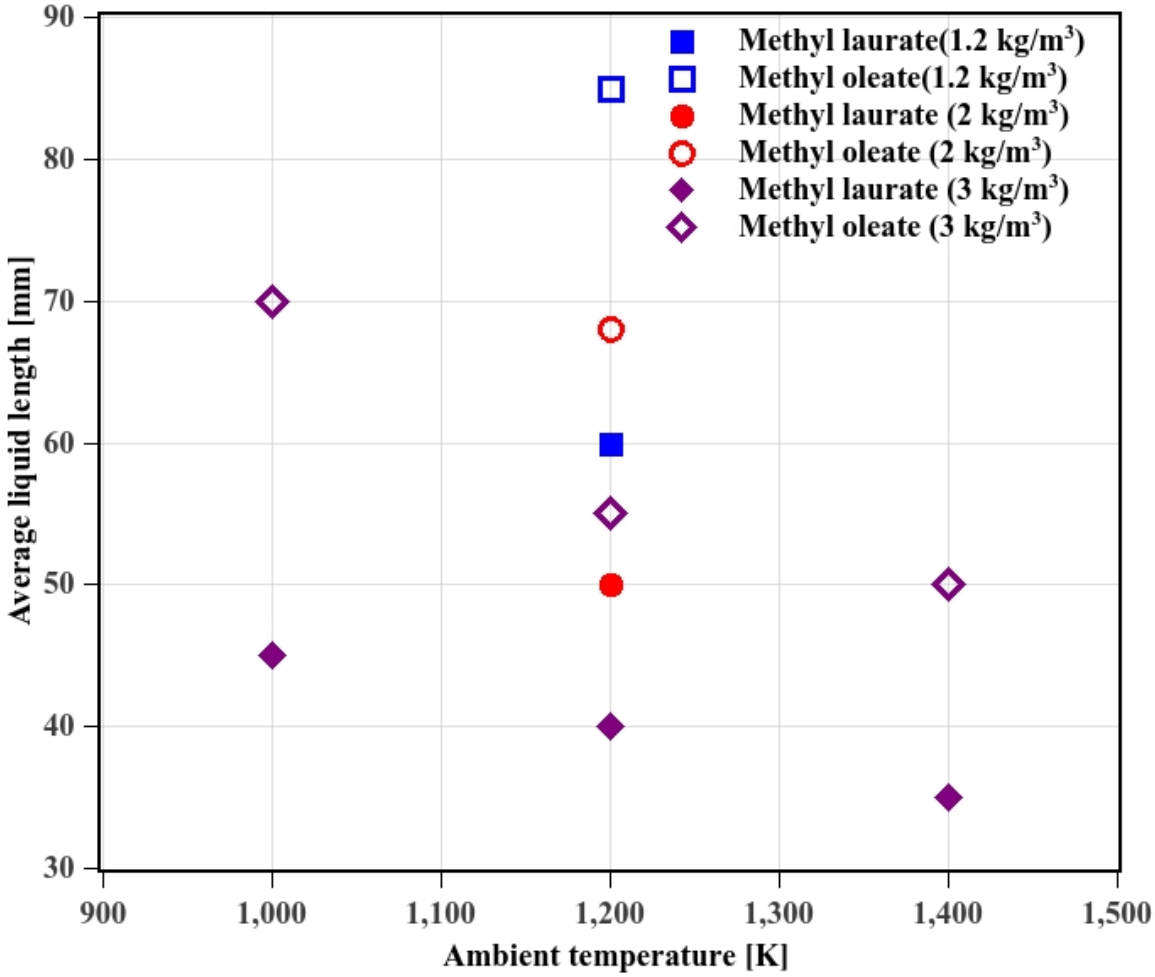

Figure 5.6: Comparison of average liquid length of methyl oleate and methyl laurate for different late-cycle post-injection conditions.

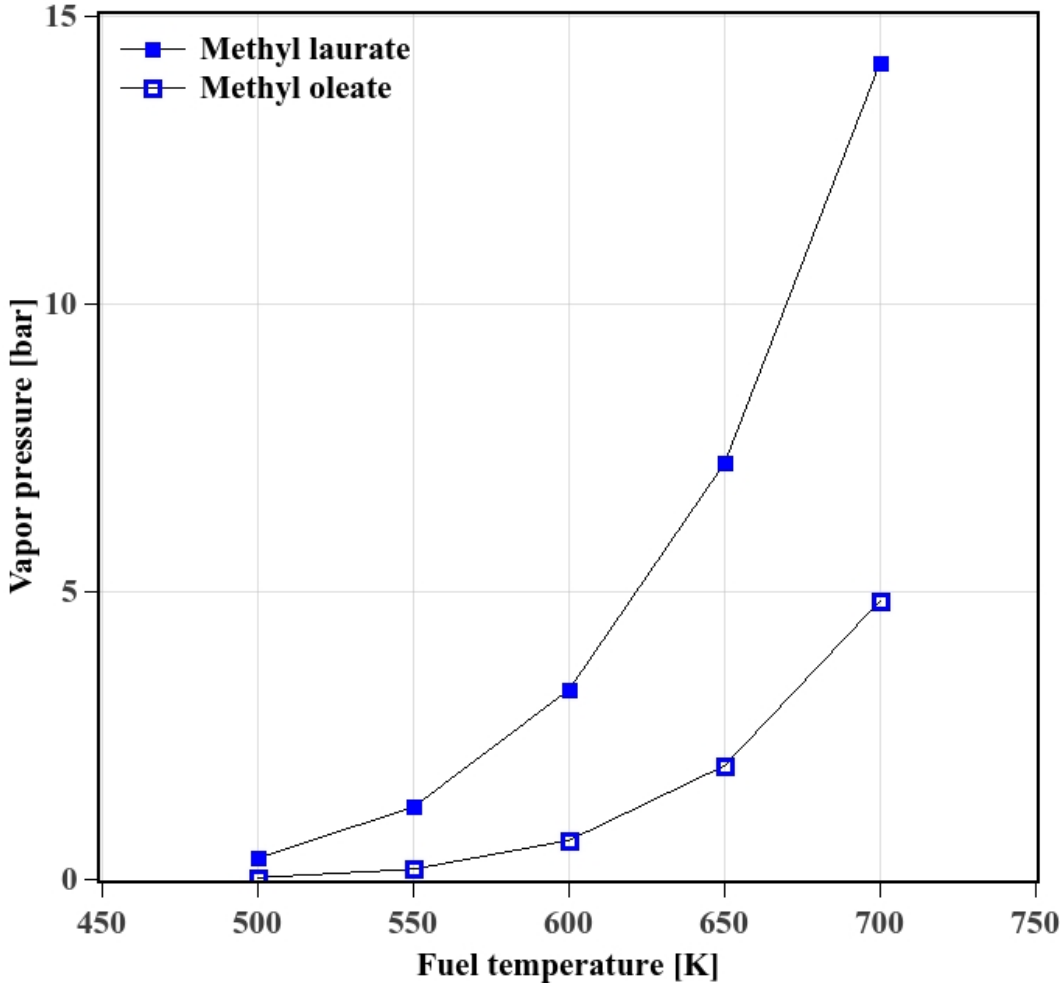

Figure 5.7: Variation of vapor pressure of methyl oleate and methyl laurate with respect to fuel temperature.

The steady-state liquid lengths for methyl oleate and methyl laurate at various late-cycle post-injection conditions are presented in the Fig.5.6. The average liquid length is defined as the average of the steady liquid length data for the time frame of around 1000 μs to 2000 μs. The liquid length at various ambient temperatures (1000 K, 1200 K, and 1400 K) and ambient gas densities (1.2 kg/m^3, 2.0 kg/m^3, and 3.0 kg/m^3) is compared. The liquid length for methyl laurate is lower than that of methyl oleate, if compared at the respective set of operating conditions ambient gas density and temperature as follows: (ρ_{gas} = 3.0 kg/m^3; T_{gas} = 1000 K, 1200 K, and 1400 K); (ρ_{gas} = 1.2 kg/m^3; T_{gas} = 1200 K) and, (ρ_{gas} = 2.0 kg/m^3; T_{gas} = 1200 K). The liquid length for methyl oleate is more than 40% higher when both are at an ambient gas density of 3.0 kg/m^3. As observed earlier, the liquid length decreases with increase in ambient gas density and the ambient gas temperature.

The effect of ambient gas temperature on the liquid length of methyl oleate is higher ($\sim$5.0 mm per 100 K) compared to methyl laurate($\sim$2.5 mm per 100 K). With a 40% increase in ambient gas temperature from 1000 K to 1400 K, the average liquid length decrease by 10 mm. Similarly, for 40% increase in ambient gas density, 1.2 to 2 kg/m^3, the average liquid length exhibits decrease of around 10 mm. The decrease in penetration with increase in temperature is due to availability of more energy from gas for evaporation. With increase in gas density penetration reduces due to higher resistance from gas leading to smaller size which increases evaporation and higher energy associated with dense gas for evaporation. The liquid length of the spray reaches the steady state as the amount of the fuel vaporized balances the amount of fuel injected. The fuel properties determining the vaporization rate are vapor pressure, liquid specific heat, and enthalpy of vaporization. The vapor pressure for methyl laurate and methyl oleate is compared and shown in the Fig.5.7 at various fuel temperatures. The vapor pressure for methyl laurate is higher than that of methyl oleate at all temperatures. This gives an indication of higher evaporation rates for methyl laurate at any given temperature compared to methyl oleate. This consequently shortens the liquid length of methyl laurate. The vapor pressure curve with respect to fuel temperature is not linear. However, a linear decrease in liquid length with an increase in temperature can be due to the cumulative effect of parameters like viscosity, surface tension and thermal conductivity of the fuel. The higher ambient gas density gives higher resistance to the incoming liquid fuel, resulting in shorter penetration of liquid and larger momentum transfer between penetrating liquid fuel and resisting surrounding gas. This effect of ambient gas density is observed to be more with methyl oleate than that of methyl laurate. The higher rate of evaporation for methyl laurate leads to a fast decrease in droplet size and higher loss of momentum leading to the shorter penetration. Thus, for the same ambient conditions of density and temperature, the liquid drop of methyl oleate will penetrate more than that of methyl laurate.

The typical light-duty diesel engine bore size is in the range of 80 mm to 90 mm [82]. The impingement of the liquid fuel is prevented if its liquid length is shorter than 40 mm to 45 mm. The averaged steady state liquid length of methyl oleate for the late-cycle post-injection condition is higher than 45 mm as seen from

the Fig.5.6. Thus, the methyl oleate liquid fuel spray may impinge on the chamber walls of the engine for the conditions studied. The commonly used biodiesel is represented by methyl oleate, hence, it can be generalized that the biodiesel spray will impinge on the wall of the combustion chamber. On the other hand, methyl laurate has the average liquid length less than 45 mm at an ambient gas density of 3 kg/m^3. Thus, for this operating condition, the coconut and palm kernel biodiesel may not impinge the wall of a typical light-duty diesel engine.

5.1.2 Liquid Length under Near Top-Dead-Center Injection Conditions

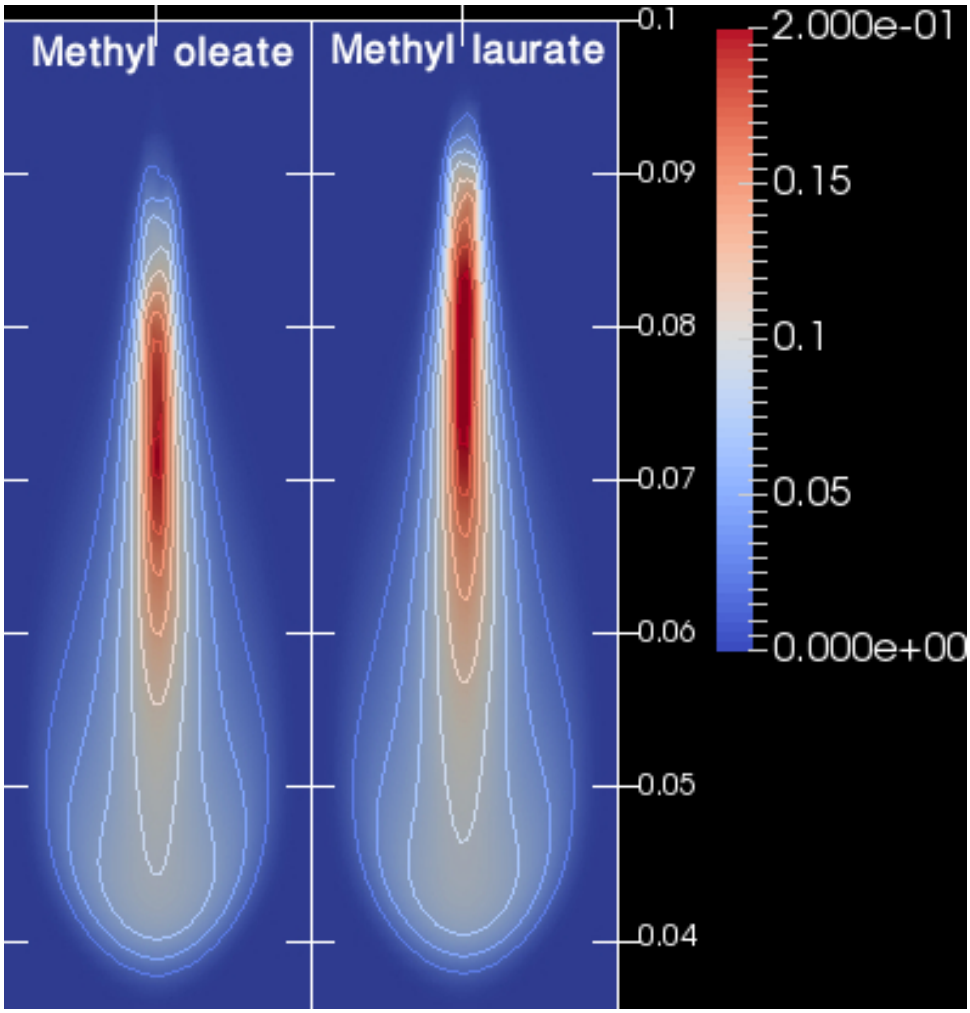

Figure 5.8: Image of spray showing contour of vapor penetration of methyl oleate and methyl laurate at an ambient gas density of 22 kg/m^3 and temperature of 1200 K.

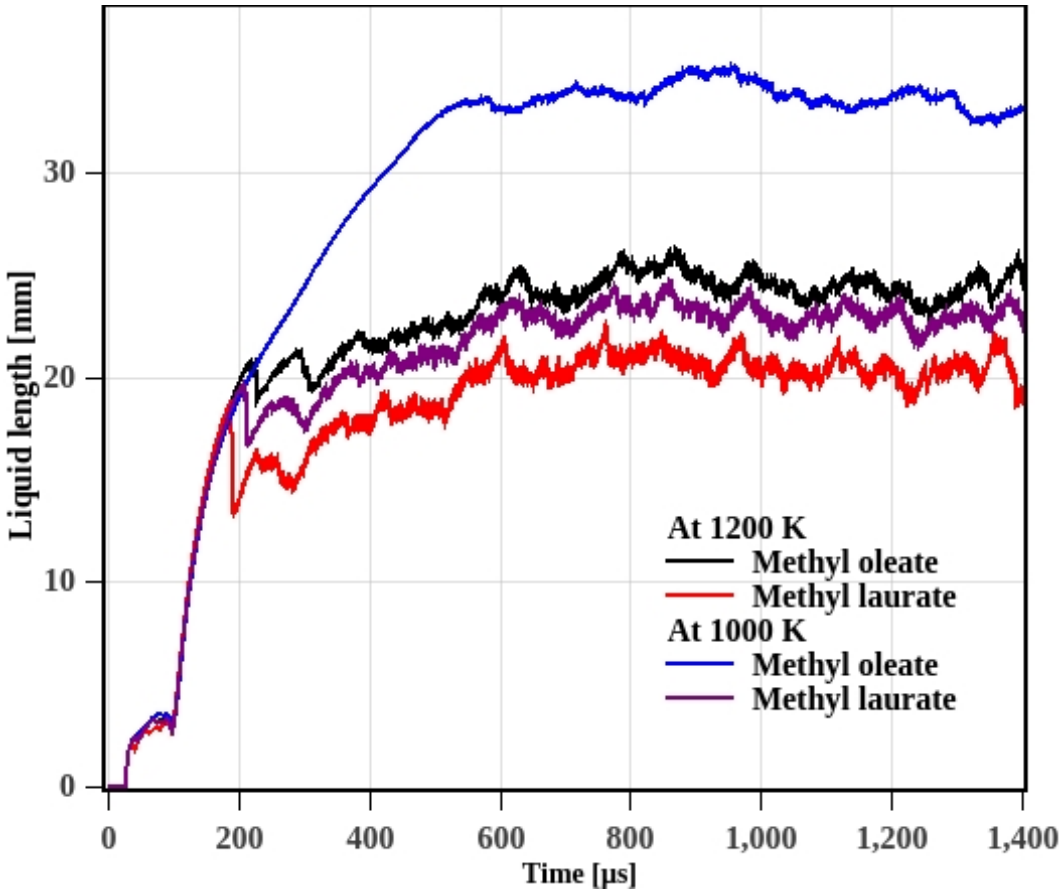

Figure 5.9: Effect of ambient gas temperature on liquid length of methyl oleate and methyl laurate at gas density of 22 kg/m^3.

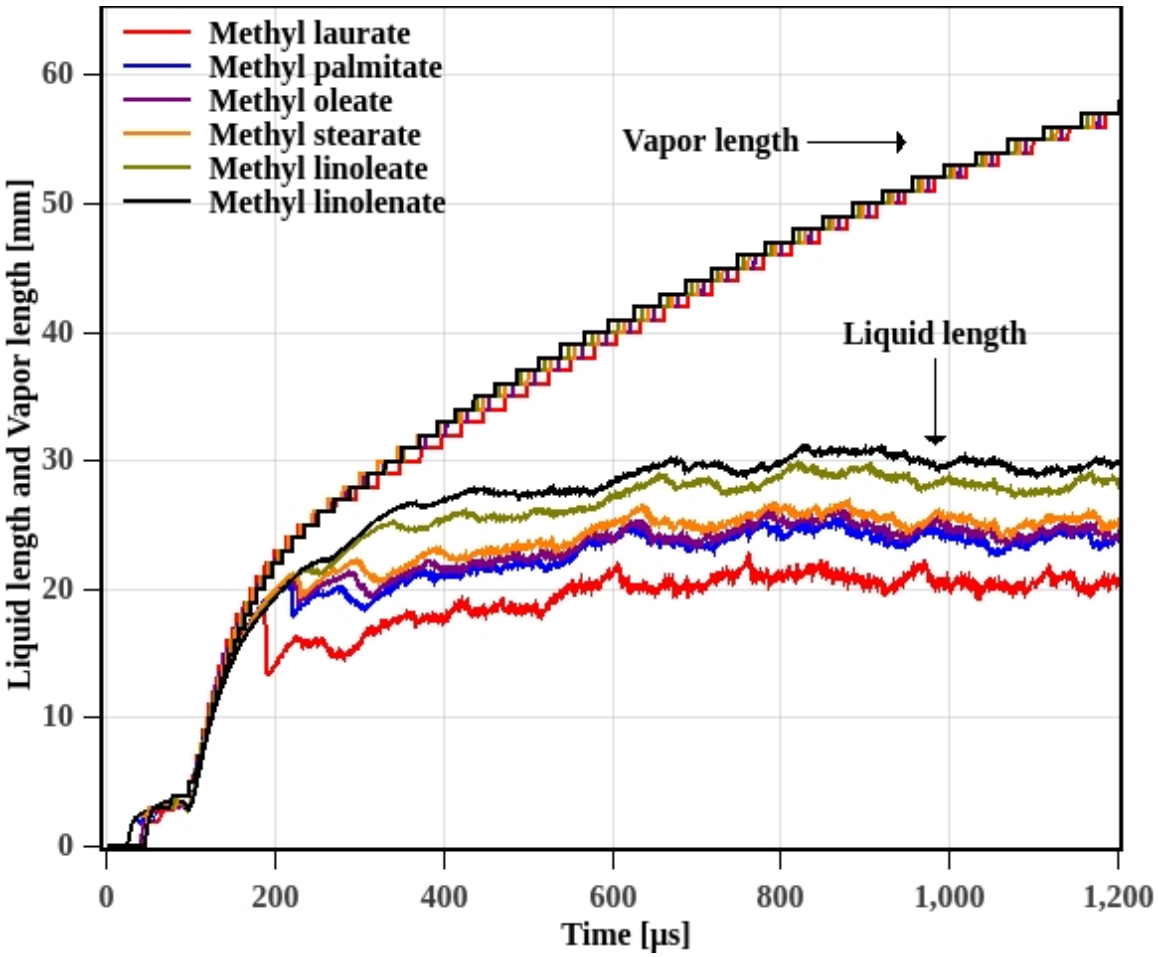

Figure 5.10: Liquid length and vapor length of FAMEs at an ambient gas temperature of 1200 K and an ambient gas density of 22 kg/m^3.

The main injection in the diesel engine occurs at the end of compression stroke, near the top-dead-center position of the piston. The ambient conditions in typical diesel engine at top-dead-center are, a temperature in the range of 900 K to 1200 K and gas density in the range of 20 kg/m^3 to 23 kg/m^3. The spray image as shown in Fig. 5.8 exhibits the difference in evaporation characteristics of methyl oleate and methyl laurate under same operating conditions of ambient gas density of 22 kg/m^3 and temperature of 1200 K. It can be observed from the Fig. 5.8 that the spread of maximum fuel vapor mass fraction as shown by red colour is wider in case of methyl laurate than that of methyl oleate. It can be said that methyl laurate evaporated earlier, as the larger vapor mass fraction is visible in upstream compared to methyl oleate. The liquid length of methyl oleate and methyl laurate is shown and compared in the Fig.5.9 at an ambient gas temperature of 1000 K and 1200 K and an ambient gas density of 22 kg/m^3. The liquid length for methyl oleate is observed to decrease by more than 35% with an increase in an ambient gas temperature from 1000 K to 1200 K. The decrease in liquid length for methyl laurate is around 20%. The methyl oleate and methyl laurate may not cause impingement on the chamber walls of typical light-duty engines with an ambient gas temperature above 1000 K and an ambient gas density of around 22 kg/m^3. To re-confirm the results, the liquid length of five pure components present in biodiesel is compared in the Fig. 5.10, at an ambient gas temperature of 1200 K and an ambient gas density of 22 kg/m^3.

The liquid length for all the pure components is observed to be less than or equal to 30 mm. Thus, it can be reasonably assumed that the liquid length of biodiesel may not go beyond 30 mm, which consequently may avoid the impingement on the chamber walls for near top-dead-center injection conditions studied.

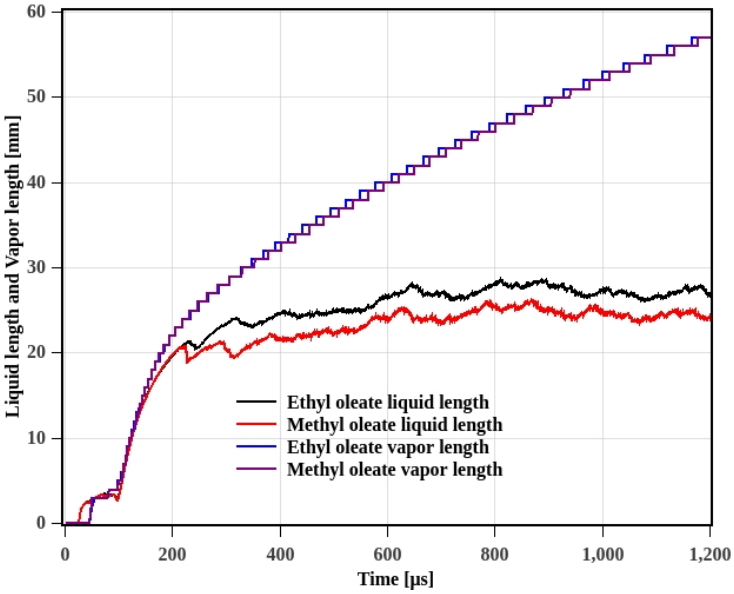

(a) At near top-dead-center (1200 K, 22 kg/m^3)

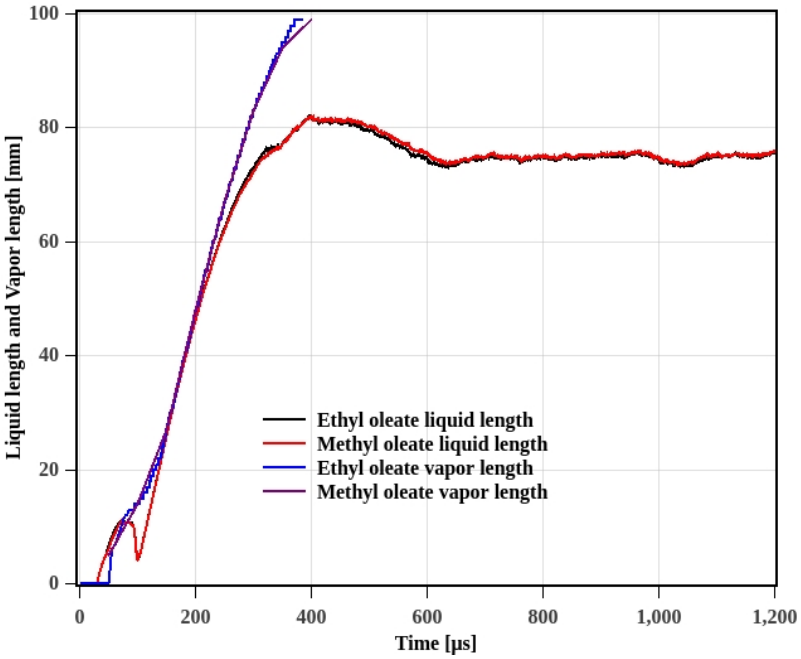

(b) At late-cycle post-injection (1400 K, 1.2 kg/m^3)

Figure 5.11: Comparison of liquid length and vapor length of methyl oleate and ethyl oleate.

Fatty Acid Ethyl Esters (FAEEs) are also used as the biodiesel fuel in diesel engine [109]. The liquid length for FAME and FAEE is compared for both near top-dead-center and late-cycle post-injection conditions, at an ambient gas temperature and an ambient gas density of (1200 K, 22 kg/m^3) and (1400 K, 1.2 kg/m^3) respectively as shown in the Fig.5.11.

The liquid length of ethyl oleate and methyl oleate for both the conditions as (Fig. 5.11a and Fig. 5.11b) shows a negligible difference. Similarly, the vapor length of methyl oleate and ethyl oleate observed to have a negligible difference for the respective conditions studied. The vapor penetrates with the momentum gained from the penetrating liquid fuel. Therefore, similar to the liquid length of ethly oleate and methyl oleate, the vapor length is also observed to follow the trend. Thus, the conclusions discussed for FAME's liquid length impingement on chamber walls should also be applicable for FAEE's.

5.2 Vapor Length Prediction

The vapor length of the fuel plays a key role in mixture formation, combustion and emission characteristics. The comparative study of vapor length for pure components of biodiesel and SVO is discussed in this section. The vapor lengths of methyl oleate and methyl laurate are compared at two ambient gas densities, 3.0 kg/m^3, and 22 kg/m^3 and two ambient temperatures, 1000 K, and 1200 K in the Fig. 5.12.

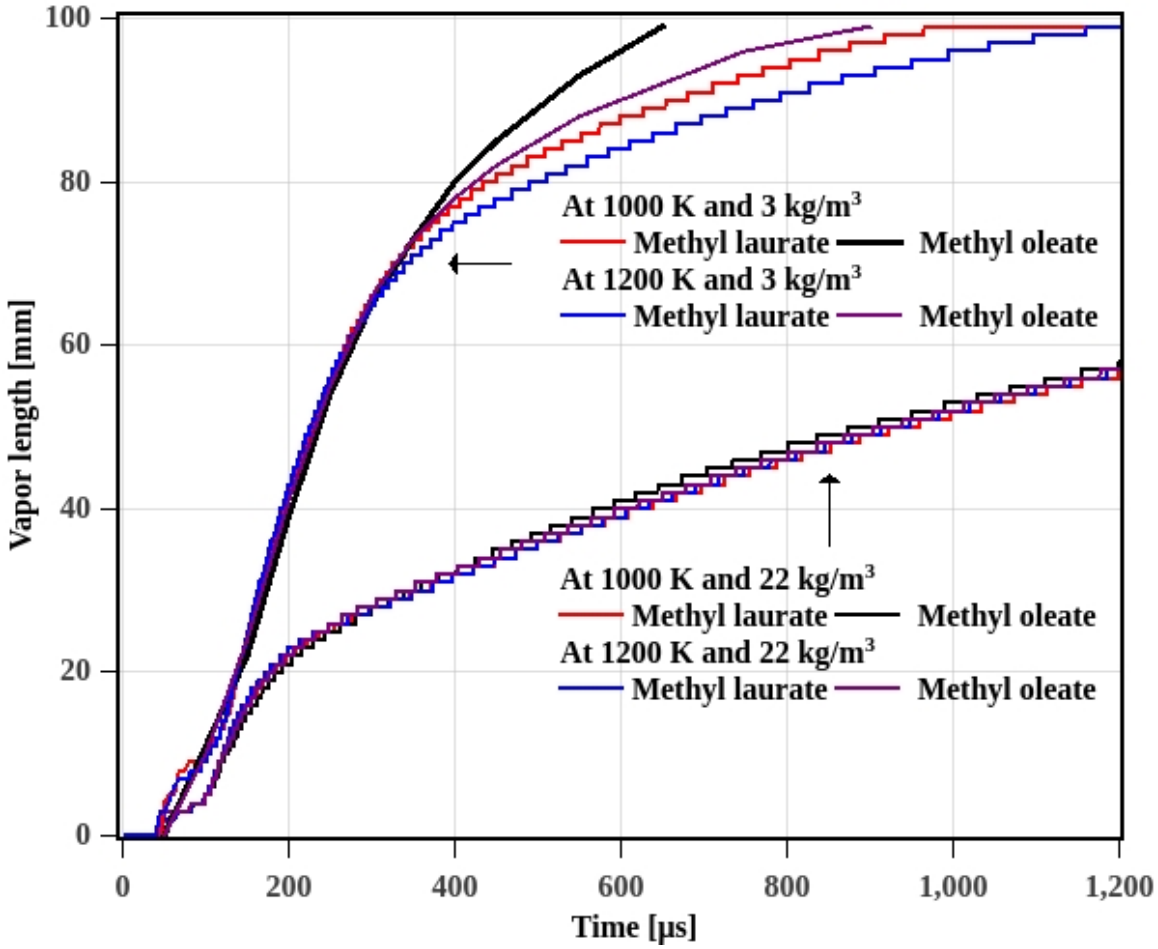

Figure 5.12: Comparison of vapor length of methyl oleate and methyl laurate at late-cycle post-injection and near top-dead-center injection conditions (temperatures 1000 K and 1200 K and densities 3 kg/m^3 and 22 kg/m^3.)

The vapor length of methyl oleate and methyl laurate is found to be similar at an ambient gas density of 22 kg/m^3 for both the temperatures. However, methyl oleate exhibits comparatively longer vapor length than that of methyl laurate at an ambient gas density of 3.0 kg/m^3. The liquid length is in transient phase during the time duration of around 300 μs. The vapor length of methyl oleate is observed to be longer than that of methyl laurate after around 300 μs. It may happen due to the longer averaged liquid length of methyl oleate than that of methyl laurate as seen from the Fig. 5.6. The methyl oleate gives higher momentum to its vapor formed due to longer liquid length than that of methyl laurate. This difference in the momentum may consequently give rise to longer vapor length of methyl oleate than methyl laurate. However, during the transient phase, the liquid length is found to be almost similar due to their similar rates of evaporation. Thus, the vapor lengths of methyl oleate and methyl laurate are found to be similar during the transient phase as seen from the Fig. 5.12. The vapor length at an ambient gas density of 22 kg/m^3 for all pure components is found to be similar as shown in the Fig. 5.10. The similarity of the vapor length observed may be attributed to the small difference among the FAMEs liquid length at 22 kg/m^3 compared to the case of 3.0 kg/m^3 ambient gas density.

The mixture formation of fuel vapor and air can be explained using a spread of vapor in the ambient air. The vapor spray area at a time 1500 μs after the start of injection is compared for different fuels in the Fig.5.13 for an ambient gas temperature of 1200 K and an ambient gas density of 22 kg/m^3.

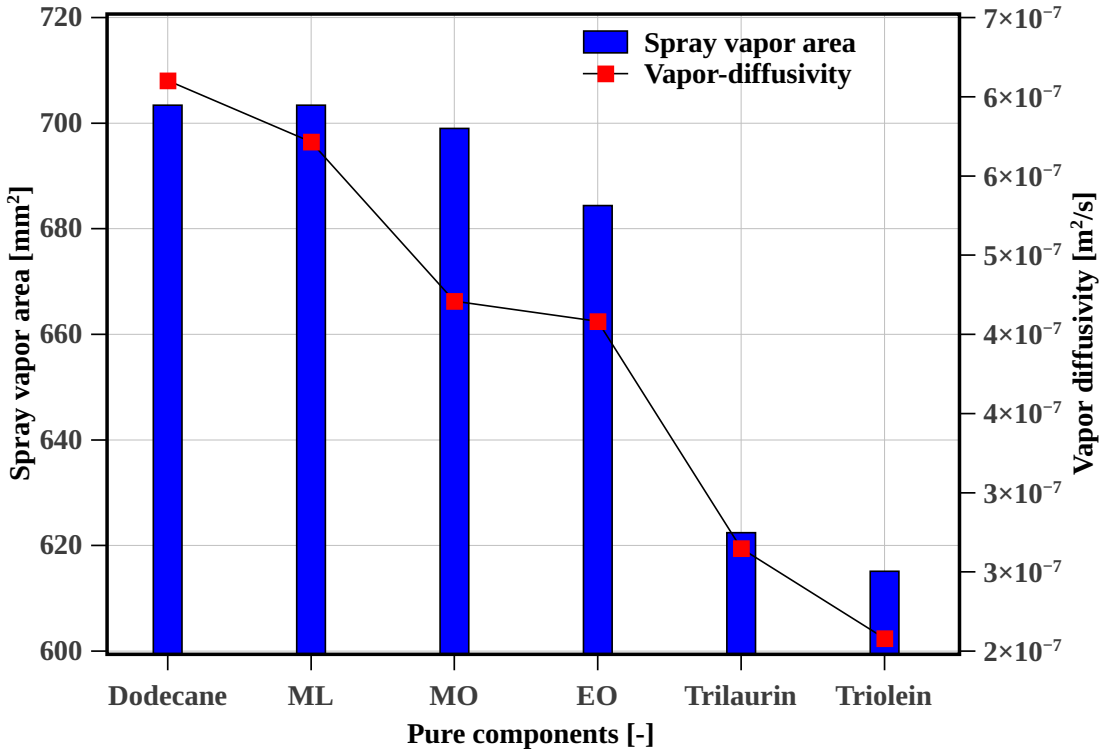

Figure 5.13: Comparison of spray vapor area and vapor diffusivity of pure components at an ambient gas temperature of 1200 K and an ambient gas density of 22 kg/m^3 (EO-ethyl oleate; ML-methyl laurate; MO-methyl oleate).

The spray vapor area is observed to be slightly larger in the case of methyl laurate than that of the methyl oleate. The larger spray vapor area of the methyl laurate can be attributed to its higher vapor diffusivity than that of the methyl oleate as seen from the Fig.5.13. Furthermore, the spray vapor area of the ethyl oleate is smaller than that of the methyl oleate. The spray vapor area of the methyl laurate is observed to be similar to dodecane, this suggests that although the vapor diffusivity of the dodecane is higher, the methyl laurate spray characteristics may be equivalent to dodecane.

5.3 SVO Pure Components

The Straight Vegetable Oils derived from plant seeds are composed of triglycerides. These SVOs can also be used as fuel in CI engines. The simple triglycerides are those which have one type of fatty acid attached to the glycerol molecule. The trilaurin and triolein are the simple triglycerides selected for the study which can represent the commonly used SVOs. The liquid length, vapor length, and spray area are predicted for these pure components. The experimental data for SVO evaporating spray is not available in the literature, hence the spray models validated for the biodiesel are used for the SVOs. The physiochemical properties of trilaurin and triolein are implemented in the fuel library of OpenFOAM required for the spray simulations. The Fig. 5.14 shows the predicted liquid length and vapor length of trilaurin and triolein at an ambient gas temperature of 1200 K and an ambient gas density of 22 kg/m^3. Trilaurin and triolein is observed to have similar vapor length and liquid length. The liquid length of both triglycerides is 40 mm, more than 25% higher than that of FAME. It is prone to the impingement in combustion chamber wall for lower ambient gas densities or ambient gas temperatures. The spray vapor area of the trilaurin is observed to be higher than that of the triolein (Fig.5.13). This may be attributed to its higher vapor diffusivity than that of the triolein. Again, the spray vapor area for triglycerides is more than 13% lower than that of corresponding methyl esters. The lower spray vapor area indicates lower air-fuel mixing and which may be result in incomplete combustion and higher emissions.

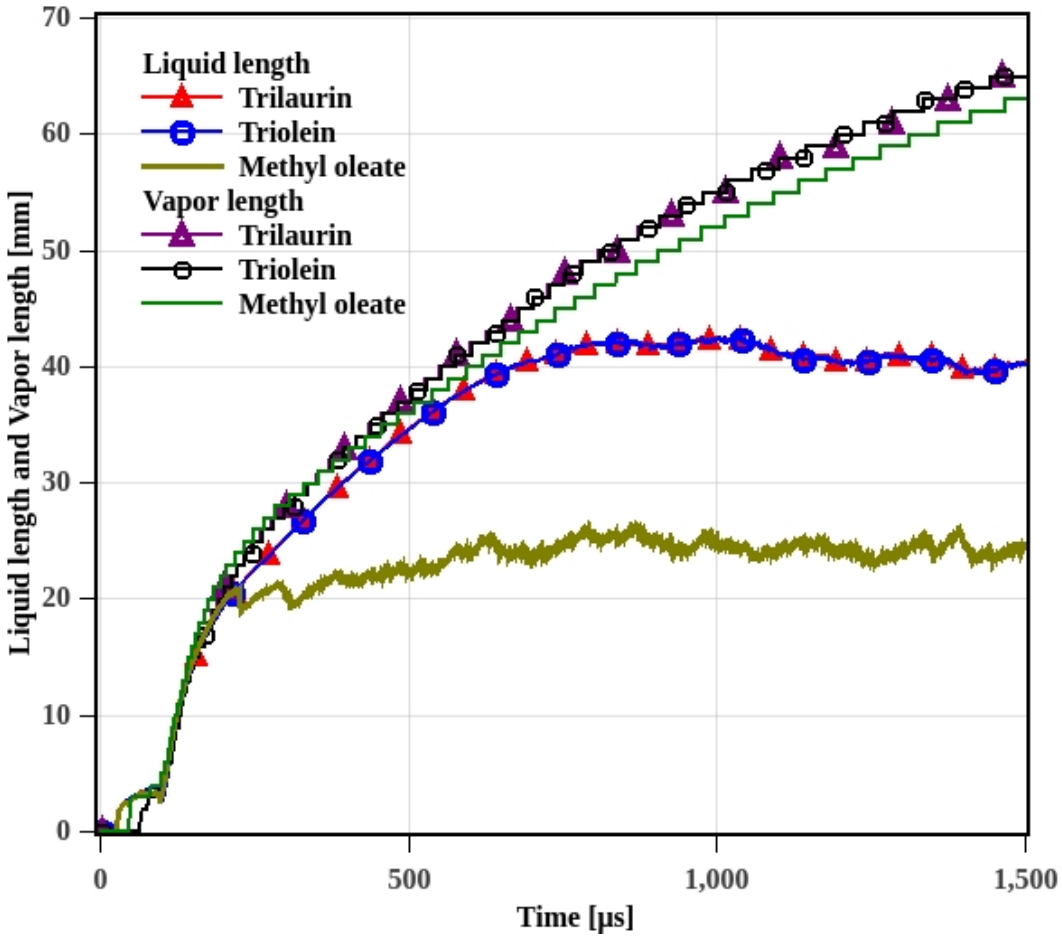

Figure 5.14: Liquid length and vapor length of SVOs pure components at an ambient gas temperature of 1200 K and an ambient gas density of 22 kg/m^3.

5.4 Specific Energy Ratio

The evaporating spray characteristics of fuel depends on the energy balance between the energy required for the evaporation of fuel and energy available from ambient gas. The amount of energy required for heating and vaporizing the spray is a function of the fuel properties such as liquid specific heat, normal boiling point and enthalpy of vaporization. The amount of energy available with ambient gas environment depends on its specific heat and temperature. The ratio of the amount of energy required to heat and vaporize the fuel spray to the amount of energy available with an ambient gas environment of the spray is known as specific energy ratio [125]. The equation of the specific energy ratio is shown in Eq.5.1.

$$\text{Specific energy ratio} = \frac{C_{p_{liq}} \times (T_{boil} - T_{fuel}) + h_{vap}}{C_{p_{gas}} \times (T_{gas} - T_{boil})} \tag{5.1}$$

In Eq. 5.1, the fuel and gas properties are: $C_{p_{liq}}$, the specific heat of liquid fuel at constant pressure; $C_{p_{gas}}$, the specific heat of an ambient gas at constant pressure; T_{boil}, the normal boiling point temperature of liquid; T_{fuel}, the fuel temperature; h_{vap}, the latent heat of vaporization; and T_{gas}, the temperature of an ambient gas. The specific energy ratio helps to understand the liquid length of different biofuels and their variation under various ambient gas temperatures. The specific energy ratio >1.0 indicates higher energy requirement of the fuel than available from the ambient gas. It lowers the rate of vaporization and thus produces longer liquid length. The fuel liquid length is observed to exhibit linear correlation with its T_{90} temperature or normal boiling point depending on whether it is a multi-component (diesel, biodiesel) or single component fuel (n-hexadecane, heptamethylnonane) [125–127].

The liquid length for the various pure component of biofuels studied and specific energy ratio is plotted against their boiling point temperature in the Fig.5.15 for the ambient condition of 1200 K and 22 kg/m^3.

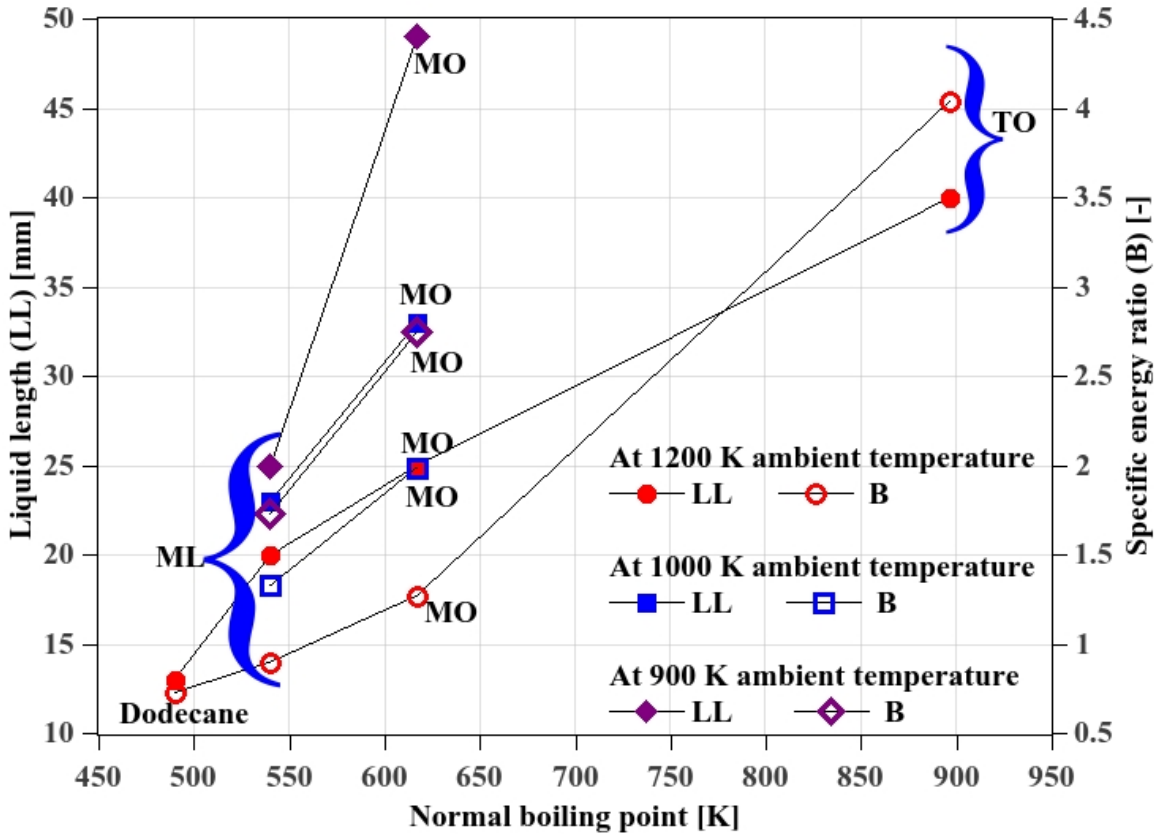

Figure 5.15: Comparison of specific energy ratio and liquid length of pure components at an ambient gas temperature of 1200 K, 1000 K and 900 K and an ambient gas density of 21 kg/m^3(TO-triolein; ML-methyl laurate; MO-methyl oleate).

The liquid length shows a linear relation for biodiesel and SVO pure components with their boiling point. The triolein exhibits longest liquid length with highest normal boiling point followed by methyl oleate, methyl laurate, and dodecane. The effect of ambient temperature conditions is shown with three temperature conditions 900 K, 1000 K and 1200 K. The specific energy ratio of methyl oleate decreases sharply with increase in an ambient gas temperature from 900 K to 1200 K with the corresponding decrease in liquid length. The similar effect is observed for energy ratio and liquid length for the methyl laurate. Thus, it can be said that the effect of specific energy ratio on the liquid length is seen to be pronounced at lower ambient gas temperature conditions [125].

5.5 Summary and Conclusions

The spray characteristics of evaporating spray, liquid length, and vapor length are predicted and compared for pure components of biodiesel and SVO at engine-relevant conditions. The CFD spray models are validated with experimental data available in the literature for various fuels under evaporating conditions. The validated spray models are then used to predict the liquid length and vapor length of pure components under late-cycle post-injection and near top-dead-center injection conditions. The predicted liquid and vapor length are found to be the function of the fuel properties and an ambient gas conditions.

The liquid length of methyl oleate is higher under late-cycle post-injection conditions studied. It may lead to impingement of liquid fuel on the combustion chamber walls. The observed wall impingement behavior for methyl oleate can be extended for all the commonly used biodiesels such as soybean, rapeseed, karanja and jatropha. The liquid length for methyl laurate at late-cycle post-injection conditions is lower than that of methyl oleate and may not impinge on the combustion chamber wall. This conclusion may be applied for coconut and palm kernel biodiesel having a higher percentage of methyl laurate. The FAME components studied under top-dead-center injection conditions are found to have a lower liquid length which can avoid wall impingement.

The vapor length at top-dead-center conditions for all the biodiesel pure com-

ponents are similar. However, at lower ambient gas density and ambient gas temperature conditions, methyl oleate is found to produce higher vapor length which decreased with increase in an ambient gas temperature. The SVO pure components, trilaurin, and triolein, have similar liquid length and vapor length, which is higher than that of their corresponding FAME. These triglycerides are more prone to wall impingement even at top-dead-center conditions.

The liquid length, vapor length and spray vapor area for methyl laurate is found to be similar to that of dodecane. This indicates that methyl laurate may have similar spray behavior as that of diesel fuel. The spray vapor area for triglycerides is significantly lower than that of FAME. The liquid length of all the pure components studied is found to be related to the specific energy ratio. Linear correlation is confirmed between the liquid length and the boiling temperature of the biofuels.

6 Multi-Component Spray Characteristics

The spray characteristics such as liquid length, vapor length, and spatial mass fraction distribution for multi-component fuel using multi-component surrogate are studied in this chapter. The evaporation characteristics of representative single component and multi-component surrogate of diesel and biodiesel are compared at engine-relevant conditions. The effect of diesel and biodiesel composition on spatial mass fraction distribution is studied with change in the percentage of a volatile component of the fuel.

6.1 Validation of Multi-Component Evaporation Model

The validation of the multi-component evaporation and heat transfer model used in the study is discussed in this section. The numerical model is validated for diesel, soybean biodiesel, and jatropha biodiesel. The composition of these fuels used for the simulation is given in Table. 6.1.

Table 6.1: Composition (liquid mass fraction) of the fuels used in the present study.

Fuel	Pure Components(Liquid mass fraction)						
Diesel	C_7H_8(0.27)	$C_{10}H_{22}$(0.12)	$C_{12}H_{26}$(0.20)	$C_{14}H_{30}$(0.21)	$C_{16}H_{34}$(0.11)	$C_{18}H_{38}$(0.09)	
Coconut	ML(0.54)	MM(0.21)	MP(0.10)	MS(0.04)	MO(0.11)		
Soybean	MP(0.08)	MS(0.04)	MO(0.25)	MLn(0.55)	MLLn(0.08)		
Palm	MM(0.01)	MP(0.41)	MS(0.04)	MO(0.43)	MLn(0.11)		

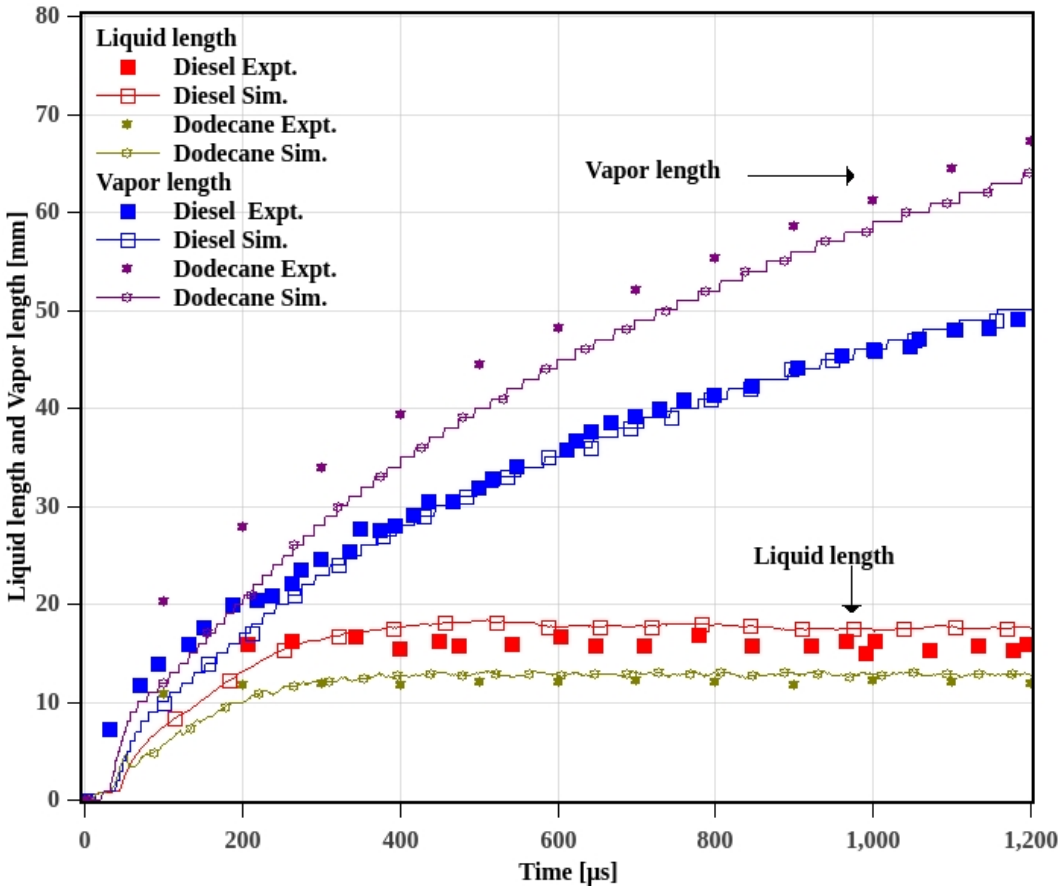

Figure 6.1: Validation of numerical model with diesel spray at an ambient gas temperature 900 K, and pressure of 60 bar [108] and dodecane spray at an ambient gas temperature 1400 K, and pressure of 30 bar [120].

The predicted liquid length and vapor length of diesel multi-component fuel at an ambient temperature of 900 K and pressure of 60 bar is observed to be comparable with the measured data (Fig. 6.1). Similarly, the predicted liquid length and vapor length of pure component dodecane are found to be in good agreement with the measurement.

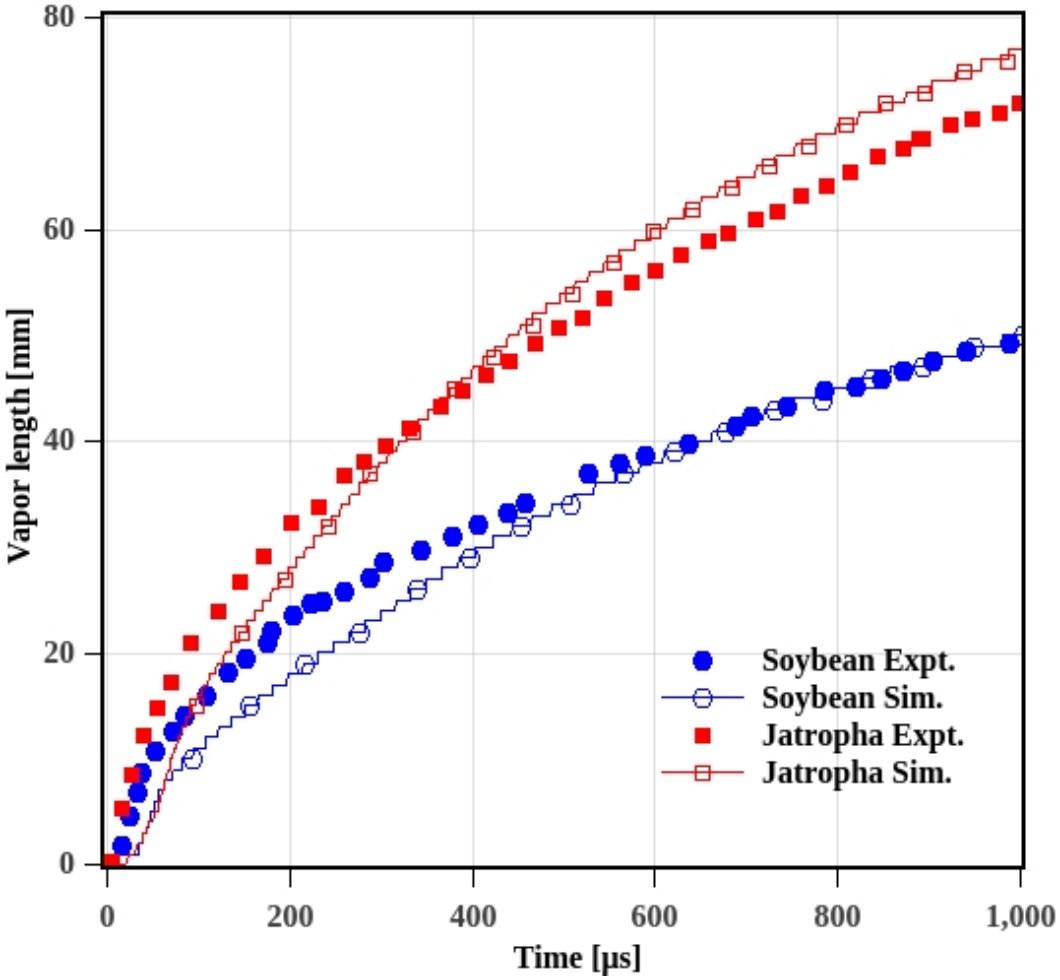

Figure 6.2: Vapor length measurement validation for biodiesel of soybean at an ambient gas temperature of 900 K, and pressure of 60 bar [90] and jatropha at an ambient gas temperature of 900 K, and pressure of 50 bar [84].

The vapor length for the biodiesel of soybean and jatropha spray are compared in the Fig. 6.2. The vapor length of this multi-component spray is also in good agreement with the measurement data.

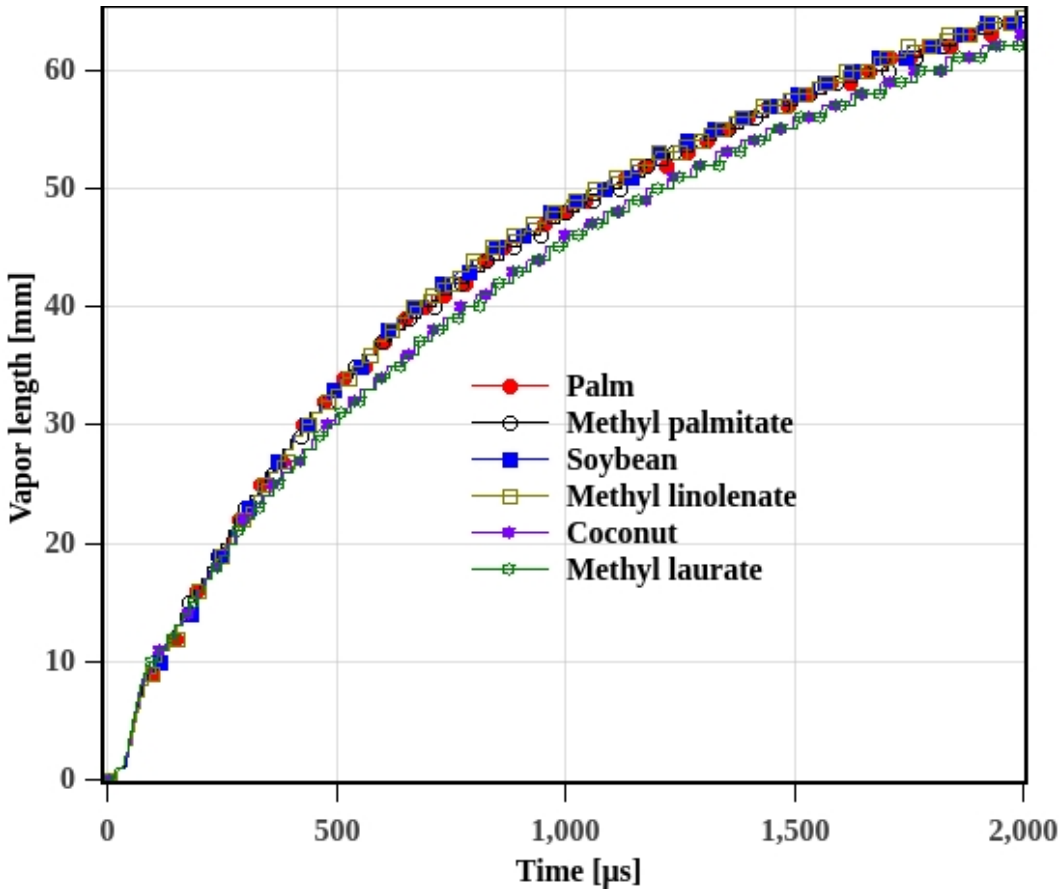

Figure 6.3: Vapor length of biodiesel and their representative surrogate single component.

The validated model is used to predict the vapor length of coconut, soybean and palm biodiesel with their respective surrogate as shown in Fig. 6.3. Methyl laurate is used as a single component surrogate for coconut biodiesel, and methyl palmitate is used as a single component surrogate for palm biodiesel. The soybean biodiesel is represented by methyl linolenate. The vapor length using a multi-component and single component representative is found to be similar. Thus, it can be said that the use of single component surrogate of real fuel is valid for predicting the liquid length and vapor length of the real multi-component fuel.

6.2 Vapor Mass Fraction of Single Component and Multi-Component Fuel

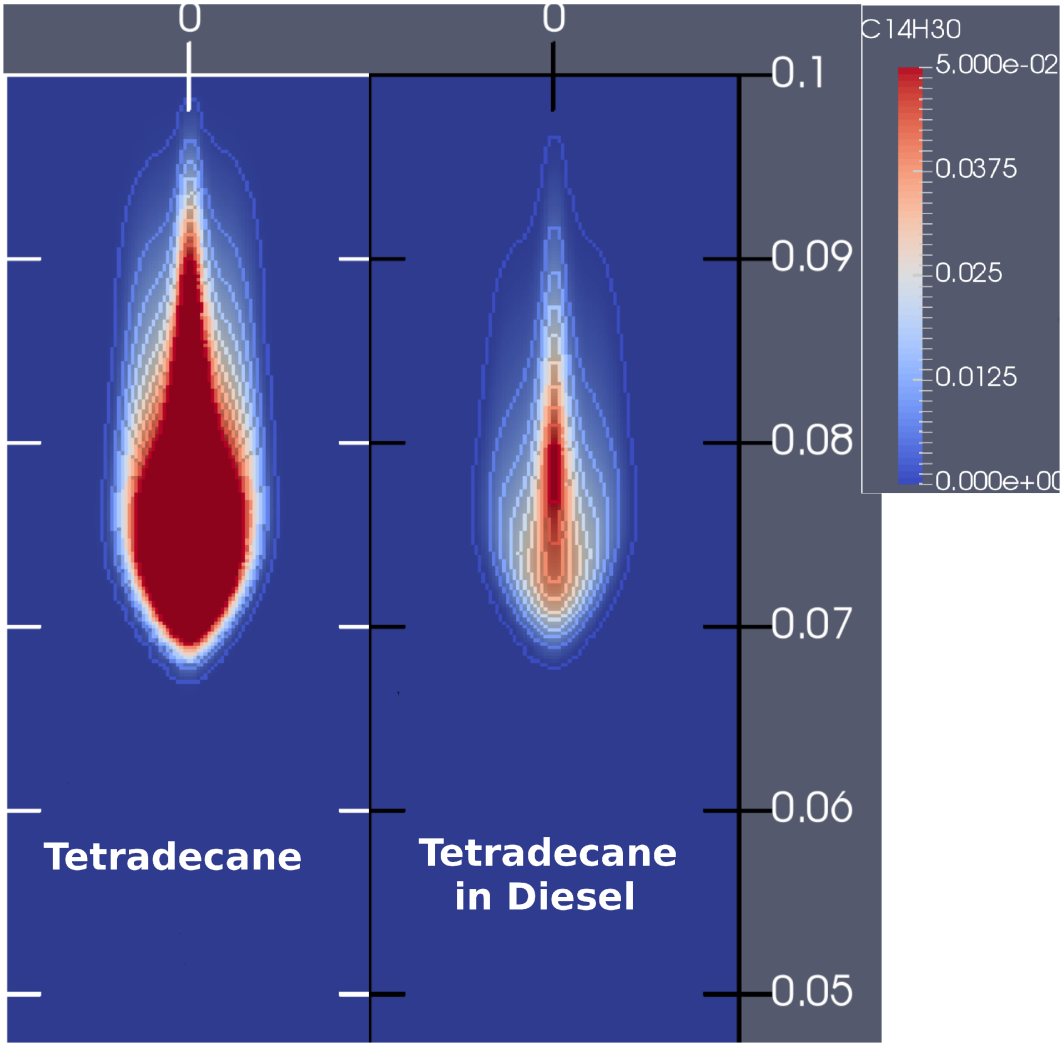

Figure 6.4: Mass fraction distribution of tetradecane in diesel spray and pure tetradecane spray at 0.5 ms after the start of injection.

The vapor mass fraction distribution which determines the equivalence ratio, ignition and combustion characteristics of the fuel are studied for both multi-component and corresponding single component surrogate. The prediction of air-fuel mixture distribution is of significance for the accurate prediction of emission profile of the particular fuel used in the CI engine. Hence, the mass fraction distribution of the spray for the multi-component and its single component surrogate is compared in this section. The diesel fuel is represented by tetradecane or dodecane as single component surrogate fuel. Similarly, various biodiesels are represented by methyl oleate or methyl laurate or methyl palmitate. It will be important to know how their vapor mass fraction distribution in a single component and multi-component fuel compares.

The distribution of vapor mass fraction of pure tetradecane spray and tetradecane in diesel spray is compared in Fig. 6.4. The spatial distribution of tetradecane is significantly different in both the sprays. The mass fraction of tetradecane is significantly low near the nozzle for multi-component spray. The multi-component diesel has 21% tetradecane and 27% toluene. The toluene having a boiling point of 380 K evaporates quickly near the nozzle whereas evaporation of tetradecane takes place at around 20 mm below the nozzle tip. The presence of toluene delays the evaporation of tetradecane. This indicates that multi-component fuel will have stratification in vapor mass fraction distribution. The vapor mass fraction distribution which determines the equivalence ratio, ignition and combustion characteristics will be different for multi-component and corresponding single component surrogate.

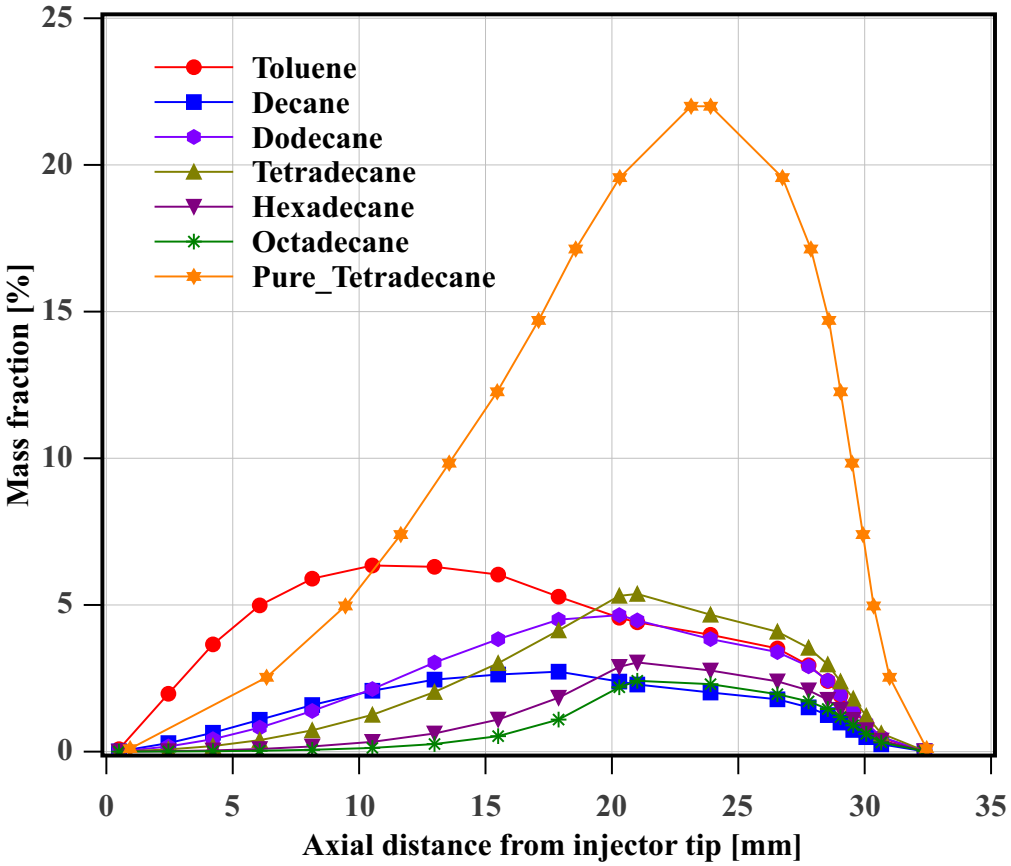

Figure 6.5: Mass fraction distribution along the axis of the spray for multi-component diesel spray and pure tetradecane spray at 0.5 *ms* after the start of injection.

The mass fraction distribution of multi-component diesel and its single component surrogate, tetradecane, at 0.5 ms after the start of injection is shown in the Fig. 6.5.

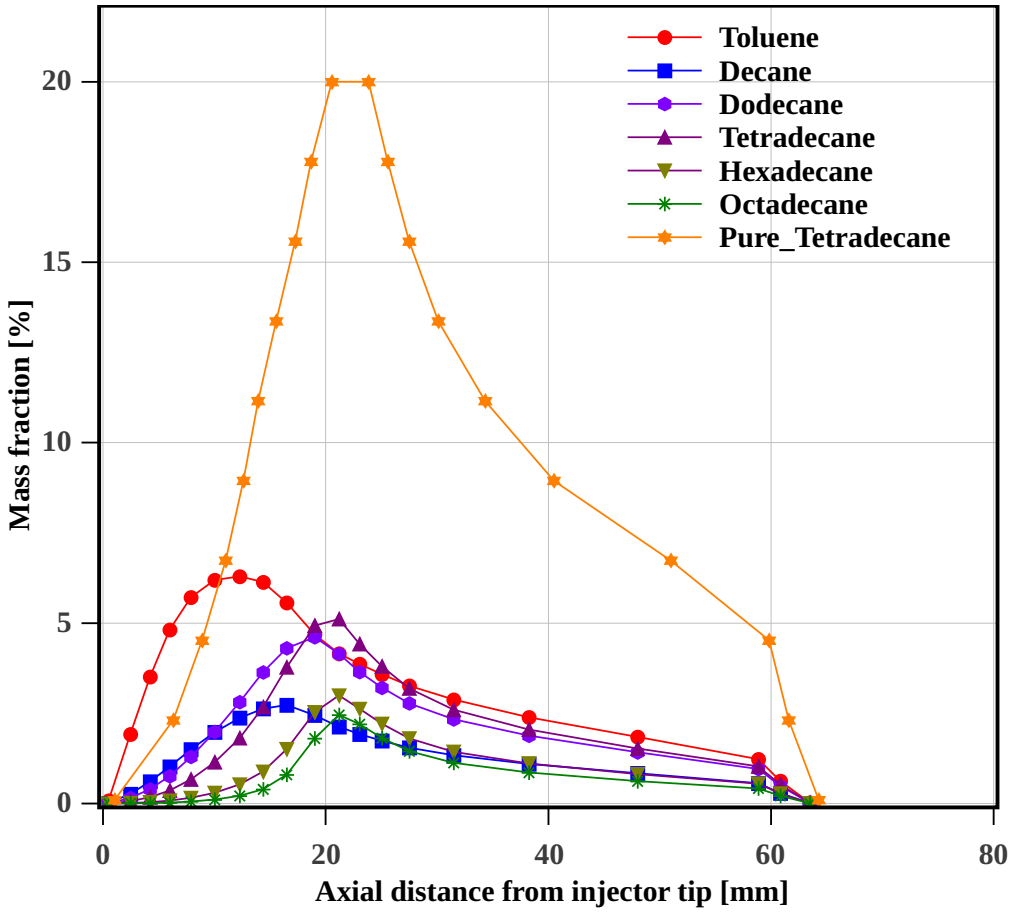

Figure 6.6: Mass fraction distribution along the axis of the spray for multi-component diesel spray and pure tetradecane spray at 2 ms after the start of injection.

The toluene, decane, and dodecane present in diesel have lower NBP (Fig. 2.1) than that of tetradecane. Higher volatility of toluene, decane, and dodecane results in peak locations of mass fraction near the nozzle tip. The peak positions are below 20 mm for both the cases of 0.5 ms (in Fig.6.5) and 2 ms (in Fig.6.6) after the start of injection. Hexadecane and octadecane which have NBP similar to that of the tetradecane, exhibit similar mass fraction profile peak positions around 20 mm from the nozzle tip. The nature of highly volatile components in the composition, tends to evaporate at a faster rate and produces a large quantity of evaporated mass near the nozzle. This nature could not be captured with single component diesel surrogate tetradecane. The mass fraction profile of single component surrogate of diesel, tetradecane, is observed to be similar to that of hexadecane and octadecane in diesel due to their similar properties specifically NBP temperature. Thus, it can be said that for diesel, the tetradecane cannot capture the nature of the mass fraction profile of highly volatile component present in the diesel.

The commonly used biodiesel contains predominantly five to six components in its composition (Table 6.1). The variation in NBP temperature of this components is small as compared to that of diesel components as seen from Fig. 2.1. The methyl laurate has a lowest boiling point of 540 K among the biodiesel constituents and methyl oleate, linoleate, and linolenate have a similar boiling point around 620 K. Biodiesels can be categorized on the basis of the similarity in the components present in its composition and their physical properties. Hence, soybean can be represented by methyl linoleate, the palm can be represented by methyl palmitate and coconut can be represented by methyl laurate.

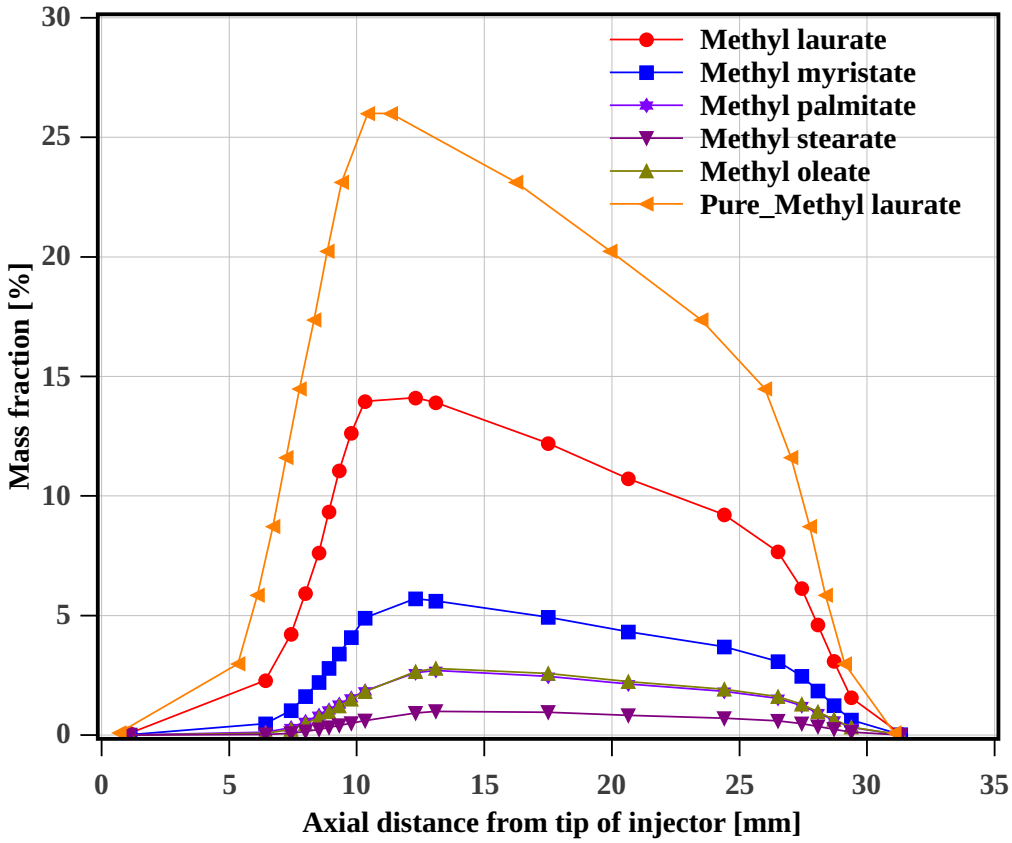

Figure 6.7: Mass fraction distribution along the axis of the spray for multi-component coconut fuel and pure component methyl laurate at 0.5 ms after the start of injection.

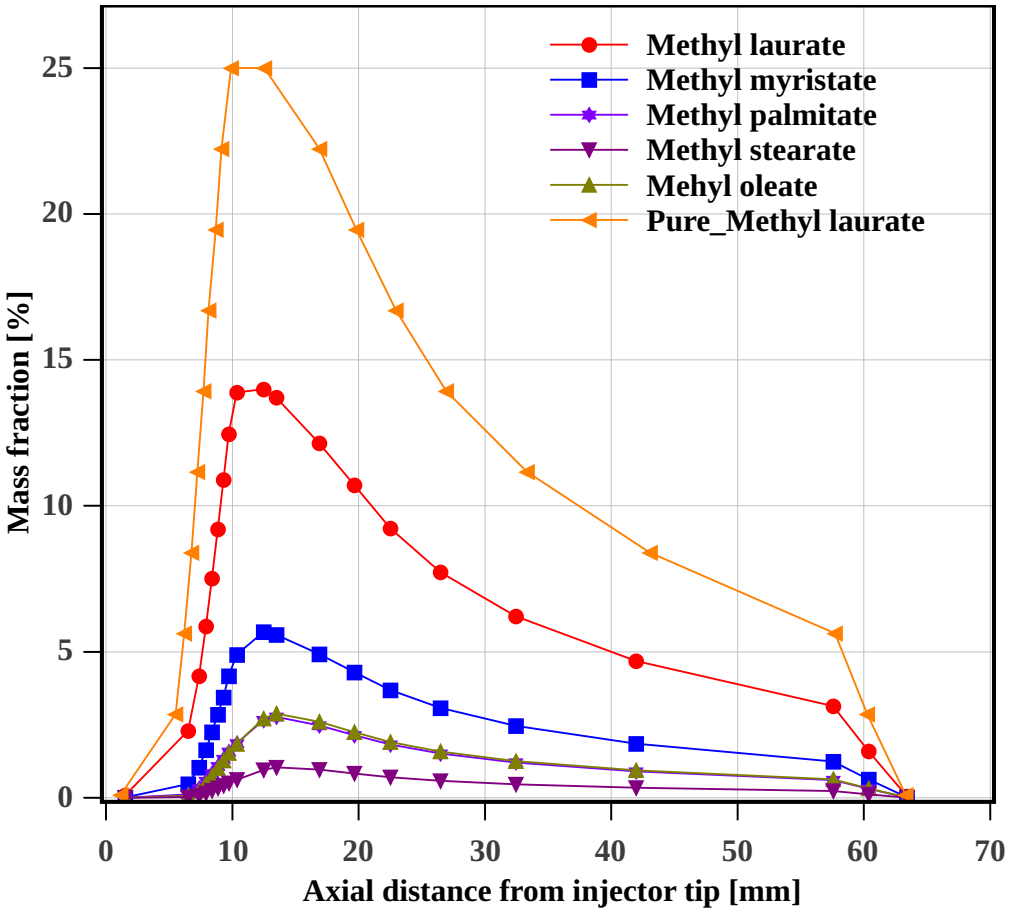

Figure 6.8: Mass fraction distribution along the axis of the spray for multi-component coconut fuel and pure component methyl laurate at 2 ms after the start of injection.

The axial mass fraction distribution of coconut biodiesel and the surrogate is compared at 0.5 ms after the start of injection in Fig. 6.7 and for 2 ms in the Fig. 6.8. The coconut biodiesel is modeled using five components while methyl laurate is used as a single component surrogate. It is observed that the mass fraction peaks of multi-component fuel is in accordance to the volatility of the pure components. The methyl laurate (largest liquid mass fraction and highest volatility), has the peak value of 14% evaporated mass fraction at 10 mm below the nozzle tip. The methyl stearate, with the highest boiling point, exhibits lowest mass fraction peak value of around 1% at 15 mm below the nozzle tip. The mass fraction distribution curve of methyl palmitate and methyl oleate overlaps due to negligible difference between their NBP and similar proportion in the coconut biodiesel. The mass fraction distribution curve in case of pure component spray is identical to that of methyl laurate except with higher values. This spatial distribution of multi-component vapor mass is not available with single component model. This is important as there is a difference in chemical kinetics of each component and their mixture. This affects the prediction of real fuel ignition and combustion characteristics and engine-out emissions.

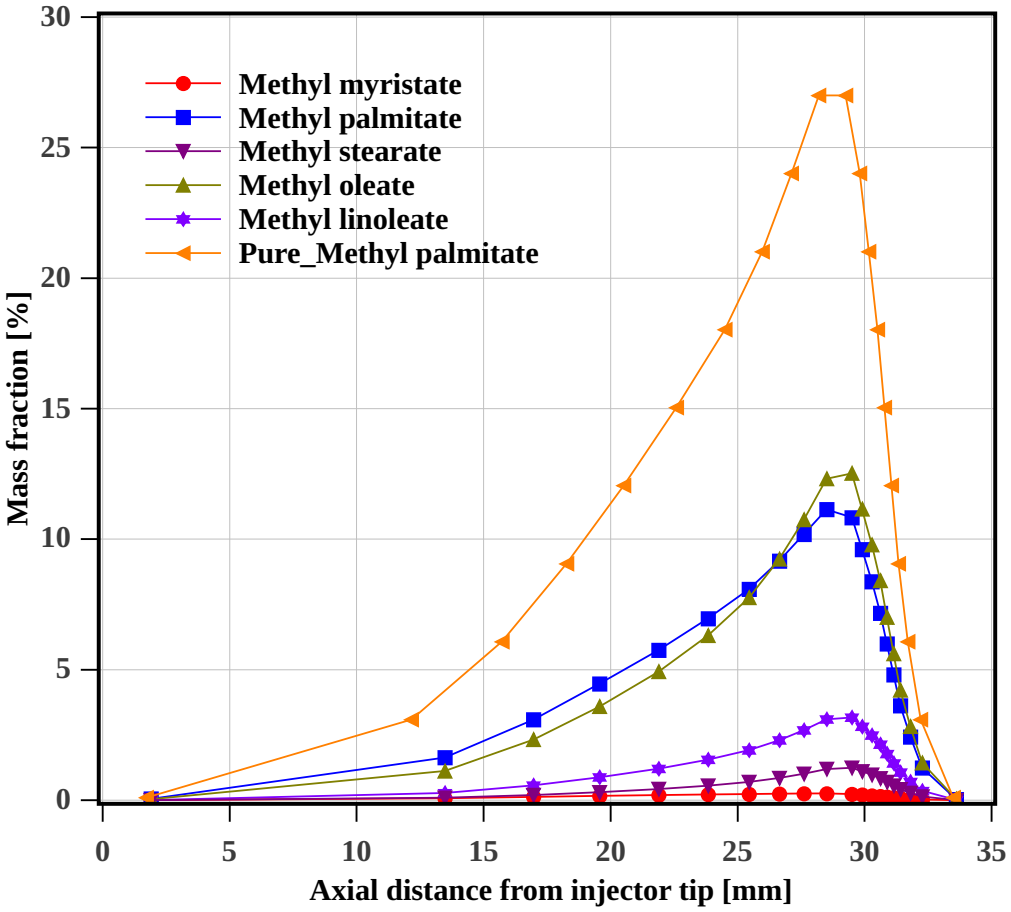

Figure 6.9: Mass fraction distribution along the axis of the spray for multi-component palm biodiesel and pure component methyl palmitate at 0.5 ms after the start of injection.

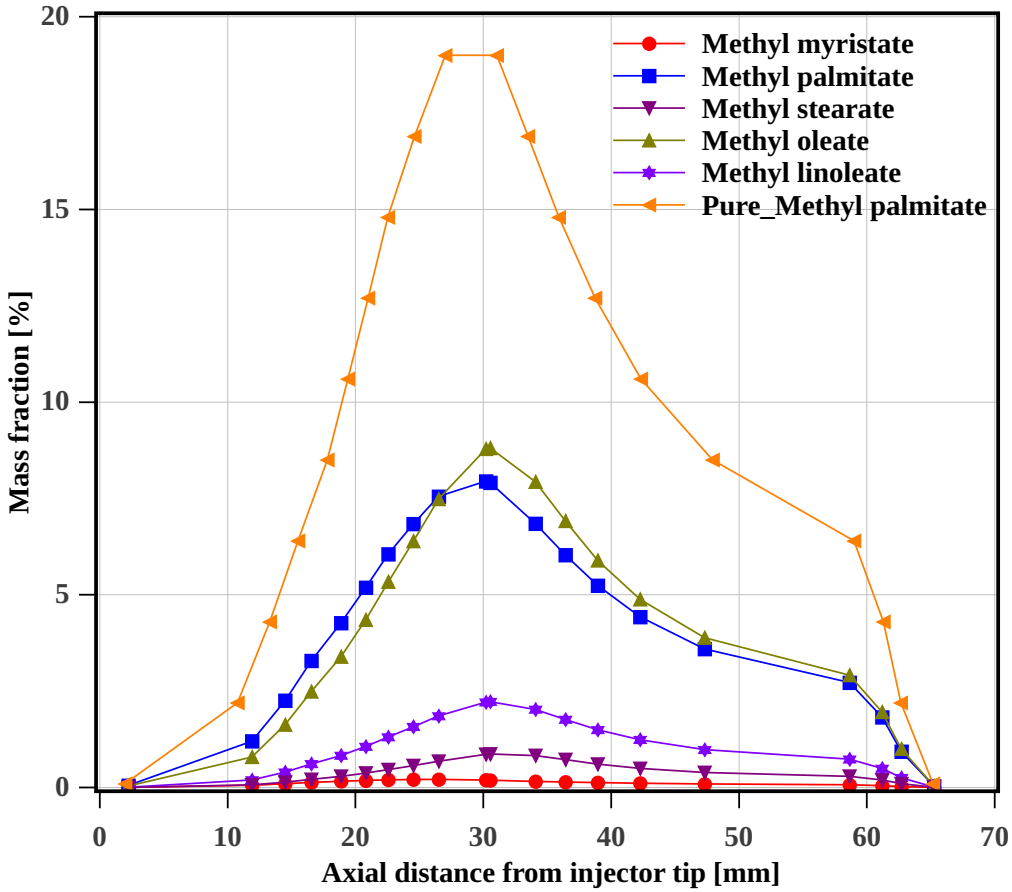

Figure 6.10: Mass fraction distribution along the axis of the spray for multi-component palm biodiesel and pure component methyl palmitate at 2 ms after the start of injection.

The vapor distribution of palm biodiesel and its representative methyl palmitate is shown in the Fig. 6.9. It is observed that mass fraction distribution curve for a single component and multi-component surrogate fuel sprays are similar except a difference in absolute value. This similarity is observed due to similar NBP temperature for all the components in the multi-component fuel. The palm biodiesel contains the similar percentage of methyl palmitate and methyl oleate and their NBP temperature is also comparable. This results in their identical spatial mass fraction distribution as seen in both the cases of 0.5 ms and 2 ms in the Fig. 6.9 and Fig. 6.10 respectively. The spatial mass fraction distribution with a single component surrogate, in case of palm biodiesel is observed to be similar to that of multi-component palm biodiesel. The highly volatile methyl myristate exhibits lowest mass fraction percentage due to its lower share of around 1% in palm biodiesel composition. Its effect is negligible on overall mass fraction profile.

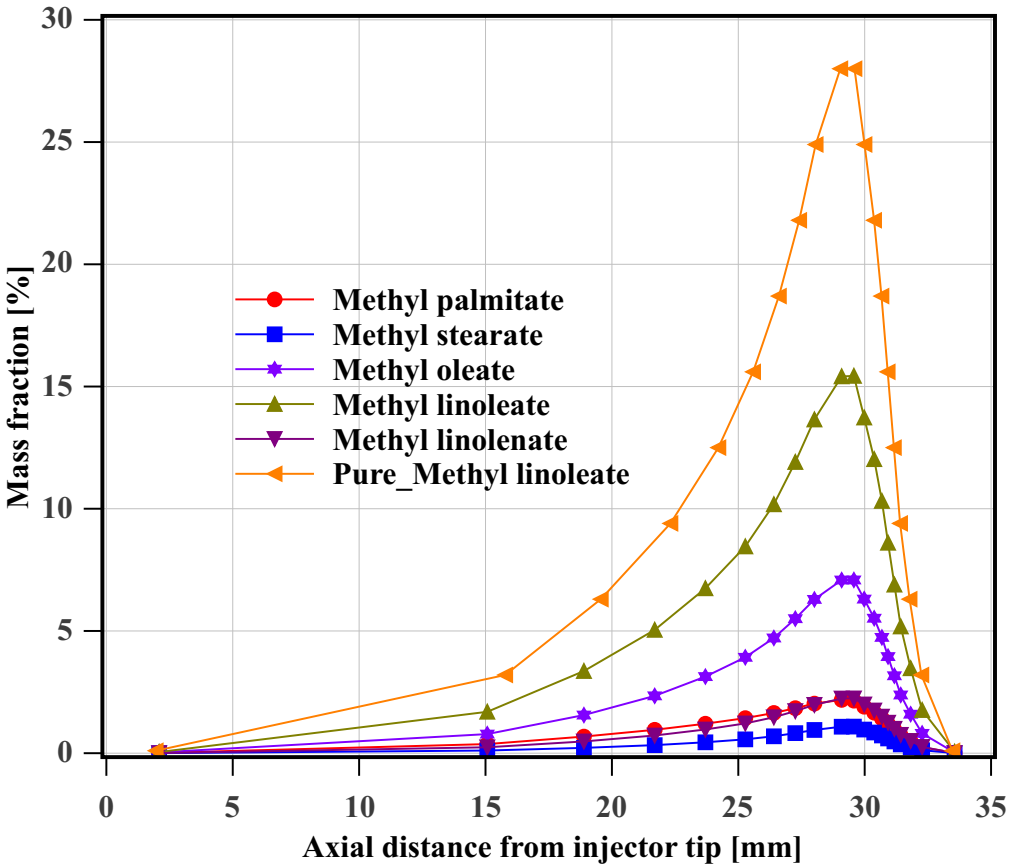

Figure 6.11: Mass fraction distribution along the axis of the spray for multi-component soybean fuel and pure component methyl linoleate at 0.5 ms after the start of injection.

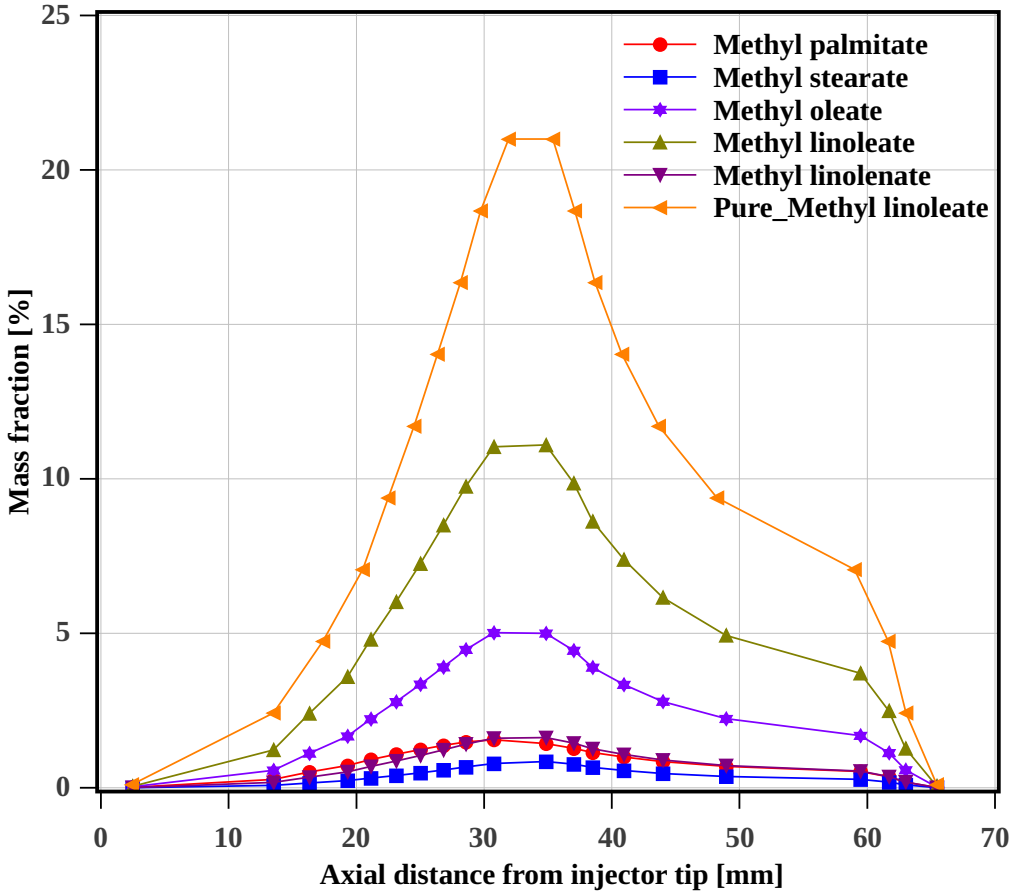

Figure 6.12: Mass fraction distribution along the axis of the spray for multi-component soybean fuel and pure component methyl linoleate at 2 ms after the start of injection.

The multi-component surrogate of soybean biodiesel and its single component surrogate methyl linoleate spray is compared. The axial mass fraction distribution at 0.5 ms after the start of injection is compared in Fig. 6.11. The mass fraction distribution of all the components including single component surrogate is observed to be similar including the case of 2 ms after the start of injection as shown in Fig. 6.12. This is due to similar normal boiling temperature for these pure components. The observed variation in the peak values of each pure component is due to the difference in their respective proportion in the composition. Thus, the single component methyl linoleate is found to represent similar spatial mass fraction distribution as that of multi-component soybean biodiesel.

The studies on diesel and biodiesels of coconut, palm, and soybean indicate that the composition of the multi-component fuel and the NBP temperature of the constituent influence the vapor mass fraction distribution. Higher volatile component tend to evaporate early and shows a peak near to the nozzle while components with lower volatility evaporate at a farther distance from the nozzle tip. A percentage of a volatile component present in the composition is also observed to have an impact on overall distribution.

6.3 Mass Fraction Distribution of Hypothetical Fuel

In order to isolate the effect of pure components volatility from its proportion in biodiesel composition, the hypothetical fuel is implemented and studied. The composition of the hypothetical fuels has similar liquid mass fraction for all the pure components. The composition of the hypothetical fuels studied are shown in the Table. 6.2.

Table 6.2: Composition (liquid mass fraction) of hypothetical fuels.

Hypothetical fuels	Pure Components(Liquid mass fraction)					
Diesel	C_7H_8(0.17)	$C_{10}H_{22}$(0.17)	$C_{12}H_{26}$(0.17)	$C_{14}H_{30}$(0.17)	$C_{16}H_{34}$(0.17)	$C_{18}H_{38}$(0.16)
Coconut	ML(0.20)	MM(0.20)	MP(0.20)	MS(0.20)	MO(0.20)	
Palm	MM(0.20)	MP(0.20)	MS(0.20)	MO(0.20)	MLn(0.20)	

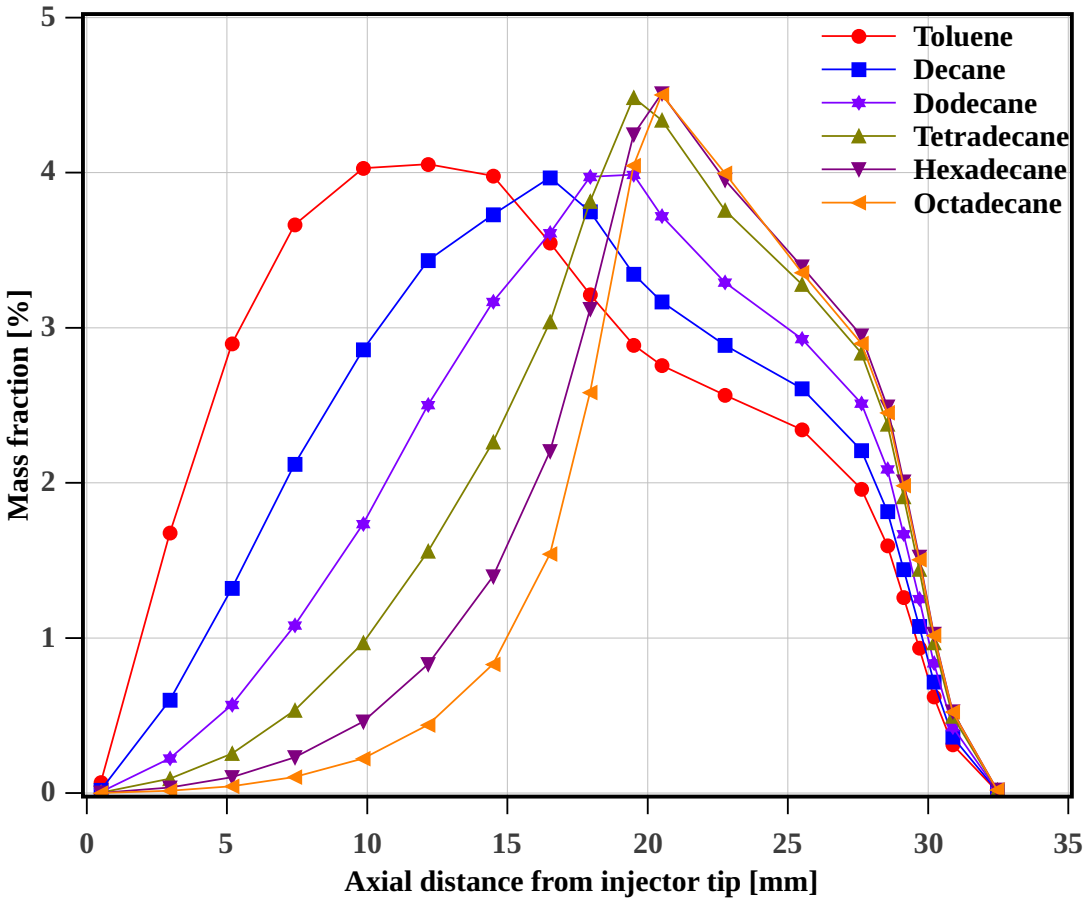

Figure 6.13: Mass fraction distribution along the axis of the spray for multi-component hypothetical diesel fuel at 0.5 ms after the start of injection.

The Fig. 6.13 and Fig. 6.14 shows the comparison of mass fraction distribution of six pure components present in hypothetical diesel fuel at 0.5 ms and 2 ms after the start of injection respectively. The mass fraction profile peaks of all the pure components are observed at different positions from the nozzle tip. The exceptions observed are hexadecane and octadecane whose profile peaks are positioned at around 20 mm below the nozzle tip. The observed difference in the locations of mass fraction profile peaks is due to the difference in their volatility, as the proportion of each component is kept same in hypothetical diesel.

This observation is valid for both the cases of 0.5 ms (in Fig. 6.13) and 2 ms (in Fig. 6.14) after the start of injection. The difference in the mass fraction values is minimum at around 60 mm downstream from the nozzle position at 2 ms (Fig. 6.14). It can be confirmed from the observations that there will be stratification of vapor mass fraction in spray for multi-component diesel fuel.

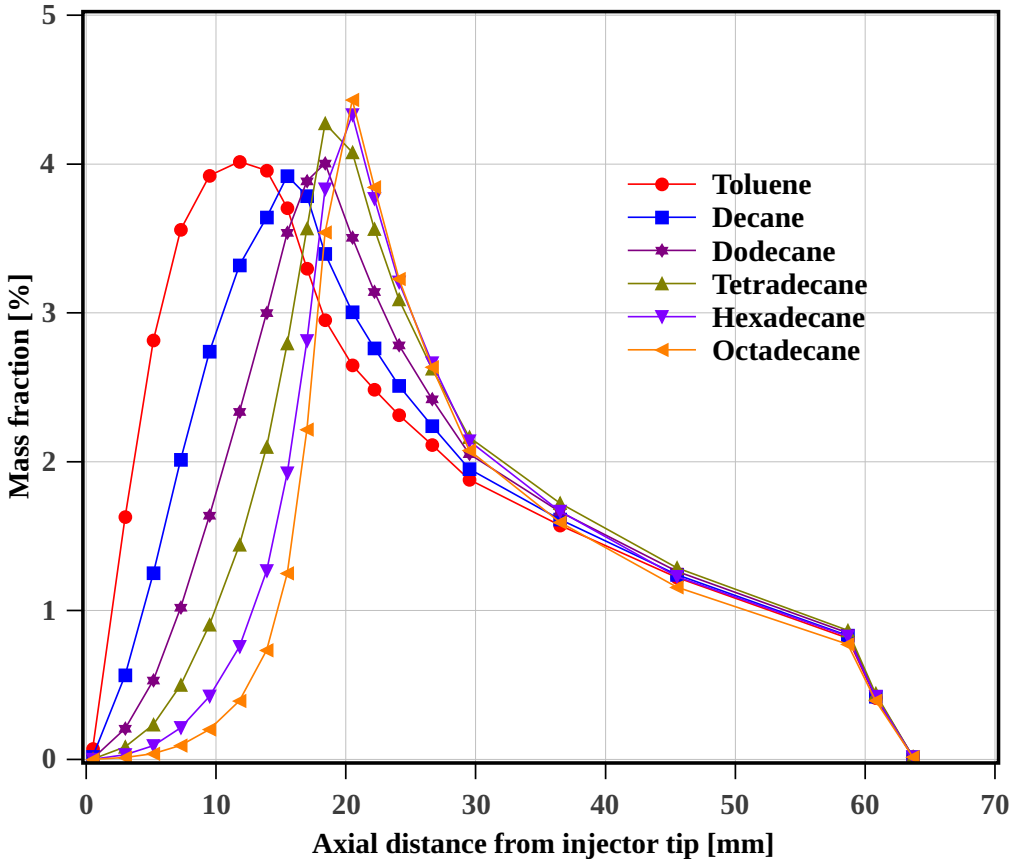

Figure 6.14: Mass fraction distribution along the axis of the spray for multi-component hypothetical diesel fuel at 2 ms after the start of injection.

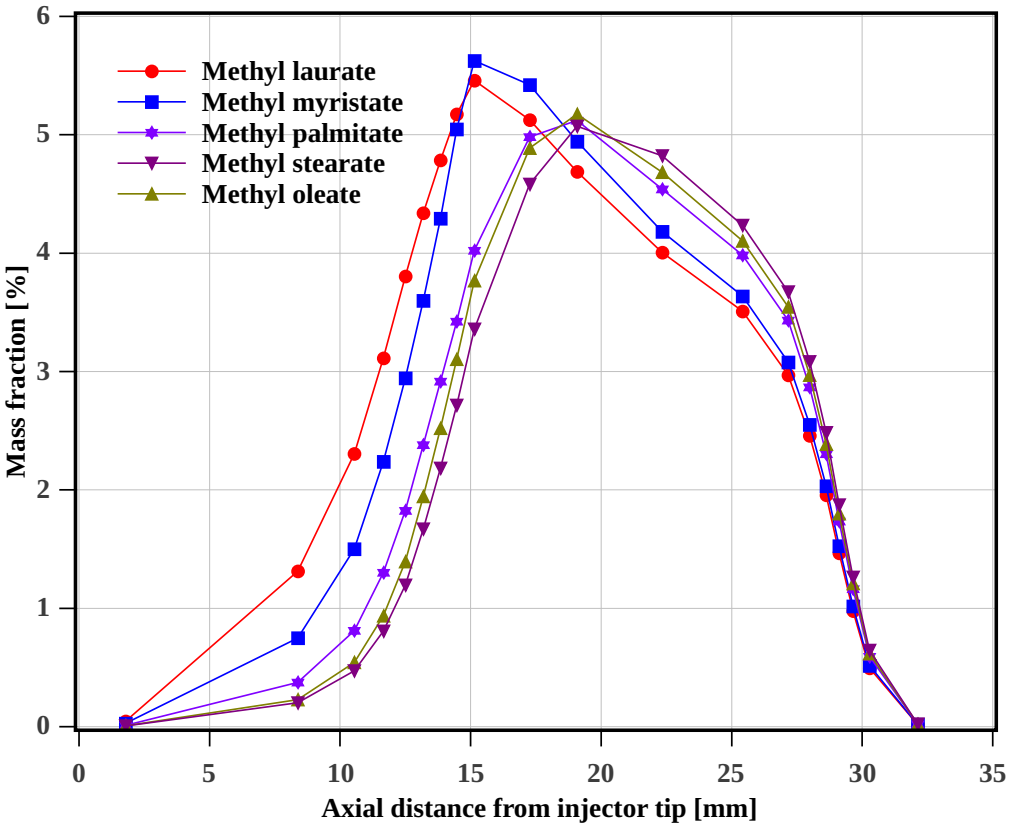

Figure 6.15: Mass fraction distribution along the axis of the spray for multi-component hypothetical coconut fuel at 0.5 *ms* after the start of injection.

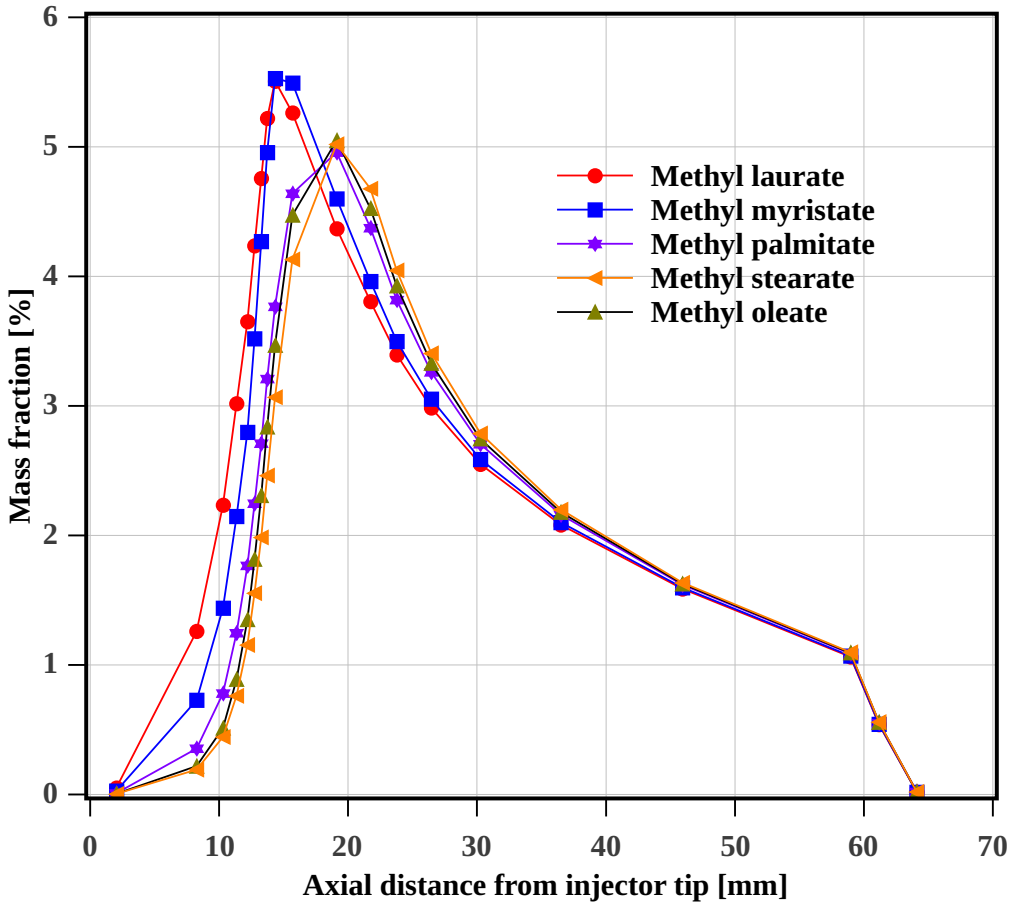

Figure 6.16: Mass fraction distribution along the axis of the spray for multi-component hypothetical coconut fuel at 2 ms after the start of injection.

The biodiesel mass fraction distribution of hypothetical biodiesels such as coconut and palm is discussed. Similar to hypothetical diesel fuel, each of the biodiesel is modeled with the equal proportion of pure components. The hypothetical biodiesels are modeled with five pure components, the composition is given in the Table. 6.2. The Fig. 6.15 and Fig. 6.16 show comparison of mass fraction distribution for five pure components present in hypothetical coconut biodiesel at 0.5 ms and 2 ms after the start of injection respectively. Unlike the diesel fuel, there is small difference in peak location of evaporated mass fraction for pure components. The peak for methyl laurate and myristate is around 10 mm below the nozzle while peak for remaining components is around 15 mm below the nozzle tip. The observation is in-line with their NBP. This also confirms that the stratification in vapor mass fraction will decrease with decrease in difference of NBP of components. The location for highest concentration of component (methyl laurate) is around 15 mm below the nozzle tip compared to 10 mm in case of diesel fuel.

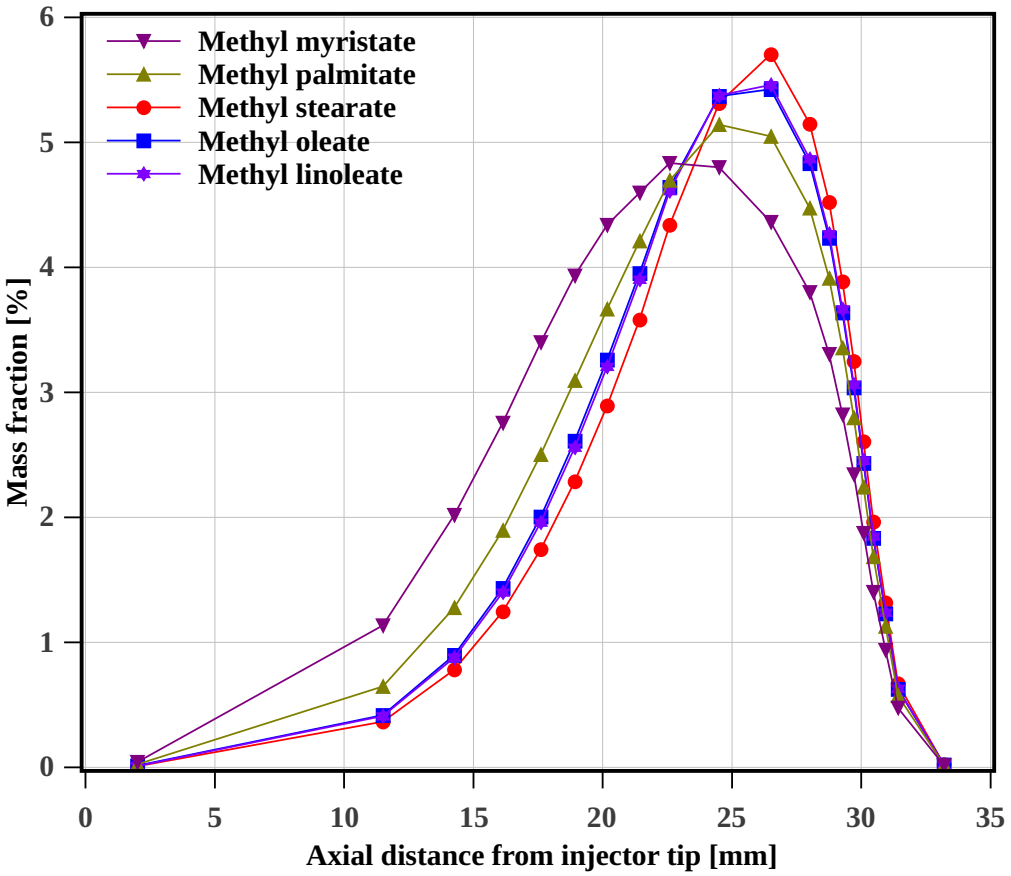

Figure 6.17: Mass fraction distribution along the axis of the spray for multi-component hypothetical palm fuel at 0.5 ms after the start of injection.

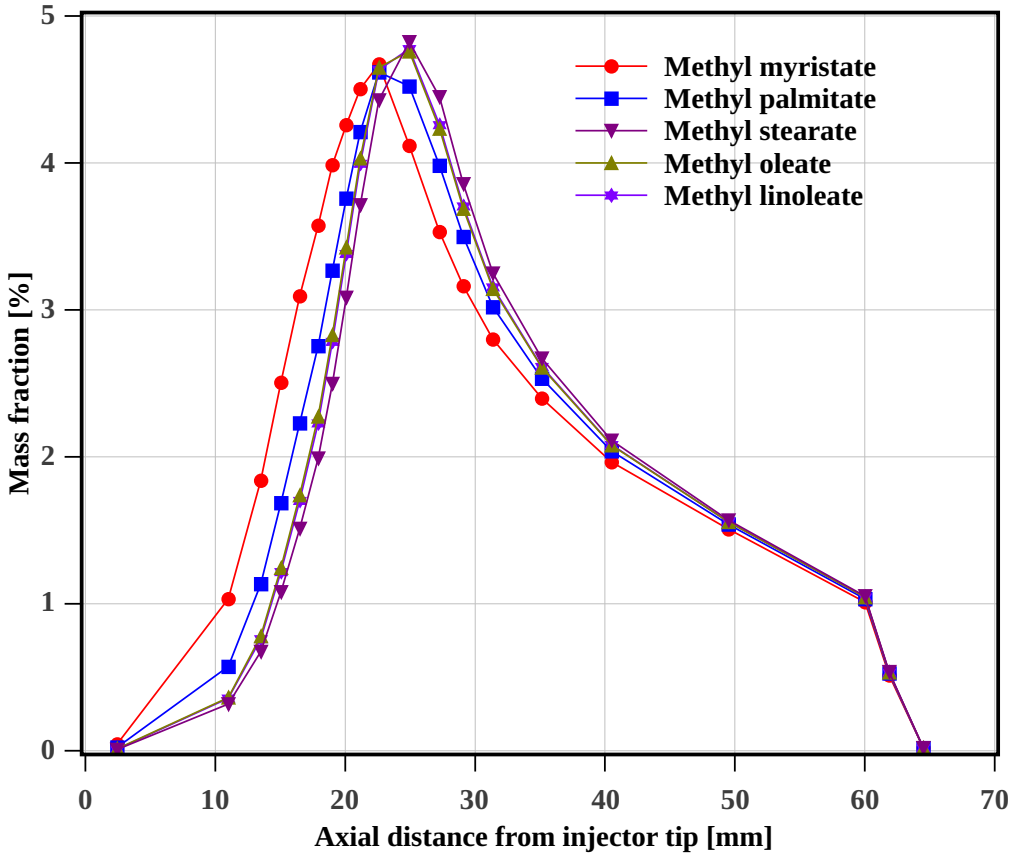

Figure 6.18: Mass fraction distribution along the axis of the spray for multi-component hypothetical palm fuel at 2 ms after the start of injection.

The evaporated mass fraction for hypothetical palm biodiesel spray is shown in Fig. 6.17 and Fig. 6.18. The location of the highest mass fraction (methyl oleate) for palm is at 20 mm below the tip. The downstream shift observed is 10 mm with respect to the hypothetical diesel fuel and 5 mm with respect to coconut biodiesel. This shift of location observed for palm biodiesel may be attributed to the absence of highly volatile pure component such as toluene or methyl laurate.

Thus, it can be concluded that the nature of volatile component present in the fuel significantly affect the mass fraction distribution profile of particular fuel which consequently determines its ignition, combustion and emission characteristics.

6.4 Effect of Fuel Composition on Mass Fraction Distribution

The axial and radial vapor mass fraction distribution on the central plane of the chamber for pure components of diesel such as toluene, dodecane, and octadecane at 0.5 ms and 2 ms after the start of injection is compared in the Fig. 6.19. The 5% vapor mass fraction represented by red color is observed to be at around 10 mm from the nozzle position for toluene, whereas, for the dodecane, 5% vapor mass fraction is present at around 20 mm downstream. The observed quantitative difference in vapor mass fraction (5%, 4%, and 2%) for toluene, dodecane and octadecane can be related to the difference in the amount of heat energy required by each component for heating and latent heat of vaporization. It is observed that evaporation of octadecane starts much below the nozzle tip (after 10 mm) compared to toluene which shows evaporated mass fraction near to nozzle tip. Hence, the NBP and volatility of each pure component present in fuel play a major role in determining the quality of mixture formed.

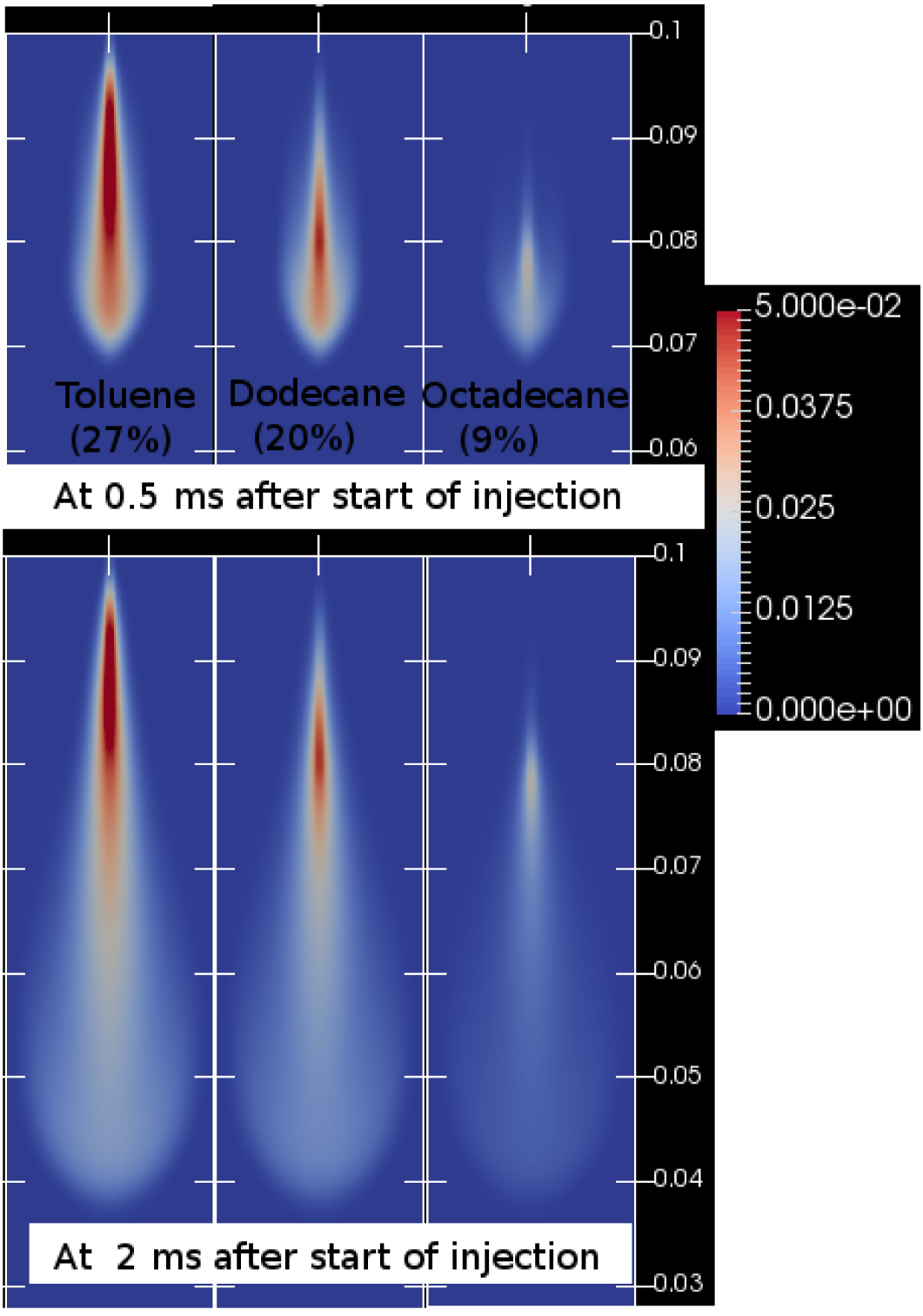

Figure 6.19: The comparison of evaporated mass fraction of toluene, dodecane and octadecane present in diesel fuel at 0.5 *ms* and 2 *ms* after the start of injection.

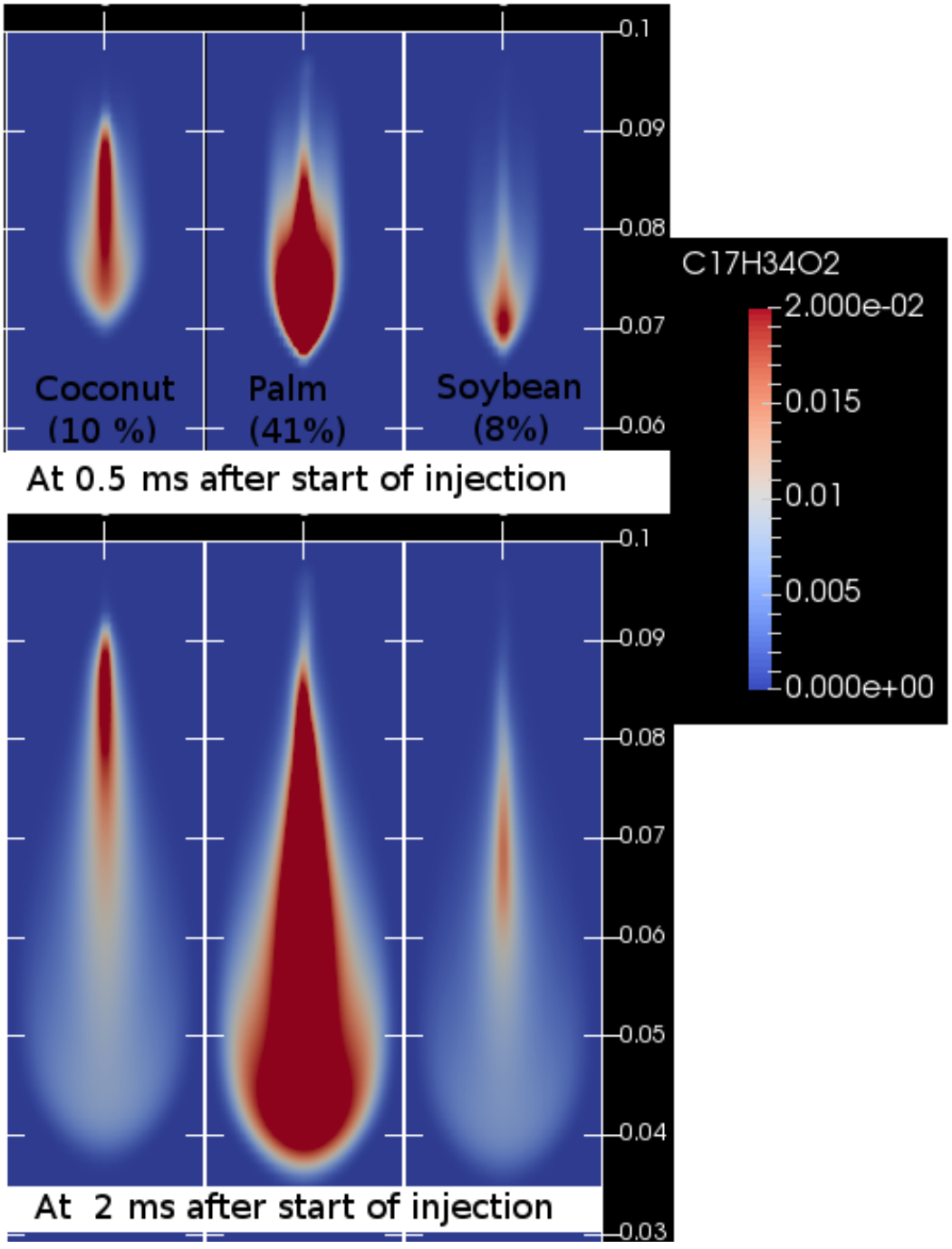

Figure 6.20: The comparison of evaporated mass fraction of methyl palmitate present in coconut, palm and soybean biodiesel at 0.5 ms and 2 ms after the start of injection.

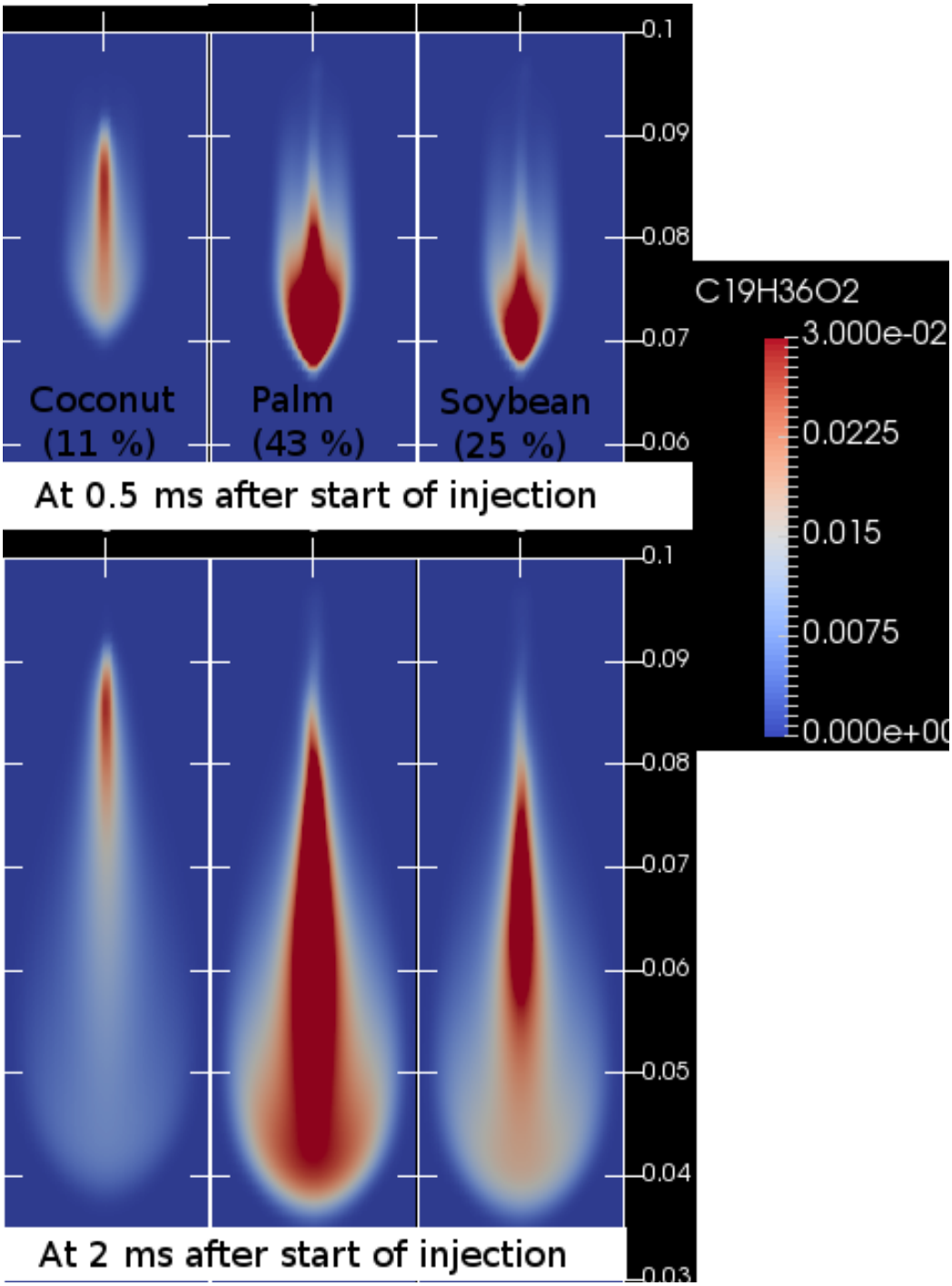

Figure 6.21: The comparison of evaporated mass fraction of methyl oleate present in coconut, palm and soybean biodiesel at 0.5 ms and 2 ms after the start of injection.

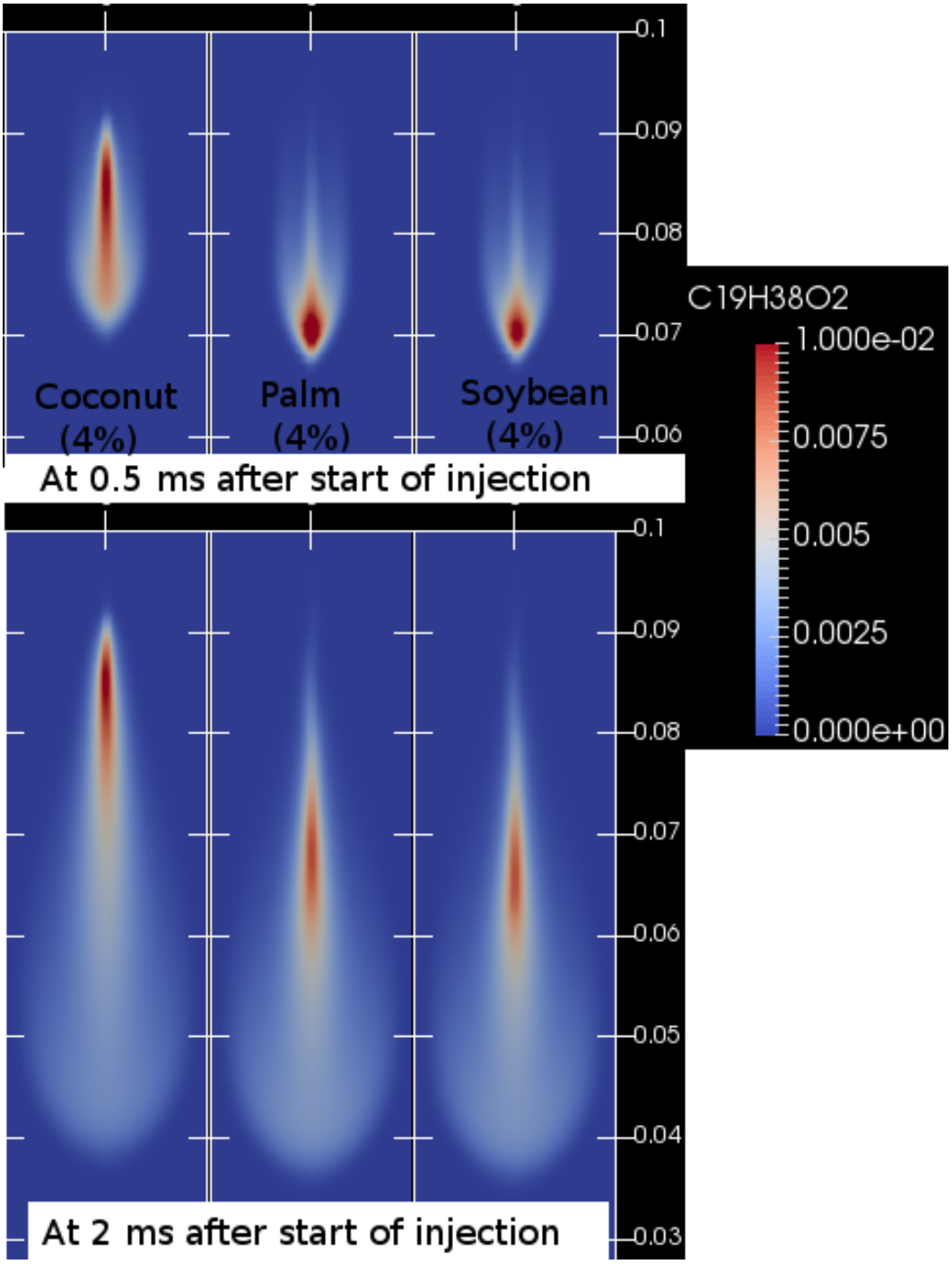

Figure 6.22: The comparison of evaporated mass fraction of methyl stearate present in coconut, palm and soybean biodiesel at 0.5 *ms* and 2 *ms* after the start of injection.

The biodiesels such as coconut, palm, and soybean pure component mass fraction are studied at 0.5 ms and 2 ms after the start of injection. The comparison of vapor mass fraction for the biodiesels is shown in the Fig. 6.20, 6.21 and 6.22. The Fig. 6.20 compares and shows the vapor mass fraction of methyl palmitate present in the different proportion in coconut, palm and soybean biodiesel at 0.5 ms and 2 ms after the start of injection. The coconut biodiesel and soybean biodiesel contains similar proportion of methyl palmitate which is 10% and 8% respectively, however, in palm biodiesel methyl palmitate is around 41%. The 2% vapor mass fraction indicated by red color is present at around 10 mm from injector position for both coconut and palm biodiesel. For soybean biodiesel the 1.5% to 2% vapor mass fraction is visible at around 30 mm downstream for both the cases of 1.5 and 2 ms. The soybean biodiesel contains heavier pure components such as methyl oleate (25%) and methyl linoleate (55%) in the significant proportion having higher NBP than that of methyl palmitate. The methyl oleate and methyl linoleate absorbs the heat from surrounding atmosphere for heating which delays the heating and vaporization of methyl palmitate. Hence, vapors of methyl palmitate are present at farther downstream at 30 mm from the injector. Unlike the case of soybean, the coconut biodiesel contains, the methyl laurate and methyl myristate in higher proportion with lower NBP than that of methyl palmitate. Thus, the evaporation of methyl palmitate is not delayed in case of the soybean. Furthermore, palm biodiesel, methyl palmitate, and methyl oleate shares similar proportion as well as around similar NBP. Thus the evaporation of the methyl palmitate is not affected by the presence of methyl oleate in palm biodiesel.

The evaporation behavior of methyl oleate in coconut, palm, and soybean biodiesel is shown and compared in the Fig. 6.21 at 0.5 ms and 2 ms after the start of injection. The evaporated mass fraction distribution of methyl oleate shown in the Fig. 6.21 and methyl palmitate vapor mass fraction as seen from the Fig. 6.20 for palm and coconut biodiesel are observed to be similar. This observed similarity may be attributed to similar NBP and proportion present in palm and coconut biodiesel. However, for soybean biodiesel, the methyl oleate vapor mass fraction distribution is observed to be significantly different than that of methyl palmitate. Specifically, in soybean biodiesel, methyl oleate 2% vapor mass fraction is observed to be present at

around 20 mm downstream to the injector position, whereas the methyl palmitate 2% vapor mass fraction is at 30 mm (in Fig. 6.20). The observed difference in the axial position of methyl oleate and methyl palmitate may be attributed to their significant difference in their proportion which dominates the lower NBP of methyl palmitate compared to methyl oleate in soybean biodiesel.

The methyl stearate vaporized mass is compared and shown in Fig. 6.22 for coconut, palm, and soybean biodiesel. The methyl stearate has higher NBP than that of methyl palmitate and methyl oleate thus, the evaporated vapor mass fraction is significantly lower than that of methyl oleate and methyl palmitate cases. On comparing methyl stearate vapor mass fraction in coconut, palm and soybean biodiesel, it can be seen that despite identical liquid mass fraction 4%, the vapor mass fraction of coconut biodiesel is different from palm and soybean biodiesel. The 1% vapor mass fraction of methyl stearate is present at around 15 mm in coconut biodiesel whereas, at 30 mm downstream for palm and soybean biodiesel. The near nozzle vapor mass fraction of methyl stearate observed for coconut biodiesel can be attributed to the presence of highly volatile components such as methyl laurate and methyl myristate.

It can be observed that the volatility of the pure components present in the fuel significantly affects the distribution of other pure components in it. Thus, it is essential to study the effect of variation in the proportion of such volatile pure components on the overall mass fraction distribution of the fuel. Hence, the effect of volatility of pure components and its proportion in fuel composition is studied by varying the composition of the multi-component fuel. The liquid mass fraction of the volatile components is varied within the range found in diesel and biodiesel available as fuel [1, 94, 108]. The composition of such fuel is given in the Table. 6.3. The volatile component such as toluene in diesel, methyl laurate in coconut biodiesel and methyl myristate in palm biodiesel is selected for the study based on their relatively lower NBP.

Table 6.3: The modified composition (liquid mass fraction) of the fuels used in the study.

Fuel	Pure Components (Liquid mass fraction)					
Dieselmodified	C_7H_8(0.15)	$C_{10}H_{22}$(0.15)	$C_{12}H_{26}$(0.23)	$C_{14}H_{30}$(0.23)	$C_{16}H_{34}$(0.13)	$C_{18}H_{38}$(0.11)
Coconutmodified	ML(0.44)	MM(0.24)	MP(0.13)	MS(0.06)	MO(0.13)	
Palmmodified	MM(0.06)	MP(0.40)	MS(0.03)	MO(0.42)	MLn(0.09)	

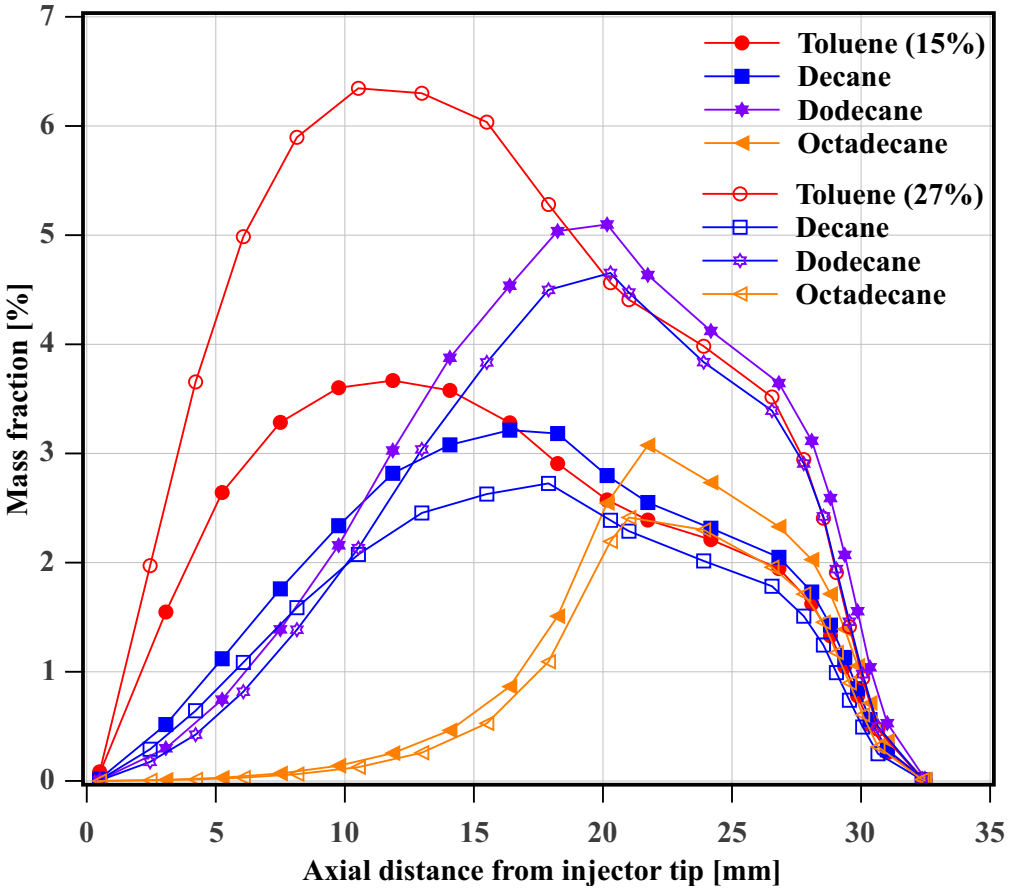

Figure 6.23: Comparison of mass fraction distribution along the axis of the spray for multi-component diesel spray with change in its composition at 0.5 ms after the start of injection.

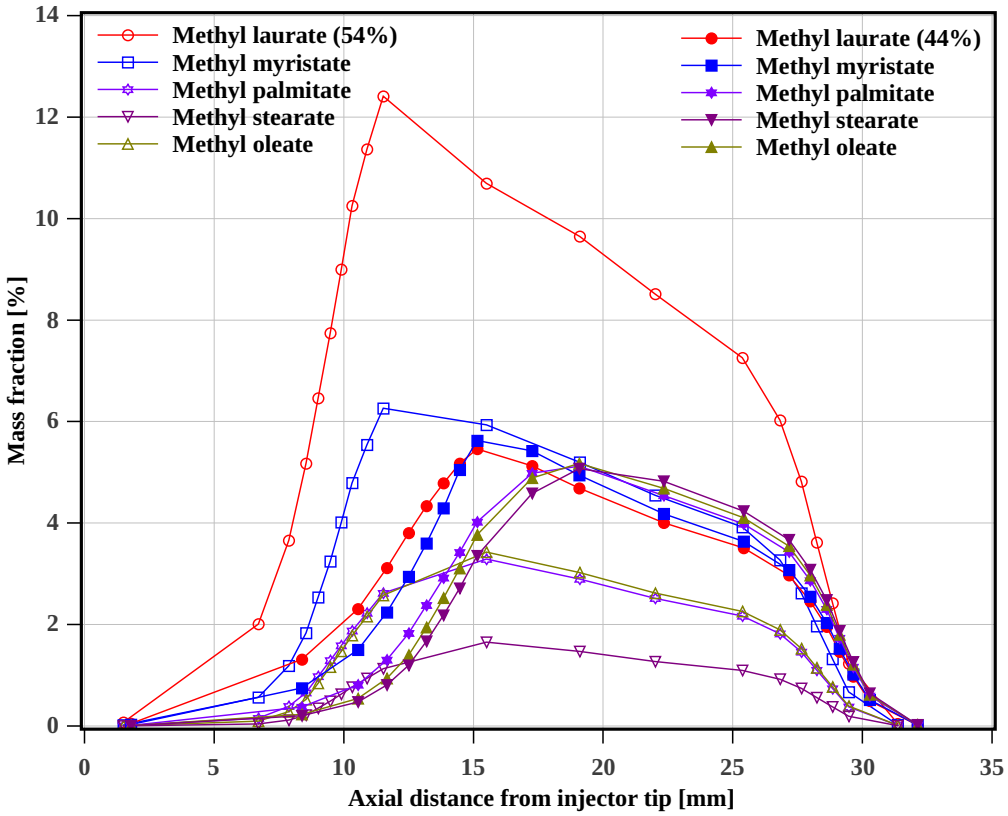

Figure 6.24: Comparison of mass fraction distribution along the axis of the spray for multi-component coconut fuel with change in its composition at 0.5 ms after the start of injection .

The vapor mass fraction distribution for diesel with two different compositions is compared in the Fig. 6.23. The diesel fuel composition with toluene 27% and 15% are compared. The composition of other components in diesel is changed with the highest component being dodecane and tetradecane (23%) in modified diesel. It is observed that the change in the evaporated mass fraction of toluene is proportionately decreased in the modified fuel. However, the mass fraction distribution curves have changed significantly. The modified diesel shows the highest percentage of dodecane vapor mass fraction (5%) at around 20 mm below the nozzle tip. The highest vapor mass fraction of toluene in modified diesel has dropped by more than half to 3.2%. The curve for tetradecane is not shown in the Fig 6.23 for clarity, and it was observed to follow the dodecane curve. It is seen that the change in the percentage of volatile component (toluene) in diesel has a significant impact on the distribution of vapor mass fraction. The components with higher NBP are not affected significantly. The change of mass fraction distribution may subsequently affect the local equivalence ratio, mixture temperature, ignition and combustion characteristics.

The vapor mass fraction distribution for coconut and modified coconut biodiesel is compared in Fig. 6.24. The liquid mass fraction of methyl laurate in coconut biodiesel is decreased from 54 to 44% in modified fuel. The overall change of its composition is shown in the Table. 6.3. The percentage of methyl laurate is still highest in the modified coconut biodiesel composition. The second largest component is methyl stearate with 24% contribution. The peak value of vapor mass fraction of methyl laurate decreased in modified biodiesel in the Fig. 6.24 similar to that of diesel. The peak value of the methyl laurate mass fraction is 6.4% for modified coconut biodiesel which is less than half of that for original composition. The decrease in vapor mass fraction is proportionately higher compared to decrease in the percentage of methyl laurate in the composition of the liquid fuel. The spatial distribution along the axis of the spray is also significantly different with the change in the composition of coconut biodiesel. The mass fraction curve of methyl laurate is shifted around 3 mm downstream to the injector position for modified biodiesel. It is observed that other three components have maximum vapor mass fraction of around 5%. A qualitatively similar shift of mass fraction for other components of the coconut biodiesel is observed. Thus, it can be said that the change in spatial mass

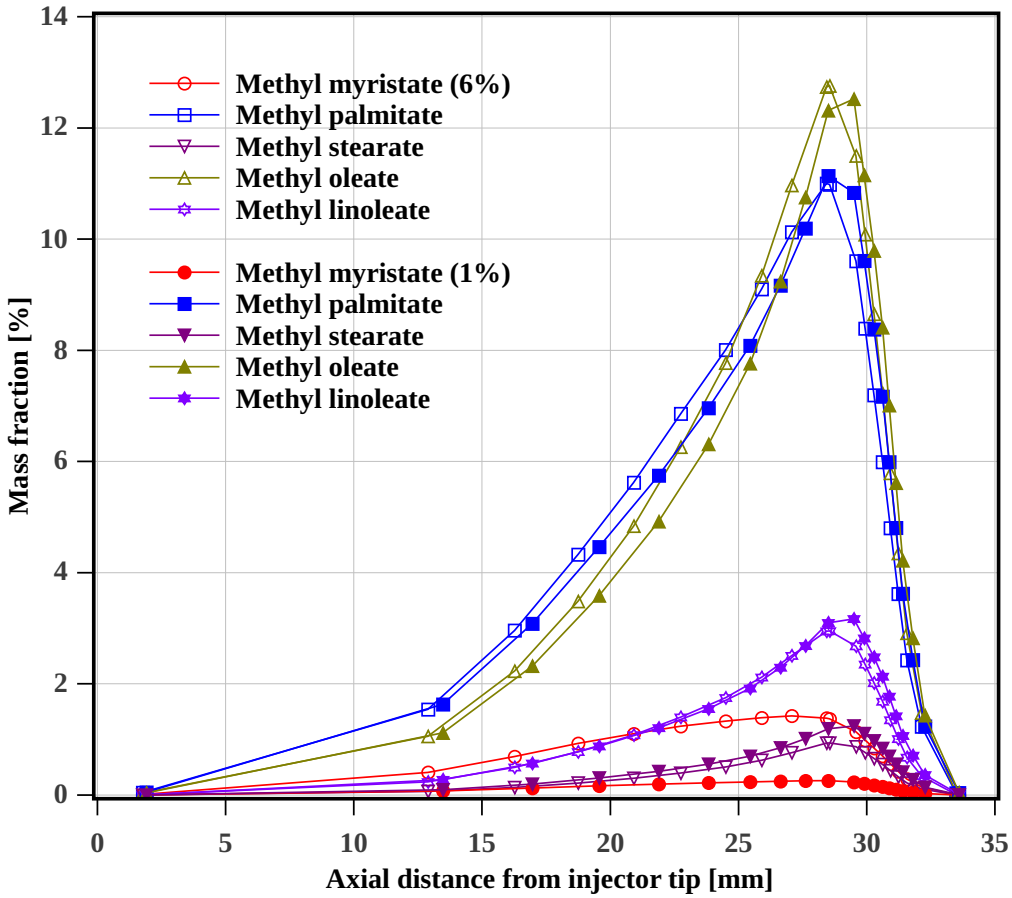

Figure 6.25: Comparison of mass fraction distribution along the axis of the spray for multi-component palm fuel with change in its composition at 0.5 ms after the start of injection.

fraction distribution should be expected with the change in biodiesel composition.

The effect on mass fraction distribution with change is palm biodiesel composition is presented in the Fig. 6.25. The methyl myristate liquid mass fraction is increased from 1 to 6% and the resultant change in the composition of the modified palm biodiesel is given in Table.6.3. The palm and modified palm biodiesel both have methyl palmitate and methyl oleate contributing maximum in their composition.

The proportionate change in the vapor mass fraction peak value is observed. However, the shift of the mass fraction curve, which is significant in case of coconut biodiesel is not present in the case of palm biodiesel. This is due to lower proportion of methyl myristate in the palm biodiesel. It can be said that the appreciable change in the spatial mass fraction distribution can be observed only when the composition of the volatile component varies significantly similar to that seen in diesel and coconut biodiesel. The minor change in the liquid mass fraction of the volatile component such as methyl myristate in palm biodiesel, would not cause a change in the vapor mass fraction distribution. It can be said that the presence of volatile pure components has a significant impact on the spatial distribution of fuel-air mixture, which consequently may affect the combustion characteristics, the nature, and quantity of the pollutants formed.

6.5 Conclusions

The composition of the biodiesel plays a significant role in determining the air-fuel mixture distribution and engine performance. In this chapter, vapor mass fraction distribution of the multi-component surrogate of diesel and biodiesel fuel is studied using multi-component evaporation model. The numerical model is validated with experimental liquid length and vapor length for diesel and biodiesel. The spray liquid length study confirms that the single component surrogate for multi-component fuel should be one having the highest contribution to the composition and representing similar physiochemical properties as that of biodiesel. The comparison of single component and the multi-component surrogate is carried out at engine-relevant conditions. The vapor distribution for a multi-component surrogate is considerably different than that of single component fuel. The tetradecane, single component surrogate for diesel has vapor mass distribution markedly different than in multi-component diesel fuel. The effect on spatial mass fraction distribution profile of biodiesel is found to be the function of the volatility differential of the pure components and their proportion in the composition. The vapor mass fraction distribution for biodiesel of palm and soybean are found to be similar to that of their single component surrogate due to a similar volatility of components of these

biodiesels. However, methyl laurate in coconut biodiesel have volatility differential with other components and also have a significant share of 40 to 50% in the coconut biodiesel composition. The change in the percentage of methyl laurate in coconut composition is found to have a strong impact on vapor distribution.

The vapor mass fraction distribution is observed to be affected by the change in the biodiesel composition specifically volatile component. However, the change is negligible for palm biodiesel with the change in methyl myristate component due to the lower proportion of methyl myristate in the palm biodiesel. The composition of the biodiesel play a significant role in determining the air-fuel mixture distribution. The biodiesel which have variation in composition, depending on the method and place of the production, may give different combustion characteristics and emission profile. The accurate determination of the biodiesel composition is essential to get the correct prediction of combustion characteristics and emission profile for the given engine conditions.

7 Conclusions and Future Work

7.1 Summary and Conclusions

The fuel spray characteristics play a key role in determining the CI engine performance, combustion, and the pollutants formed. The biodiesel fuelled CI engines are observed to produce higher NO_x emission. Advanced combustion technologies try to reduce emissions through optimal air-fuel mixture formation. This is controlled through spray atomization and evaporation. It is important to investigate the biodiesel spray characteristics in accordance with its composition and physiochemical properties to understand the cause of higher NO_x emission. This will help make the biodiesel as a viable alternative fuel for CI engine. The spray characteristics of the biodiesel, both non-evaporating and evaporating, are studied using an open-source, "OpenFOAM" CFD code. The CFD code is modified to incorporate the physiochemical properties of pure components of biodiesel from NSRDS, Design Institute for Physical Properties project 801. The numerical code can be used to model pure component fuel and also multi-component fuel using mixing rule. The multi-component droplet heating and evaporation model is incorporated in the code to simulate real fuel spray evaporation and air-fuel mixture formation.

The non-evaporating spray characteristics are validate using the experiments performed in a high-pressure spray chamber with optical access. The single component representatives are selected for commonly used biodiesels based on composition. For example, methyl oleate is chosen to represent biodiesels such as karanja, soybean, and rapeseed. The methyl laurate is selected to represent coconut and palm kernel biodiesel. A comparative experimental and numerical study is conducted to establish the significance of single component representative for biodiesel, diesel and their blend for predicting spray tip penetration. The spray tip penetration of karanja

biodiesel is found to be similar to that of the methyl oleate. The spray tip penetration of coconut biodiesel is observed to be similar to that of methyl laurate. Furthermore, the measured spray tip penetration of biodiesel and its 20% blend with diesel is also compared with their corresponding single component and multi-component representative. It is found to be in good agreement with the measured spray tip penetration.

The spray characteristics of evaporating spray, liquid length, and vapor length are predicted and compared for pure components of biodiesel and SVO at engine-relevant conditions. The spray models are validated with experimental data available in the literature for various fuels under evaporating conditions. The liquid and vapor length are found to be the function of fuel properties and an ambient gas conditions. The liquid length of methyl oleate is higher under late-cycle post-injection conditions studied. It may lead to impingement of liquid fuel on the combustion chamber walls. The liquid length for methyl laurate at late-cycle post-injection conditions is lower than that of methyl oleate and may not impinge on the combustion chamber wall. The FAME components studied under near top-dead-center injection conditions are noted to have a lower liquid length, which can avoid wall impingement.

The vapor length for all the biodiesel pure components is similar at near top-dead-center conditions. However, at lower ambient gas density and ambient gas temperature conditions, methyl oleate is found to produce higher vapor length. The vapor length decreases with increase in an ambient gas temperature. The pure components of SVOs have higher liquid length than that of their corresponding FAME. The liquid length, vapor length and spray vapor area for methyl laurate is found to be similar to that of dodecane. The spray vapor area for triglycerides is significantly lower than that of FAMEs. A linear correlation is confirmed between the liquid length and the boiling temperature of the biofuels.

The vapor mass fraction distribution of the multi-component surrogate of diesel and biodiesel fuel is studied using multi-component evaporation model. The single component and the multi-component surrogate spray is compared at engine-relevant conditions. The vapor distribution for a multi-component surrogate is considerably different than that of single component fuel. The spatial mass fraction distribution of biodiesel is observed to be the function of the volatility differential of the

pure components and their proportion in the composition. The vapor mass fraction distribution for biodiesel of palm and soybean is found to be similar to that of their single component surrogate due to a similar volatility of components of these biodiesels. The change in the percentage of methyl laurate in coconut composition is found to have a strong impact on vapor distribution. The vapor mass fraction distribution is observed to be affected by the change in the biodiesel composition specifically volatile component. The accurate determination of the biodiesel composition is essential to achieve the correct prediction of combustion characteristics and emission profile for the given engine conditions.

The important conclusions from the present experimental and numerical investigations are discussed below:

1. A single component representative of biodiesel is sufficient to predict the non-evaporating spray characteristics of biodiesel and its blend in their respective category.

2. It is necessary to have knowledge of the composition of the biodiesel and FAME component dominating physical properties of biodiesel to model the biodiesel spray.

3. The observed wall impingement behavior for methyl oleate can be extended for all the commonly used biodiesels, such as soybean, rapeseed, karanja and jatropha.

4. Similarly, the results of methyl laurate can be applied for coconut and palm kernel biodiesel.

5. The triglycerides, representing SVOs, are more prone to wall impingement even at high ambient gas pressure and temperature conditions.

6. The liquid length of all the pure components studied is found to be related to the specific energy ratio.

7. The composition of the biodiesel play a significant role in determining the air-fuel mixture distribution. The biodiesel have variation in composition depending on the method of production and their raw material. This may result in variation in combustion characteristics and emissions.

8. The volatility differential of pure components and their proportion in the composition strongly influence the spatial mass fraction distribution profile of biodiesel.

9. The biodiesel with pure components having similar boiling point, have less impact of composition on vapor mass fraction distribution.

7.2 Future Work

1. The multi-component evaporation model can be utilized to study the ignition behavior of individual pure components of biofuels.

2. The evaporating spray experiments of biofuel pure components in optical engine can help to understand the effect of flow field turbulence and on air-fuel mixture formation.

Bibliography

[1] R. D. Lanjekar, D. Deshmukh, A review of the effect of the composition of biodiesel on NO_x emission, oxidative stability and cold flow properties, Renewable & Sustainable Energy Reviews 54 (2016) 1401 – 1411.

[2] A. Demirbas, Progress and recent trends in biodiesel fuels, Energy Conversion and Management 50 (1) (2009) 14–34.

[3] A. Demirbas, Biodiesel production via non-catalytic SCF method and biodiesel fuel characteristics, Energy Conversion and Management 47 (15) (2006) 2271–2282.

[4] S. P. Singh, D. Singh, Biodiesel production through the use of different sources and characterization of oils and their esters as the substitute of diesel: A review, Renewable & Sustainable Energy Reviews 14 (1) (2010) 200–216.

[5] M. S. Graboski, R. L. McCormick, Combustion of fat and vegetable oil derived fuels in diesel engines, Progress in Energy and Combustion Science 24 (2) (1998) 125–164.

[6] C. A. W. Allen, Prediction of biodiesel fuel atomization characteristics based on measured properties, Ph.D. thesis, Dalhousie University Daltech (1998).

[7] G. Knothe, Improving biodiesel fuel properties by modifying fatty ester composition, Energy & Environmental Science 2 (7) (2009) 759–766.

[8] P. Ye, Investigation of impact of fuel injection strategy and biodiesel fueling on engine emissions and performance, Ph.D. thesis, The Pennsylvania State University (2011).

[9] G. Knothe, Dependence of biodiesel fuel properties on the structure of fatty acid alkyl esters, Fuel Processing Technology 86 (10) (2005) 1059–1070.

[10] S. K. Hoekman, C. Robbins, Review of the effects of biodiesel on NO_x emissions, Fuel Processing Technology 96 (2012) 237–249.

[11] S. K. Hoekman, A. Broch, C. Robbins, E. Ceniceros, M. Natarajan, Review of biodiesel composition, properties, and specifications, Renewable and Sustainable Energy Reviews 16 (1) (2012) 143–169.

[12] E. G. Giakoumis, A statistical investigation of biodiesel physical and chemical properties, and their correlation with the degree of unsaturation, Renewable Energy 50 (2013) 858–878.

[13] R. L. McCormick, M. S. Graboski, T. L. Alleman, A. M. Herring, K. S. Tyson, Impact of biodiesel source material and chemical structure on emissions of criteria pollutants from a heavy-duty engine, Environmental Science & Technology 35 (9) (2001) 1742–1747.

[14] M. S. Graboski, R. L. McCormick, T. L. Alleman, A. M. Herring, The effect of biodiesel composition on engine emissions from a DDC series 60 diesel engine, technical report NREL/SR-510-31461, National Renewable Energy Laboratory; (2003).

[15] G. Martínez, N. Sánchez, J. M. Encinar, J. F. González, Fuel properties of biodiesel from vegetable oils and oil mixtures. Influence of methyl esters distribution, Biomass and Bioenergy 63 (2014) 22–32.

[16] G. Knothe, K. R. Steidley, Kinematic viscosity of biodiesel fuel components and related compounds. Influence of compound structure and comparison to petrodiesel fuel components, Fuel 84 (9) (2005) 1059–1065.

[17] H. M. Teeter, J. C. Cowan, Viscometric properties of higher fatty acids and their derivatives, Journal of the American Oil Chemists' Society 33 (4) (1956) 163–169.

[18] C. A. W. Allen, K. C. Watts, R. G. Ackman, M. J. Pegg, Predicting the viscosity of biodiesel fuels from their fatty acid ester composition, Fuel 78 (11) (1999) 1319–1326.

[19] B. Kegl, Influence of biodiesel on engine combustion and emission characteristics, Applied Energy 88 (5) (2011) 1803–1812.

[20] E. Torres-Jimenez, M. Kegl, R. Dorado, B. Kegl, Numerical injection characteristics analysis of various renewable fuel blends, Fuel 97 (2012) 832 – 842.

[21] M. Battistoni, C. N. Grimaldi, Numerical analysis of injector flow and spray characteristics from diesel injectors using fossil and biodiesel fuels, Applied Energy 97 (2012) 656–666.

[22] Q. Li, F. Schwarzmuller, R. Stegmann, G. Wachtmeister, Optical analysis of spray behavior with a modern common rail injector in canola oil operation, Atomization and Sprays 26 (6) (2016) 607–631.

[23] P. Emberger, D. Hebecker, P. Pickel, E. Remmele, K. Thuneke, Emission behaviour of vegetable oil fuel compatible tractors fuelled with different pure vegetable oils, Fuel 167 (2016) 257–270.

[24] E. Jiaqiang, T. Liu, W. M. Yang, J. Li, J. Gong, Y. Deng, Effects of fatty acid methyl esters proportion on combustion and emission characteristics of a biodiesel fueled diesel engine, Energy Conversion and Management 117 (2016) 410–419.

[25] S. Pinzi, P. Rounce, J. M. Herreros, A. Tsolakis, M. P. Dorado, The effect of biodiesel fatty acid composition on combustion and diesel engine exhaust emissions, Fuel 104 (2013) 170–182.

[26] G. Knothe, Improving biodiesel fuel properties by modifying fatty ester composition, Energy & Environmental Science 2 (7) (2009) 759–766.

[27] J. Thangaraja, K. Anand, P. S. Mehta, Predicting surface tension for vegetable oil and biodiesel fuels, RSC Advances 6 (88) (2016) 84645–84657.

[28] S. G. Musharraf, M. A. Ahmed, N. Zehra, Quantification of fames in biodiesel blends of various sources by gas chromatography tandem mass spectrometry, Analytical Methods 7 (8) (2015) 3372–3378.

[29] S. K. Hoekman, A. Broch, C. Robbins, E. Cenicero, Investigation of biodiesel chemistry, carbon footprint and regional fuel quality, Tech. Rep. AVFL-17a, Coordinating Research Council, Inc., 3650 Mansell Road Suite 140 Alpharetta, GA 30022 (2011).

[30] C. E. Ejim, B. A. Fleck, A. Amirfazli, Analytical study for atomization of biodiesels and their blends in a typical injector: surface tension and viscosity effects, Fuel 86 (10) (2007) 1534–1544.

[31] E. Mancaruso, L. Sequino, B. M. Vaglieco, First and second generation biodiesels spray characterization in a diesel engine, Fuel 90 (9) (2011) 2870–2883.

[32] J. Galle, J. Demuynck, J. Vancoillie, S. Verhelst, Spray parameter comparison between diesel and vegetable oils for non-evaporating conditions, in: SAE Technical Paper 2012-01-0461, SAE International, 2012.

[33] A. Azetsu, S. Dodo, T. Someya, C. Oikawa, A study on the structure of diesel spray (2-D visualization of the non-evaporating spray), in: COMODIA, Vol. 90, 1990, pp. 199–204.

[34] Y. Gao, J. Deng, C. Li, F. Dang, Z. Liao, Z. Wu, L. Li, Experimental study of the spray characteristics of biodiesel based on inedible oil, Biotechnology Advances 27 (5) (2009) 616–624.

[35] E. Jiaqiang, T. Liu, W. M. Yang, J. Li, J. Gong, Y. Deng, Effects of fatty acid methyl esters proportion on combustion and emission characteristics of a biodiesel fueled diesel engine, Energy Conversion and Management 117 (2016) 410–419.

[36] B. Mohan, W. Yang, K. L. Tay, W. Yu, Experimental study of spray characteristics of biodiesel derived from waste cooking oil, Energy Conversion and Management 88 (2014) 622–632.

[37] J. B. Heywood, Internal combustion engine fundamentals, Mcgraw-Hill New York, 1988.

[38] S. R. Turns, Understanding NO_x formation in nonpremixed flames: Experiments and modeling, Progress in Energy and Combustion Science 21 (5) (1995) 361–385.

[39] J. E. Dec, Advanced compression-ignition engines understanding the in-cylinder processes, Proceedings of the Combustion Institute 32 (2) (2009) 2727–2742.

[40] M. Shahabuddin, A. M. Liaquat, H. H. Masjuki, M. A. Kalam, M. Mofijur, Ignition delay, combustion and emission characteristics of diesel engine fueled with biodiesel, Renewable & Sustainable Energy Reviews 21 (2013) 623–632.

[41] E. Ozturk, Performance, emissions, combustion and injection characteristics of a diesel engine fuelled with canola oil–hazelnut soapstock biodiesel mixture, Fuel Processing Technology 129 (2015) 183–191.

[42] Y. Zhang, A. L. Boehman, Impact of biodiesel on NO_x emissions in a common rail direct injection diesel engine, Energy & Fuels 21 (4) (2007) 2003–2012.

[43] A. Monyem, J. H. Van Gerpen, M. Canakcl, The effect of timing and oxidation on emissions from biodiesel–fueled engines, Carbon 44 (1) (2001) 35–42.

[44] M. E. Tat, J. H. Van Gerpen, Measurement of biodiesel speed of sound and its impact on injection timing, technical report NREL/SR-510-31462, National Renewable Energy Laboratory; (2003).

[45] A. L. Boehman, D. Morris, J. Szybist, E. Esen, The impact of the bulk modulus of diesel fuels on fuel injection timing, Energy & Fuels 18 (6) (2004) 1877–1882.

[46] M. Canakci, J. H. Van Gerpen, Comparison of engine performance and emissions for petroleum diesel fuel, yellow grease biodiesel, and soybean oil biodiesel, Transactions of the American Society of Agricultural Engineers 46 (4) (2003) 937–944.

[47] M. Johansson, J. Yang, R. Ochoterena, S. Gjirja, I. Denbratt, NO_x and soot emissions trends for RME, SME and PME fuels using engine and spray experiments in combination with simulations, Fuel 106 (2013) 293–302.

[48] G. A. Ban-Weiss, J. Y. Chen, B. A. Buchholz, R. W. Dibble, A numerical investigation into the anomalous slight NO_x increase when burning biodiesel; A new (old) theory, Fuel Processing Technology 88 (7) (2007) 659–667.

[49] A. Gopinath, S. Puhan, G. Nagarajan, Effect of unsaturated fatty acid esters of biodiesel fuels on combustion, performance and emission characteristics of a DI diesel engine, International Journal Of Energy And Environment 1 (3) (2010) 411–430.

[50] J. Pullen, K. Saeed, Factors affecting biodiesel engine performance and exhaust emissions–part I: Review, Energy 72 (2014) 1–16.

[51] R. L. McCormick, T. L. Alleman, The biodiesel handbook, Vol. 1, AOCS press Champaign, IL, 2005, Ch. Exhaust Emissions, pp. 163–181.

[52] V. T. Wyatt, M. A. Hess, R. O. Dunn, T. A. Foglia, M. J. Haas, W. N. Marmer, Fuel properties and nitrogen oxide emission levels of biodiesel produced from animal fats, Journal of the American Oil Chemists' Society 82 (8) (2005) 585–591.

[53] G. Knothe, C. A. Sharp, T. W. Ryan, Exhaust emissions of biodiesel, petrodiesel, neat methyl esters, and alkanes in a new technology engine, Energy & Fuels 20 (1) (2006) 403–408.

[54] H. T. C. Machacon, Y. Matsumoto, C. Ohkawara, S. Shiga, T. Karasawa, H. Nakamura, The effect of coconut oil and diesel fuel blends on diesel engine performance and exhaust emissions, JSAE Review 22 (3) (2001) 349–355.

[55] M. A. Kalam, M. Husnawan, H. H. Masjuki, Exhaust emission and combustion evaluation of coconut oil-powered indirect injection diesel engine, Renewable Energy 28 (15) (2003) 2405–2415.

[56] M. Ono, M. Nakajima, K. Yoshida, H. Shoji, A. Iijima, Influence of various biodiesel fuels on diesel engine performance, Society of Automotive Engineers of Japan 20097100 (2009).

[57] H. Mohamed Ismail, H. K. Ng, S. Gan, X. Cheng, T. Lucchini, Investigation of biodiesel–diesel fuel blends on combustion characteristics in a light duty diesel engine using OpenFOAM, Energy & Fuels 27 (1) (2012) 208–219.

[58] E. Kinoshita, T. Myo, K. Hamasaki, H. Tajima, Z. R. Kun, Diesel combustion characteristics of coconut oil and palm oil biodiesels, Tech. rep., SAE Technical Paper (2006).

[59] T. Myo, E. Kinoshita, H. Tsuru, K. Hamasaki, Combustion characteristics of a DI diesel engine with palm kernel oil biodiesel and its blend (B20), Society of Automotive Engineers of Japan 20076568 (2007).

[60] A. Shaheed, E. Swain, Performance and exhaust emission evaluation of a small diesel engine fuelled with coconut oil methyl esters, SAE Technical Paper 981156 (1998).

[61] M. Han, K. Cho, C. S. Sluder, R. M. Wagner, Soybean and coconut biodiesel fuel effects on combustion characteristics in a light-duty diesel engine, Tech. rep., SAE Technical Paper (2008).

[62] C. A. Amann, D. C. Siegla, Diesel particulates–what they are and why, Aerosol Science and Technology 1 (1) (1981) 73–101.

[63] M. J. Murphy, J. D. Taylor, R. L. McCormick, Compendium of experimental cetane number data, technical report NREL/SR-540-36805, National Renewable Energy Laboratory; (2004).

[64] M. Bennett, J. Volckens, R. Stanglmaier, A. P. McNichol, W. D. Ellenson, C. W. Lewis, Biodiesel effects on particulate radiocarbon (14C) emissions from a diesel engine, Journal of Aerosol Science 39 (8) (2008) 667–678.

[65] P. K. Sahoo, L. M. Das, Combustion analysis of Jatropha, Karanja and Polanga based biodiesel as fuel in a diesel engine, Fuel 88 (6) (2009) 994–999.

[66] A. S. Cheng, A. Upatnieks, C. J. Mueller, Investigation of the impact of biodiesel fuelling on NO_x emissions using an optical direct injection diesel engine, International Journal of Engine Research 7 (4) (2006) 297–318.

[67] C. J. Mueller, A. L. Boehman, G. C. Martin, An experimental investigation of the origin of increased NO_x emissions when fueling a heavy-duty compression-ignition engine with soy biodiesel, SAE 2009-01-1792 (2009).

[68] N. Mizushima, D. Kawano, H. Ishii, Y. Goto, H. Arai, Effect of fuel properties of biodiesel on its combustion and emission characteristics, in: SAE Technical Paper, SAE International, 2011.

[69] W. Zhang, K. Nishida, J. Gao, D. Miura, An experimental study on flat-wall-impinging spray of microhole nozzles under ultra-high injection pressures, Proceedings of the institution of mechanical Engineers, Part D: Journal of Automobile Engineering 222 (9) (2008) 1731–1741.

[70] R. Payri, F. J. Salvador, J. Gimeno, V. Soare, Determination of diesel sprays characteristics in real engine in-cylinder air density and pressure conditions, Journal of mechanical science and technology 19 (11) (2005) 2040–2052.

[71] C. F. Taylor, The Internal-combustion Engine in Theory and Practice: Combustion, fuels, materials, design, Vol. 2, MIT press, 1985.

[72] P. Pogorevc, B. Kegl, L. Skerget, Diesel and biodiesel fuel spray simulations, Energy & Fuels 22 (2) (2008) 1266–1274.

[73] H. M. Ismail, H. K. Ng, S. Gan, T. Lucchini, Computational study of biodiesel–diesel fuel blends on emission characteristics for a light-duty diesel engine using openfoam, Applied Energy 111 (2013) 827–841.

[74] S. M. Palash, M. A. Kalam, H. H. Masjuki, B. M. Masum, I. M. R. Fattah, M. Mofijur, Impacts of biodiesel combustion on NO_x emissions and their reduction approaches, Renewable & Sustainable Energy Reviews 23 (2013) 473–490.

[75] G. Knothe, C. A. Sharp, T. W. Ryan, Exhaust emissions of biodiesel, petrodiesel, neat methyl esters, and alkanes in a new technology engine, Energy & Fuels 20 (1) (2006) 403–408.

[76] S. K. Hoekman, C. Robbins, Review of the effects of biodiesel on NO_x emissions, Fuel Processing Technology 96 (2012) 237–249.

[77] T. Myo, K. Hamasaki, E. Kinoshita, H. Tajima, Diesel combustion characteristics of single compositions of fatty acid methyl esters, in: SAE Technical Paper 2005-32-0042, no. 2005-32-0042, SAE International, 2005.

[78] D. Deshmukh, A. M. Mohan, T. N. C. Anand, R. V. Ravikrishna, Spray characterization of straight vegetable oils at high injection pressures, Fuel 97 (2012) 879–883.

[79] P. Hellier, N. Ladommatos, T. Yusaf, The influence of straight vegetable oil fatty acid composition on compression ignition combustion and emissions, Fuel 143 (2015) 131–143.

[80] M. S. Shehata, S. M. A. Razek, Experimental investigation of diesel engine performance and emission characteristics using jojoba/diesel blend and sunflower oil, Fuel 90 (2) (2011) 886–897.

[81] B. Mohan, W. Yang, S. Kiang Chou, Fuel injection strategies for performance improvement and emissions reduction in compression ignition enginesâĂŤa review, Renewable & Sustainable Energy Reviews 28 (2013) 664–676.

[82] C. L. Genzale, L. M. Pickett, S. Kook, Liquid penetration of diesel and biodiesel sprays at late-cycle post-injection conditions, SAE International Journal of Engines 3 (2010) 479–495.

[83] T. Wang, X. Meng, X. Song, M. Jia, Modeling the spray behaviors of fatty acid methyl esters in biodiesel fuels under engine-relevant conditions, in: SAE Technical Paper 2014-01-2736, SAE International, 2014.

[84] P. Boggavarapu, R. V. Ravikrishna, Experimental studies on evaporating sprays of diesel and jatropha methyl ester (JME), in: Proceedings of the 18th

Annual Conference on Liquid Atomization and Spray Systems-Asia, Chennai, India (18th ILASS 2016), ILASS, 2016.

[85] H. M. Ismail, H. K. Ng, X. Cheng, S. Gan, T. Lucchini, G. D'Errico, Development of thermophysical and transport properties for the CFD simulations of in-cylinder biodiesel spray combustion, Energy & Fuels 26 (8) (2012) 4857–4870.

[86] S. Som, D. E. Longman, A. Ramírez, S. K. Aggarwal, A comparison of injector flow and spray characteristics of biodiesel with petrodiesel, Fuel 89 (12) (2010) 4014–4024.

[87] S. H. Park, H. J. Kim, H. K. Suh, C. S. Lee, Experimental and numerical analysis of spray-atomization characteristics of biodiesel fuel in various fuel and ambient temperatures conditions, International journal of heat and fluid flow 30 (5) (2009) 960–970.

[88] D. Jarrahbashi, S. Kim, C. L. Genzale, Simulation of combustion recession after end-of-injection at diesel engine conditions, Journal of Engineering for Gas Turbines and Power 139 (10) (2017) 102804.

[89] B. Mohan, W. Yang, W. Yu, Effect of internal nozzle flow and thermo-physical properties on spray characteristics of methyl esters, Applied Energy 129 (2014) 123–134.

[90] J. G. Nerva, C. L. Genzale, S. Kook, J. M. GarcÃŋa-Oliver, L. M. Pickett, Fundamental spray and combustion measurements of soy methyl-ester biodiesel, International Journal of Engine Research 14 (4) (2013) 373–390.

[91] V. Gopalakrishnan, J. Abraham, An investigation of ignition behavior in diesel sprays, Proceedings of the Combustion Institute 29 (1) (2002) 641–646.

[92] S. K. Aggarwal, Ignition behavior of a multicomponent fuel spray, Combustion and Flame 76 (1) (1989) 5–15.

[93] J. A. Bittle, B. M. Knight, T. J. Jacobs, Interesting behavior of biodiesel ignition delay and combustion duration, Energy & Fuels 24 (8) (2010) 4166–4177.

[94] Y. Ra, R. D. Reitz, A vaporization model for discrete multi-component fuel sprays, International Journal of Multiphase Flow 35 (2) (2009) 101–117.

[95] F. P. Karrholm, N. Nordin, Numerical investigation of mesh/turbulence/spray interaction for diesel applications, in: SAE Technical Paper 2005-01-2115, SAE International, 2005.

[96] D. I. P. P. R, DIPPR Project 801 - Full Version, Design Institute for Physical Property Research/AIChE, 2005-2016.

[97] S. R. Turns, et al., An introduction to combustion, Vol. 499, McGraw-hill New York, 1996.

[98] I. Glassman, R. A. Yetter, N. G. Glumac, Combustion, Academic press, 2014.

[99] G. Faeth, Current status of droplet and liquid combustion, in: Energy and Combustion Science, Elsevier, 1979, pp. 149–182.

[100] R. Payri, F. J. Salvador, J. Gimeno, G. Bracho, A new methodology for correcting the signal cumulative phenomenon on injection rate measurements, Experimental techniques 32 (1) (2008) 46–49.

[101] H. G. Weller, G. Tabor, H. Jasak, C. Fureby, A tensorial approach to computational continuum mechanics using object-oriented techniques, Computers in physics 12 (6) (1998) 620–631.

[102] J. C. Beale, R. D. Reitz, Modeling spray atomization with the kelvin-helmholtz/rayleigh-taylor hybrid model, Atomization and Sprays 9 (6) (1999) 623–650.

[103] M. Turner, S. Sazhin, J. Healey, C. Crua, S. Martynov, A breakup model for transient diesel fuel sprays, Fuel 97 (2012) 288–305.

[104] E. Babinsky, P. Sojka, Modeling drop size distributions, Progress in energy and combustion science 28 (4) (2002) 303–329.

[105] B. Abramzon, W. A. Sirignano, Droplet vaporization model for spray combustion calculations, International journal of heat and mass transfer 32 (9) (1989) 1605–1618.

[106] W. A. Sirignano, Fuel droplet vaporization and spray combustion theory, Progress in Energy and Combustion Science 9 (4) (1983) 291–322.

[107] Y. Ra, R. D. Reitz, The application of a multicomponent droplet vaporization model to gasoline direct injection engines, International Journal of Engine Research 4 (3) (2003) 193–218.

[108] S. Kook, L. M. Pickett, Liquid length and vapor penetration of conventional, fischer-tropsch, coal-derived, and surrogate fuel sprays at high-temperature and high-pressure ambient conditions, Fuel 93 (2012) 539–548.

[109] G. Knothe, Historical perspectives on vegetable oil-based diesel fuels, Inform 12 (11) (2001) 1103–1107.

[110] C. Caldeira, F. Freire, E. A. Olivetti, R. Kirchain, Fatty acid based prediction models for biodiesel properties incorporating compositional uncertainty, Fuel 196 (2017) 13–20.

[111] J. Gimeno, G. Bracho, P. Martí-Aldaraví, J. E. Peraza, Experimental study of the injection conditions influence over n-dodecane and diesel sprays with two ECN single-hole nozzles. part I: Inert atmosphere, Energy Conversion and Management 126 (2016) 1146–1156.

[112] R. Payri, F. J. Salvador, J. Gimeno, J. E. Peraza, Experimental study of the injection conditions influence over n-dodecane and diesel sprays with two ECN single-hole nozzles. part II: Reactive atmosphere, Energy Conversion and Management 126 (2016) 1157–1167.

[113] J. M. Desantes, J. V. Pastor, J. M. García-Oliver, F. J. Briceño, An experimental analysis on the evolution of the transient tip penetration in reacting diesel sprays, Combustion and flame 161 (8) (2014) 2137–2150.

[114] F. KaraosmanoÇğlu, G. Kurt, T. Özaktaş, Long term CI engine test of sunflower oil, Renewable Energy 19 (1) (2000) 219–221.

[115] R. Altın, S. Cetinkaya, H. S. Yücesu, The potential of using vegetable oil fuels as fuel for diesel engines, Energy Conversion and Management 42 (5) (2001) 529–538.

[116] D. C. Rakopoulos, C. D. Rakopoulos, E. G. Giakoumis, A. M. Dimaratos, M. A. Founti, Comparative environmental behavior of bus engine operating on blends of diesel fuel with four straight vegetable oils of greek origin: sunflower, cottonseed, corn and olive, Fuel 90 (11) (2011) 3439–3446.

[117] J. San José, M. A. Sanz-Tejedor, Y. Arroyo, Effect of fatty acid composition in vegetable oils on combustion processes in an emulsion burner, Fuel Processing Technology 130 (2015) 20–30.

[118] B. Esteban, J. R. Riba, G. Baquero, R. Puig, A. Rius, Characterization of the surface tension of vegetable oils to be used as fuel in diesel engines, Fuel 102 (2012) 231–238.

[119] S. Y. No, Application of straight vegetable oil from triglyceride based biomass to IC engines - A review, Renewable & Sustainable Energy Reviews 69 (2017) 80–97.

[120] Sandia National Laboratories. Engine Combustion Network experimental data archive, http://www.sandia.gov/ecn/.

[121] S. Kumar, J. S. Yadav, V. K. Sharma, W. Lim, J. H. Cho, J. Kim, I. Moon, Physicochemical properties of jatropha curcas biodiesel + diesel fuel no. 2 binary mixture at T = (288.15 to 308.15) K and atmospheric pressure, Journal of Chemical & Engineering Data 56 (3) (2011) 497–501.

[122] P. Benjumea, J. Agudelo, A. Agudelo, Basic properties of palm oil biodiesel–diesel blends, Fuel 87 (10) (2008) 2069–2075.

[123] S. Pinzi, I. L. Garcia, F. J. Lopez-Gimenez, M. D. Luque de Castro, G. Dorado, M. P. Dorado, The ideal vegetable oil-based biodiesel composition: a review of social, economical and technical implications, Energy & Fuels 23 (5) (2009) 2325–2341.

[124] C. Allen, E. Toulson, D. Tepe, H. Schock, D. Miller, T. Lee, Characterization of the effect of fatty ester composition on the ignition behavior of biodiesel fuel sprays, Fuel 111 (2013) 659–669.

[125] B. S. Higgins, C. J. Mueller, D. L. Siebers, Measurements of fuel effects on liquid-phase penetration in di sprays, in: SAE Technical Paper 1999-01-0519, SAE International, 1999.

[126] D. L. Siebers, Liquid-phase fuel penetration in siesel sprays, in: SAE Technical Paper 980809, SAE International, 1998.

[127] D. L. Siebers, Scaling liquid-phase fuel penetration in diesel sprays based on mixing-limited vaporization, in: SAE Technical Paper 1999-01-0528, SAE International, 1999.

List of publications

Journal papers:

1. Lanjekar R. D., Deshmukh D., Experimental and numerical investigations on spray characteristics of fatty acid methyl esters, Royal Society Open Science 5(2) (2018): 171121. Doi: http://dx.doi.org/10.1098/rsos.171121

2. Lanjekar, R. D., and Deshmukh, D., Biofuel pure component spray characteristics at engine-relevant conditions, Energy & Fuels 31 (9)(2017):9438-9445. Doi: http://dx.doi.org/10.1021/acs.energyfuels.7b00848

3. Lanjekar, R. D., and Deshmukh, D., A review of the effect of the composition of biodiesel on NO_x emission, oxidative stability and cold flow properties, Renewable & Sustainable Energy Reviews 54 (2016): 1401-1411. Doi: http://dx.doi.org/10.1016/j.rser.2015.10.034

International Conference papers:

1. Lanjekar, R.D., and Deshmukh,D., Experimental and numerical characterization of fatty acid and methyl ester sprays, Proceedings of the ILASS-Asia 2016, 18th Annual Conference on Liquid Atomization and Spray Systems - Asia, Chennai, India, 2016.

2. Lanjekar, R.D., and Deshmukh,D., Modeling influence of alcohol moiety and chain length on pure fatty acid ester spray, Proceedings of the 13th International Conference on Liquid Atomization and Spray Systems (13th ICLASS 2015), 2015.